INVESTIGATION OF FAILURE MODES AND MECHANISMS OF ALIBEY EARTH DAM BY SOLID-FLUID COUPLED NONLINEAR DYNAMIC FINITE ELEMENT SIMULATION

by

AHMET ALPER PARKER

B.S., Civil Engineering, Istanbul Technical University, 1999
B.S., Management Engineering, Istanbul Technical University, 2002
M.S., Management Engineering, Istanbul Technical University, 2003

Submitted to the Kandilli Observatory and
Earthquake Research Institute in partial fulfillment of
the requirements for the degree of
Master of Science

Graduate Program in Earthquake Engineering
Bogazici University
2006

INVESTIGATION OF FAILURE MODES AND MECHANISMS
OF ALIBEY EARTH DAM BY SOLID-FLUID COUPLED NONLINEAR DYNAMIC
FINITE ELEMENT SIMULATION

APPROVED BY:

Assoc. Prof. Bilge Siyahi (Thesis Supervisor)	.....
Prof. Mustafa Erdik	.....
Prof. Niyazi Turkelli	.....

DATE OF APPROVAL:

ACKNOWLEDGEMENTS

I would like to express my sincere gratitude to my thesis supervisor Bilge Siyahi for her guidance and support during preparation of this dissertation. I am grateful to Prof. Mustafa Erdik and Prof. Niyazi Turkelli for providing me additional time for working on the study at the last minute; I am thankful to them. Also, I would like to acknowledge Assistant Professor Sami And Kilic, Associate Professor Fazil Onder Sonmez from Mechanical Engineering Department, Zuhal Ozdemir, Gokce Tonuk, Muammer Ozbek, Banu Sanli, Cuneyt Tuzun, Muge Balkaya from Istanbul Technical University, Bulent Hakan Akman, Mine Betul Demircioglu, Onur Eren, Sezin Sarioguz and Orcun Sarioguz for their valuable comments, suggestions and support for developing the research.

I would like to recognize open source community, especially the developers of OpenSees framework for their effort on developing the code and maintaining support for code specific issues.

This thesis was supported by Bogazici University Research Fund 06T104. I would like to acknowledge their generous support.

Finally, I want to thank to my family for their love and support throughout my life.

ABSTRACT

INVESTIGATION OF FAILURE MODES AND MECHANISMS OF ALIBEY EARTH DAM BY SOLID-FLUID COUPLED NONLINEAR DYNAMIC FINITE ELEMENT SIMULATION

In this study, earthquake resistance of Alibey Earth Dam was investigated. Dam was modeled with four node plane-strain finite elements and displacement-pore pressure coupled finite element analyses were performed. Nonlinear material models such as pressure dependent and independent multi yield materials were implemented during the analyses. Transient dynamic finite element analyses were performed with Newmark method. Newton-Raphson solution scheme was adopted during the solution of the equations. Liquefaction and/or cyclic mobility effects were considered during the analysis. For the finite element analyses OpenSees (Open System for Earthquake Engineering Simulation) framework was adopted.

ÖZET

ALİBEY TOPRAK BARAJI'NIN GÖÇME MOD VE MEKANİZMALARININ KATI-SIVI BİLEŞİK DOĞRUSAL OLMAYAN DİNAMİK SONLU ELEMANLAR BENZETİMİ İLE İNCELENMESİ

Bu çalışmada Alibey Toprak Barajı'nın deprem dayanımı araştırılmıştır. Baraj, dört düğüm noktalı düzlem şekil değiştirme sonlu elemanlarıyla modellenmiş ve deplasman-boşluk suyu basıncı bileşik sonlu elemanlar analizleri gerçekleştirilmiştir. Analizler sırasında basınç bağımlı ve bağımsız çoklu akma malzemeleri gibi doğrusal olmayan malzeme modelleri uygulanmıştır. Geçişken dinamik sonlu elemanlar analizleri Newmark metoduyla gerçekleştirilmiştir. Denklemlerin çözümü sırasında Newton-Raphson çözüm yöntemi kullanılmıştır. Sıvılaşma ve devirsel hareketlilik etkileri de analizlerde gözönüne alınmıştır. Sonlu elemanlar analizleri için OpenSees (Deprem Mühendisliği Benzetimi için Açık Sistem) çerçevesi kullanılmıştır.

TABLE OF CONTENTS

LIST OF FIGURES

LIST OF TABLES

1. INTRODUCTION

1.1. Motivation for this Study

Earth dams are engineering structures that are used for many purposes such as irrigation, flood control, power generation and water storage. However, failure of an earth dam can cause significant economic damages and loss of human life. Engineers design dams to withstand the effect of extreme events such as floods and earthquakes. One of the major events that cause such catastrophic failures is earthquakes [1].

This study is conducted to investigate the failure modes and mechanisms of Alibey Earth Dam to evaluate the seismic performance of the dam. If the resistance of the dam to earthquakes can be predicted, economic damage and loss of human life can be prevented.

1.2. Objectives and Scope

There are previous studies performed for Alibey Earth Dam including coupled and uncoupled consolidation studies [2], [3], [4], [5], [6], [7], [8], [9], [10], [11] and seismic response investigations[12]. A study conducted by Cimilli [12] investigates the response of Alibey Earth dam by both numerical and experimental methods.

To further the previous researches on Alibey Dam in terms of seismic resistance investigations including nonlinear and liquefaction and/or cyclic mobility effects was the primary objective of this study. Modal analysis was performed which considers the soil below the dam and previous experimental results were compared with the current model.

In this study, first, description of the Alibey Earth Dam has been given, with emphasize on the material properties of the dam's foundation soil. Then, literature survey specific to earth dam failures and seismic analysis methodologies of earth dams have been outlined. Strong ground motion estimations were performed for the region where Alibey Dam is located. Finite element formulations were discussed and constitutive models adopted during analysis of the dam were examined. Also, descriptions of the boundary conditions and an effective seismic input definition have been given. The numerical model was explained in detail. Transient dynamic time history finite element simulations were

performed to investigate the performance of the dam under seismic excitation. The finite element formulations adopted in the study have the option to consider the effects of displacement and pore-pressure coupling. Pressure dependent and independent multi yield material properties were implemented that considers the liquefaction effects in the model. For the analyses, the primary numerical tool to implement finite element simulations was the OpenSees software framework. Verifications and validation of numeric modeling were given. Interpretation of results and comparisons with previous studies are discussed. Conclusions derived from the study are given at the end of the study.

2. DESCRIPTION OF THE STRUCTURE

2.1. Introduction

Alibey Dam is located in Istanbul, Turkey at the coordinates of 41^{o} 06’ 04’’ N, 28^{o} 55’ 11.7’’ E. Alibey Dam is an earth dam located at North-West Turkey on Alibey Stream. Figure 2 - 1, Figure 2 - 2 and Figure 2 - 3 shows the satellite views of the dam. Design and engineering supervision of the project was carried out by State Hydraulic Works, owner of the dam.

The dam serves as a domestic and industrial water supply for its vicinity and it also prevents floods in the Alibeykoy region. Failure of the dam may cause excessive damage to Alibeykoy and may result in loss of human life.

2.2. Underlying Soil Conditions and the Method Used During the Construction

1,970,000 m^3 earth and rock-fill materials were used during the construction of the Alibey dam. The dam is composed of several different types of materials. In the central part of the dam, a clay core was implemented (plastic clay). Top of the slopes are composed of decomposed rock material. At the top of the flat parts of the dam, sound rock materials exist. On the clay core, two different types of gravely sands were used. Dam body is commonly composed of sandy clay materials. Also, filter materials, clayey sand and grave and tunnel deposits exist in the dam. Figure 2 - 4 shows the cross section of the dam.

In cases where bearing capacity of foundation layers were insufficient, staged construction and pre-loading methods were applied. During the construction, significant settlement problems were encountered. As a result of this problem, staged construction continued for 8 years from 1975 to 1983. Also, sand drains were implemented for consolidation.

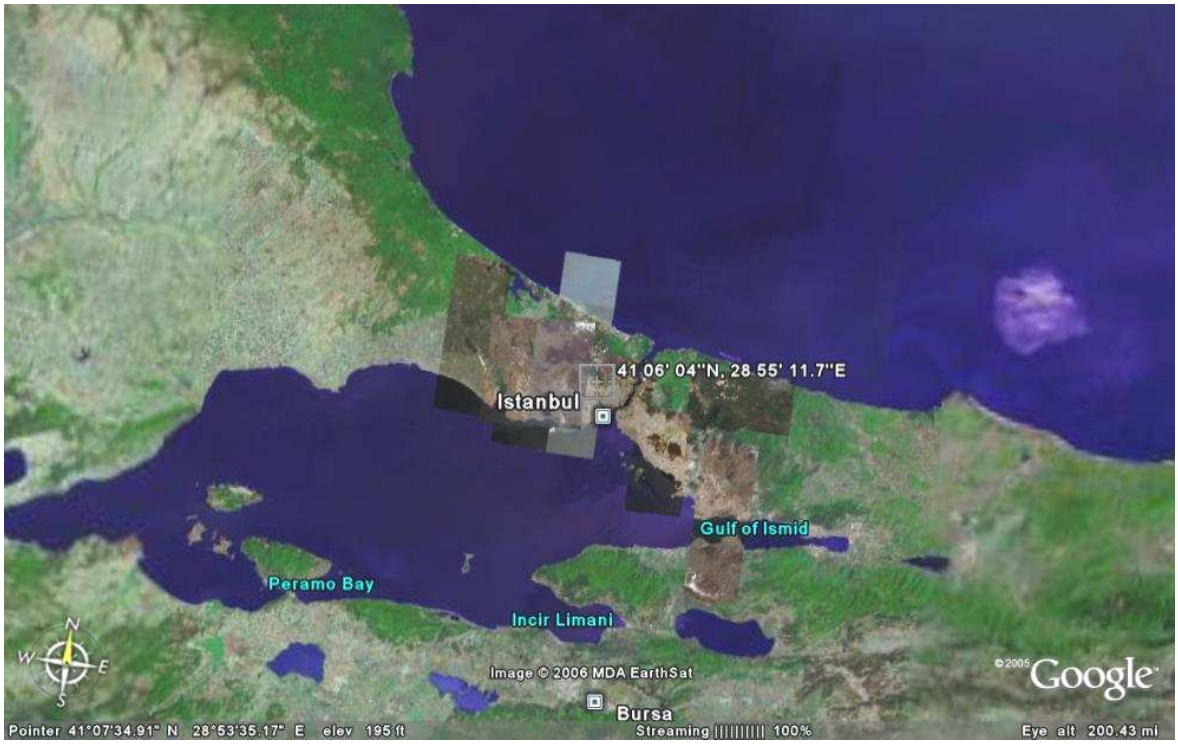

Figure 2 - 1: Satellite view of Alibey Earth Dam. Courtesy of Google Incorporation. Google Earth Virtual Globe Software, 2006.

Figure 2 - 2: Satellite view of Alibey Earth Dam. Courtesy of Google Incorporation. Google Earth Virtual Globe Software, 2006.

Figure 2 - 3: Satellite view of Alibey Earth Dam. Courtesy of Google Incorporation. Google Earth Virtual Globe Software, 2006.

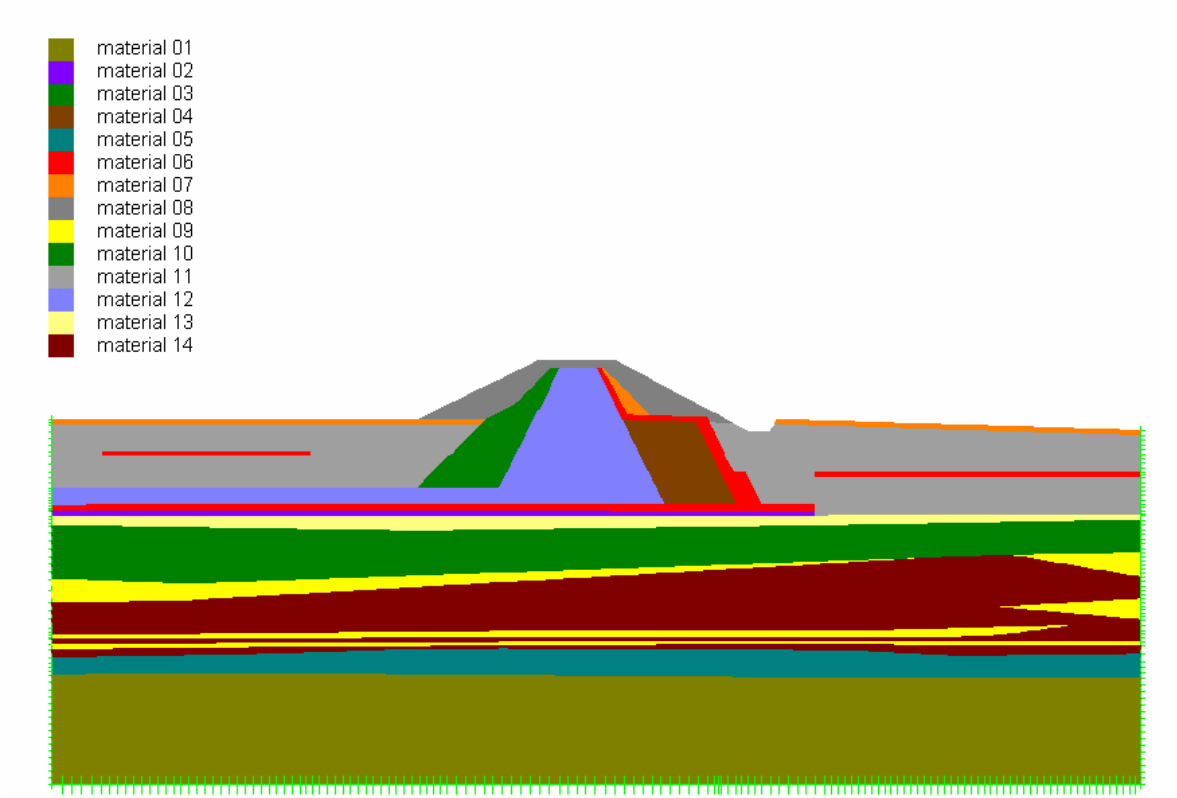

Figure 2 - 4: Cross-section of the dam with respect to different material properties.

Material names and their properties are given in Table 2 - 1.

Table 2 - 1: Material properties of the dam and foundation [11].

Material Label	Material Name	Material Type	E (kN/m^2)	ν
Material 01	Greywacke	Rock	68400000	0.20
Material 02	Fill	Fill	140000	0.30
Material 03	Gravelly-Sand Material	Sand-Gravel	140000	0.30
Material 04	Sands with Gravels	Sand-Gravel	140000	0.30
Material 05	Sand with Gravel	Sand-Gravel	140000	0.30
Material 06	Filter Material	Fill	140000	0.30
Material 07	Light-Weight Rock Material	Fill	140000	0.30
Material 08	Strong Rock Materials	Fill	100000	0.20
Material 09	Sand	Sand Band	140000	0.30
Material 10	Green Clay	Green Clay	140000	0.30
Material 11	Sandy-Clay	Fill	140000	0.30
Material 12	Plastic Clay	Yellow Clay	140000	0.30
Material 13	Yellow Clay	Yellow Clay	140000	0.30
Material 14	Black Clay	Black Clay	140000	0.30

2.3. Size of the Dam and Reservoir

The crest elevation of the dam is 34 meters and the crest length is 304 meters. Its height from the riverbed is 28 meters. The reservoir volume at the normal water surface elevation is 66.8 hm^3. Its area at normal water surface elevation is 4.66 km^2. Maximum water surface elevation is 32 meters and normal water surface elevation is 26 meters. The spillway is frontal and gated type [12].

Table 2 - 2: Data about Alibey Earth Dam and the reservoir [13].

Location	Eyup – Istanbul
River	Alibey
Purpose	Domestic and industrial water supply, flood protection
Embankment Type	Earth-fill
Ground Base	Earth – Rock
Construction (Starting and Completion) Year	1975 - 1983
Dam Volume	1,927,000 m^3
Talveg Level	6.00 m

Height (from River Bed)	28.00 m
Drainage Area	160.00 km^2
Crest Length	304.00 m
Crest Weight	15.00 m
Crest Level	34.00 m
Maximum Water Level	32.00 m
Normal Water Level	26.00 m
Minimum Water (Operation) Level	11.25 m
Minimum Operation Area	$0.426 * 10^6$ m^2
Maximum Reservoir Capacity	$65 * 10^6$ m^3
Maximum Reservoir Area	$4.76 * 10^6$ m^2
Reservoir Volume	34.87 hm^3/year
Reservoir Volume at Normal Water Surface Elevation	66.80 hm^3
Reservoir Area at Normal Water Surface Elevation	4.66 km^2
Annual Domestic Water	39 hm^3
Useful Reservoir Volume	34.00 hm^3/year
Full Spillway Capacity	500 m^3/s
Annual Performance (Active Volume)	35.00 hm^3/year
Dead Volume	$0.487 * 10^6$ m^3
Annual Mean Precipitation	800 mm/year
Annual Mean Flow	280 mm/year
Predicted Flow	160 * 280 km^2 * mm/year
Downstream River Capacity	80 m^3/s
Flood Peak	1000 m^3/s

3. REVIEW OF PREVIOUS RESEARCH

3.1. Introduction

In this section, types of failures in earth dams are discussed and seismic analysis methods special to earth dams have been explained.

3.2. Types of Failures in Earth Dams

Over the years, several types of earthquake damage have been observed in earth dams and embankments. Three major factors affect the stability and performance of an embankment during an earthquake:

a) Section geometry (upstream and downstream slopes).
b) Construction method and compaction procedure.
c) Type of embankment and foundation material.

The possible ways in which an earth dam might fail during an earthquake include:

1. Failure due to disruption of the dam by major fault movement in the foundation.
2. Slope failures induced by ground motions.
3. Loss of freeboard due to differential crest settlement.
4. Piping failure through cracks induced by the ground movements.
5. Overtopping of the dam due to failure of the spillway or outlet works.

In general, the principle types of damage can be classified as sliding failure, liquefaction failure, longitudinal cracks, transverse cracks, and piping failure [14].

3.2.1. Sliding Failure

Sliding, as shown in Figure 3 - 1 is a major type of damage that can occur in earth dams subjected to earthquake ground motions. Sliding initially causes settlement and subsequently leads to dam failure. The slope stability of earth dams is usually evaluated in terms of the shear strength of soils and the Mohr-Coulomb strength criterion is often used to characterize local failure. According to the Mohr-Coulomb criterion, the shear strength of the soil, τ_f is expressed as

$$\tau_f = c + \tau' \tan\phi \qquad \text{(Eq. 3.1)}$$

where τ' is the effective normal stress on the failure surface, and c and ϕ are the cohesion and angle of internal friction, respectively. When earthquake-induced maximum shear stress exceeds the shear strength of soils, local yielding is expected to occur. Consequently, if the shear strength along a trial sliding surface cannot resist destabilizing seismic forces, sliding failure may occur [14].

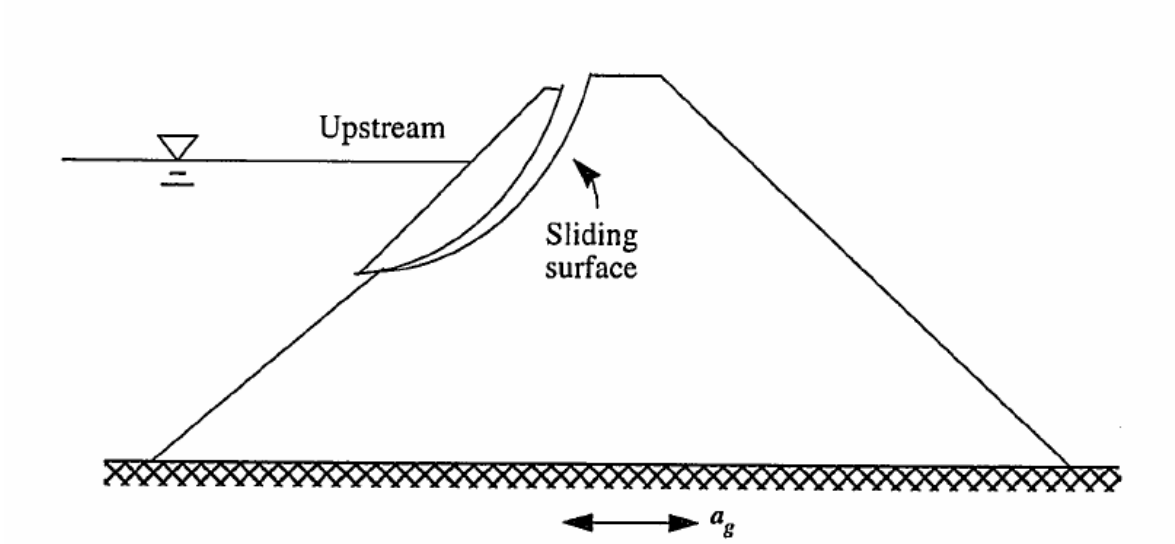

Figure 3 - 1: Sliding Failure of an earth dam [14].

3.2.2. Liquefaction Failure

Under earthquake conditions, due to rapid cyclic straining, gravity loading is transferred from soil solids to the pore-water. This results in an increase of pore-water pressure with a reduction in the capacity of the soil to resist loading. This process by which loss of strength occurs in soil is called liquefaction. The phenomenon of soil liquefaction is primarily associated with medium- to fine-grained saturated cohesionless soils. Sliding of a slope is attributed to the dam losing stability due to variation in stress, and the soil losing resistance due to vibration and the rise of pore-water pressure. Such damage induced by ground motions occur most often at the upstream slope as shown in Figure 3 - 2. If the earth dam is saturated at the upstream side, it may liquefy when subjected to vibration exceeding a certain limit.

The occurrence of liquefaction failure is usually related to the volumetric strain in the soil which is given by

$$\varepsilon_v = \varepsilon_1 + \varepsilon_2 + \varepsilon_3 \qquad \text{(Eq. 3.2)}$$

where ε_1, ε_2 and ε_3 are the principal strains for 3D problems.

Another method to evaluate possible liquefaction is the use of a threshold strain. If the cyclic shear strain in soil as a result of an earthquake does not exceed a certain threshold level, liquefaction should not occur. The peak shear strain caused by an earthquake ground motion can be estimated by

$$\gamma_{\max} = \frac{1.2\, a_{\max} h}{v_s^2} \qquad \text{(Eq. 3.3)}$$

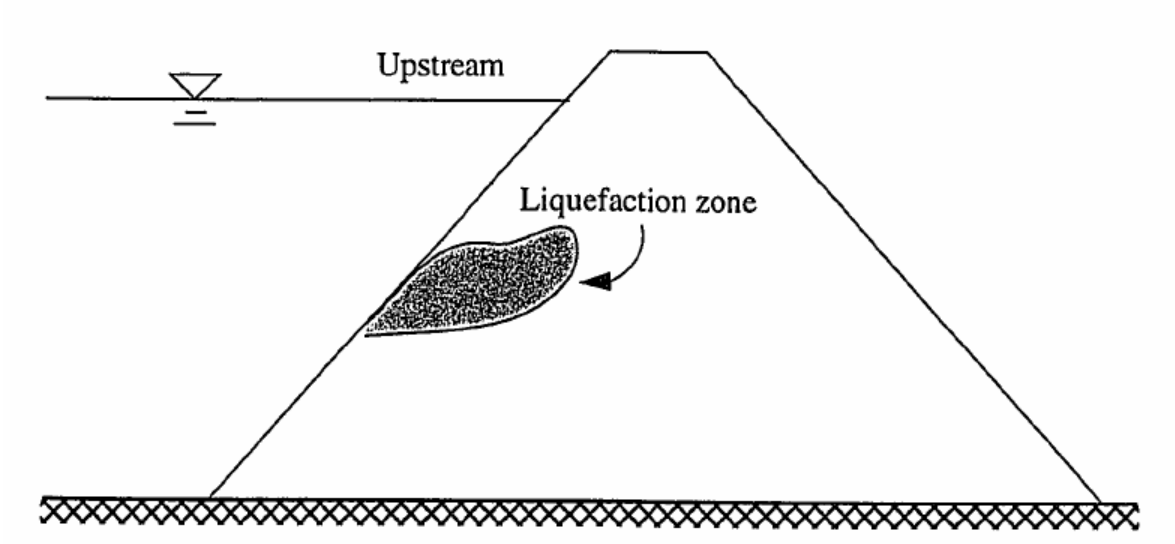

Figure 3 - 2: Liquefaction failure of an earth dam [14].

in which a_{max} is the peak acceleration of earthquake motions, h is the depth from the crest and v_s is the shear wave velocity in the soil [14].

3.2.3. Longitudinal Cracks

Longitudinal cracks take place mostly in the crest area shown in Figure 3 - 3. The formation of wide longitudinal cracks is considered to be due to tensile stresses produced at the surface. Shear sliding deformation may also contribute to such failure. Another cause of longitudinal cracks is the uneven settlement of the core or foundation. Uneven settlement usually occurs when the strength of the foundation is not uniform or when loose river deposits are left unexcavated. It should be noted that longitudinal cracks are sometimes concealed. The internal cracks formed in the Hachi Dam in Niigata, Japan were

discovered when the dam was excavated to repair sluiceways damaged in the Niigata earthquake. Therefore, careful investigation is necessary even when no damage is visible [14].

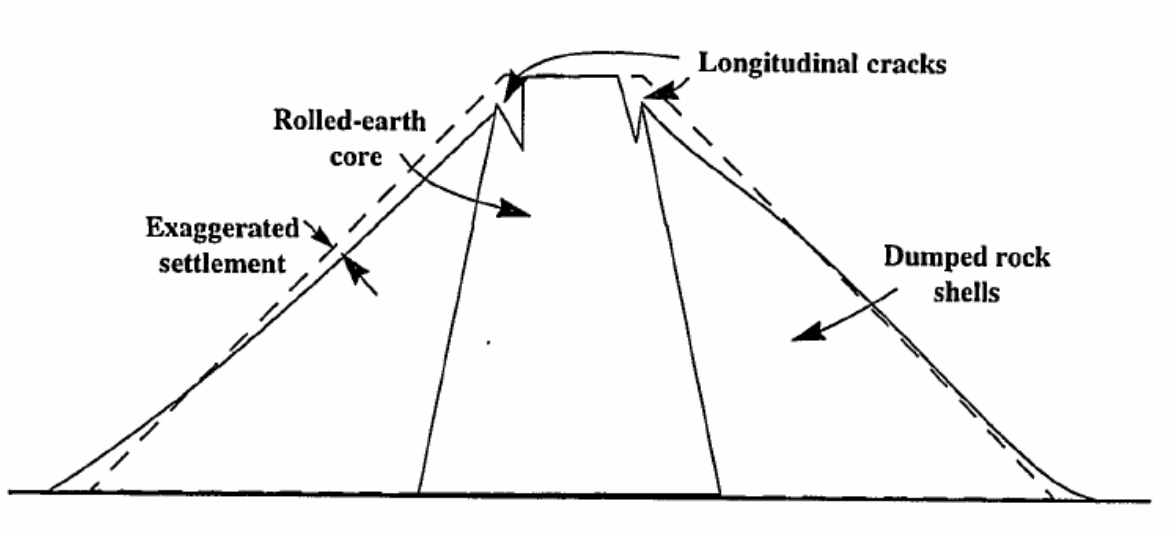

Figure 3 - 3: Failure in terms of longitudinal cracks in an earth dams [14].

3.2.4. Transverse Cracks

Transverse cracks consist of four types:

a) Those formed due to violent vibration in the direction parallel to dam axis
b) Those formed near both ends of an embankment because of the difference in the vibration characteristics of the embankment and the banks
c) Those formed due to nonuniformity of consolidation within the dam when repairs were made on sluiceways
d) Those due to uneven settlement of the foundation.

Typical transverse cracks due to differential settlement are shown in Figure 3 - 4. Generally, transverse cracks are fewer than the number of longitudinal cracks, but these can serve as water channels, causing breaking, so early repair is necessary [14].

3.2.5. Embankment and Foundation Piping

Piping, or progressive erosion of concentrated leaks, has caused a number of catastrophic failures. As water seeps through the compacted soil of an embankment or the natural soil of a foundation, the pressure head is dissipated in overcoming the viscous drag

forces which resist the flow through the small soil pores. Conversely, the seeping water generates erosive forces which tend to pull the soil particles with it in its travel through and under the dam. If the forces resisting erosion are less than those which tend to cause it, the soil particles are washed away and piping occurs. The resisting forces depend on the cohesion and the weight of the soil particles, as well as on the action of the downstream filter [14].

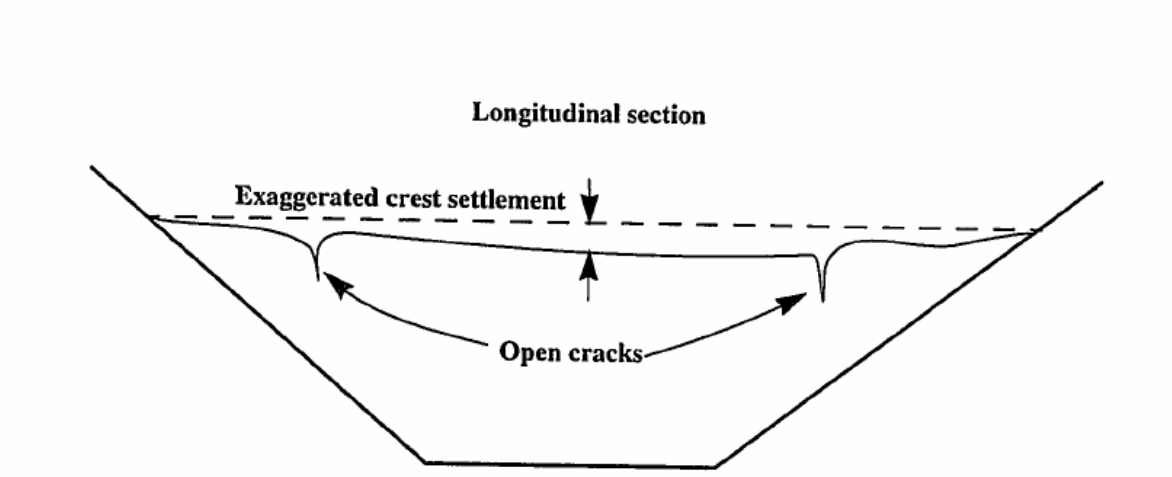

Figure 3 - 4: Transverse cracks due differential settlements in an earth dam [14].

3.3. Previous Earth Dam Seismic Response Studies

In the study called “Shear vibration of vertically inhomogeneous earth dams” by (Gazetas, G., 1982), a closed-form solution to the problem of free vibrations of vertically inhomogeneous earth dams, modeled as truncated-wedge-shaped shear beams, was obtained by implementing an inverse procedure in which the determination of the function describing the inhomogeneity constitutes part of the problem. According to the study, the resulting cube-root variation of the shear-wave velocity with distance from the crest compares very favorably with measurements in two Japanese dams. Method’s results were presented in the form of natural periods, modal shapes and average seismic coefficients for a number of truncation ratios in the study. Also, the study states that, compared with an “equivalent” homogeneous dam, the inhomogeneous experiences sharper amplification of modal displacements and greater average seismic coefficients near the crest and has natural periods which are closer to each other. Gazetas concludes by an observation stating that this behavior is in better agreement with the observed response of a 37 m-high dam during five earthquake motions [15].

(Chugh, A.K., 1985) studied the dynamic response analysis of embankment dams. According to his study, a one-dimensional wave propagation method for earthquake response analysis of horizontally-layered sites of infinite lateral extent is adopted to account for the finite cross-sectional dimensions of an embankment dam overlying a foundation deposit which may be considered infinite in its lateral extent. The procedure adopted in the paper is used to study the response of an existing embankment dam for an actual earthquake record. For this case, a two-dimensional dynamic finite element analysis was also performed. For the site, the records of ground acceleration at an outcropping base rock and at the crest of the dam are available and the comparisons of computed and observed responses support the modified use of the simple numerical procedure [16].

According to the study conducted by (Prevost, J.H. Abdel-Ghaffar, A.M. and Lacy, S.J., 1984) under the title “Nonlinear dynamic analyses of an earth dam”, the following investigations were presented. Firstly, comparison between the results of 2D nonlinear and 3D nonlinear dynamic finite element analyses of an earth dam subject to two very different input ground motions; and secondly, comparison between measured and computed earthquake responses of the dam. Their study was based on rigorous nonlinear hysteretic analyses utilizing a multi-surface plasticity theory. In their study, the backbone shear stress-strain curve was assumed hyperbolic and symmetrical about the origin. In the study, detailed comparisons induced stresses, strains, accelerations, and permanent deformations at various locations in the dam were presented. They also assessed the effects of three-dimensionality on the dynamic response, particularly on resulting permanent deformations. They also evaluated the suitability of 2D analyses in determining the dynamic behavior of such structures [17].

The study called “Elasto-plastic earthquake shear-response of one-dimensional earth dam models” by (Elgamal, A.-W. Abdel-Ghaffar, A.M. and Prevost, J.H., 1985) adopts a simplified analysis procedure for the nonlinear hysteretic earthquake response of earth dams. In their study, the dam was modeled as a one-dimensional hysteretic shear-wedge subjected to base excitation. Dam materials’ hysteretic stress-strain behavior was modeled by using elasto-plastic constitutive equations based on multi-surface kinematic plasticity theory. The method they adopted in their study is based on a Galerkin formulation of the equations of motion in which the solution is expanded using eigenmodes of the linearized problem defined over the spatial domain occupied by the dam. For the nonlinear dynamic response of an earth dam subjected to two very different input ground motions, this

analysis technique is applied. In the paper, the following four investigations are presented. (i) Comparison between the results obtained using two soil models taking different nonlinear properties is given, (ii) comparison between the results of the one-mode and the multi-mode solution expansions are presented, (iii) comparison with the results obtained through an elaborate finite element representation of the dam is given, (iv) comparison with the results obtained through the Makdisi-Seed iterative procedure for earth dam analysis is presented. In the study, the comparisons show that the proposed technique can be used to determine adequately the transient earthquake response of long earth dams. Also, the writers conclude by sating that the efficiency and low computational cost make the technique very attractive and this technique can easily and systematically be extended to two- and three-dimensional calculations of earth dam response [18].

(Gazetas, 1987) discussed the recent developments at the time his paper was published at the paper called “Seismic response of earth dams: some recent developments). At his paper he focused on theoretical methods for estimating the dynamic response of earth dams to earthquake ground excitation. He outlined the historical developments in this field and he introduced basic concepts/models for response analysis. He also elucidated their salient features, advantages and limitations. He identified and studied the major phenomena associated with, and factors influencing, the response. He accorded particular emphasis to inhomogeneity due to dependence of soil stiffness on confining pressure, nonrectangular canyon geometry, and nonlinear-inelastic soil behavior. Several new formulations that have evolved up to his time were outlined. The simplicity of some of these formulations was underlined and attempts were made to compare their predictions with measurements from full-scale, natural and man-made, forced vibration tests. In the study, the basic validity as well as the limitations of the proposed analysis methods was demonstrated and topics of needed further research were suggested [19].

(Lacy, S.J. and Prevost, J.H., 1987) studied the nonlinear seismic response analysis of earth dams. They proposed a general and efficient numerical procedure for analyzing the dynamic response of geotechnical structures, which are considered as both nonlinear and two phase systems. They outlined the appropriate coupled dynamic field equations for the response of a two-phase soil system. They described the finite element spatial discretization of the field equations and discussed the time integration for the resulting nonlinear semi-discrete finite element equations. They examined iterative techniques for the solution of the global nonlinear system of finite element equations. According to the

paper, a large amount of computational effort was expended in the iterative phase of the solution and they needed such an iterative procedure both reliable and efficient. They discussed three iterative procedures: Newton-Raphson, Modified Newton-Raphson and Quasi-Newton methods, including BFGS and Broyden updates. They also presented the elasto-plastic earthquake response analysis of a two phase nonhomogeneous earth dam. They compared the results of the numerical calculations to the recorded response of the dam [20].

(Lin, J. and Chao, B., 1990) studied the estimation of shear moduli and damping factors of earth dam materials in their paper. They state that, Abdel-Ghaffar and Scott developed a procedure for extracting the shear moduli and damping factors of soils based upon strong motion records from earth dams, and, it is a very efficient procedure for earth dams that exhibited predominantly first mode response along the upstream-downstream direction. They state that Abdel-Ghaffar and Scott employed digital band-pass filters on the crest and abutment acceleration records and constructed the hysteresis loops of soils by treating these filtered records as the input-output to a nonlinear SDOF structure. According to them, in their process an important superposition assumption was implicitly introduced. Their study looked into the implications of this linear superposition assumption on presumed nonlinear systems. Specifically, they conducted numerical simulations in finding out whether or not such a procedure is capable of extracting a known input dynamic behavior of soils. They found that the hysteresis loops were generally distorted, and to minimize errors only those loops of larger strain amplitudes should be used. They also suggested simple guidelines in their study. They carried out applications to real records from two dams which follows the proposed guidelines. They also explored the results of such applications [21].

(Zeghal, M. and Abdel-Ghaffar, M., 1992) studied the behavior of earth dam using strong-motion earthquake records. In the study, the seismic records of the Long Valley Earth Dam were utilized in order to shed some light on the salient features of the dam nonlinear behavior. They instrumented the dam with 22 accelerographs tied with a common triggering. The dam was shaken in the 1980’s by a series of earthquakes that varied in intensity and maximum induced accelerations. Their analysis is based on ideas of system-identification techniques. They performed preliminary pattern recognition, based on a spectral analysis; and it shows evidence of three dimensionality and nonlinearity in the dam behavior and of seismic wave propagation at its boundaries. Their investigations

show that, although constitutive hysteretic models provide reasonable approximations, they are insufficient to fully account for all the vibration dissipation mechanisms. The results conclude that the model response in the upstream-downstream direction has a better quality of fitness to the recorded response than do the responses in the longitudinal and vertical directions. Also, their analyses show an insufficiency of the instrumentation at the structures boundaries. Their study showed them seismic records can be utilized to produce a wealth of information not available by other means [22].

(Davis, C.A. and Bardet, J.P., 1996) evaluated the performance of two reservoirs during 1994 Northridge Earthquake. According to their study, the 1994 Northridge Earthquake affected two geotechnical structures of the Van Norman Complex, the Los Angeles Reservoir (LAR) and the Power Plant Tailrace, in different ways. They report that, both the Los Angeles Dam and North Dike of the LAR slightly moved and settled, and sustained small superficial cracks. They reported that, the North Dike underwent a noticeable increase in seepage, without significantly impeding normal reservoir operations. They state that, The Northridge Earthquake uplifted and shifted the foundation of the LAR by 30 cm, and provided them with a unique example of tectonic effects on embankments. Also, they state that, in contrast to the LAR, which performed well, the nearby rolled fill dike of the Power Plant Tailrace slowly failed by piping due to transverse cracks and differential lateral spreading induced by liquefaction. Both of the cases supplied valuable information about the response of embankments subjected to near-source ground motion [23].

(Uddin, N., 1997) discovered a single-step procedure for estimating seismically-induced displacements in earth structures. Up to his time, estimation of the permanent deformations of embankment dams is, in practice, based upon the simplifying assumption that dynamic-acceleration response and wedge sliding are two separate processes (decoupled “elastic” and “rigid-slip” features of the dynamic response). He proposed an alternative hypothesis, namely that these two processes occur simultaneously [24].

(Dakoulas, P. and Abouseeda, H., 1997) studied the response of earth dams to Rayleigh waves using coupled FE-BE method in their paper. They emphasized the importance of the foundation flexibility and the spatial variability of the ground motion. Their study is based on a rigorous hybrid numerical formulation that combines the efficiency and versality of the finite element (FE) method and the ability of the boundary element (BE) method to account for the radiation conditions. They used a two dimensional

formulation in the frequency domain to investigate the response of infinitely long earth and rockfill dams subjected to Rayleigh waves traveling across the dam width. Their study demonstrates the dramatic effect of the flexibility of the foundation rock in reducing the overall response of the dam. Their study also shows that the spatial variability of the vertical component of the ground motion caused by the Rayleigh waves induced additional rocking motion that contributes significantly to increasing the horizontal response, especially in the upper part of the dam body, while reducing the vertical vibration [25].

Same authors (Abouseeda, H. and Dakoulas, P., 1998) studied the nonlinear dynamic earth dam-foundation interaction using a BE-FE method. In their study they presented a general rigorous, coupled Boundary Element-Finite Element (BE-FE) formulation for nonlinear seismic soil-structure interaction in two dimensions. They have applied the BE-FE method to investigate the inelastic response of earth dams to transient SV waves [26].

(Liang, R.Y. Nusier, O.K. and Malkawi, A.H., 1999) outlined a reliability based approach for evaluating the slope stability of embankment dams. According to the study, the determination of variables such as soil strength parameters, pore pressure and other pertinent properties involves uncertainties, which cannot be handled in the traditional deterministic methods. They developed reliability and probability theories in their paper for assessing the reliability index and the corresponding probability of failure of multi-layered embankment dams and slopes [27].

(Chen, M. and Harichandran, R.S., 2001) studied the stochastic response of the Santa Felicia earth dam, in southern California, to spatially varying earthquake ground motion (SVEGM). They used an SVEGM model that accounts for both incoherence and propagation of seismic waves and compared the results with those for various simplified excitations, and investigated the sensitivity of the responses to coherency models proposed by different researchers [28].

(Wu, G. 2001) analyzed the earthquake-induced deformations of the Upper San Fernando Dam under the 1971 San Fernando Earthquake. The writer described a nonlinear effective stress finite element approach for dynamic analysis of soil structure in the paper. His approach include the use of a third parameter in the two-parameter hyperbolic stress-strain model, a modified expression for unloading-reloading modulus in the Martin-Finn-Seed pore-water pressure model, and an additional pore-water pressure model based on cyclic shear stress. Then the writer conducted dynamic analyses to simulate the seismically

induced soil liquefaction and ground deformation of the Upper San Fernando Dam under the 1971 San Fernando Earthquake [29].

(Cascone, E. and Rampello, S., 2003) investigated the decoupled seismic analysis of an earth dam. They evaluated the seismic stability of an earth dam via the decoupled displacement analysis using the accelerograms obtained by ground response analysis to compute the earthquake-induced displacements. They carried out the response analysis of the dam under both 1D and 2D conditions, incorporating the nonlinear soil behavior through the equivalent linear method [30].

(Zerfa, F.Z. and Loret, B. 2003) conducted coupled dynamic elastic-plastic analysis of earth structures. They developed a fully coupled finite element code based on mixture theory. They tailored Prevost's multi-surface constitutive model to three dimensional loads and used them to predict effective stresses. Also, they implemented a new viscous boundary to avoid wave reflections towards the structure [31].

(Ming, H.Y. and Li, X.S., 2003) conducted a fully coupled analysis of failure and considered remediation of Lower San Fernando Dam. They determined the extent of flow deformation in an embankment dam by the driving forces and the residual strength of the soil, as well as by the kinematic constraints. They presents a set of fully coupled finite element analyses of the responses of the well-known lower San Fernando Dam during the 1971 earthquake in their paper. To describe soil behavior over the full range of loading conditions encountered, a critical state model incorporating the concept of state-dependent dilatancy was employed [32].

(Gudehus, G. Cudmani, R.O. Libreros-Bertini, A.B. and Buhler, M.M., 2004) studied the in-plane and anti-plane strong shaking of soil systems and structures. They introduced the concept of in-plane and anti-plane shaking with a rigid block on a plane surface with Coulomb friction [33].

(Khoei, A.R. Azami, A.R. and Haeri, S.M., 2004) studied the implementation of plasticity based models in dynamic analysis of earth and rockfill dams with a comparison of Pastor-Zienkiewicz and cap models. In the paper, a unified finite element formulation associated with saturated and unsaturated soils is presented. The writers applied the finite element method to the governing equations for the spatial discretization, followed by a generalized Newmark scheme used for the time domain discretization. They used time stepping scheme in the fully implicit coupled method and a direct solution procedure is used for the coupled equation system. The framework of generalized plasticity was

presented and numerical results of three saturated-unsaturated earth and rockfill dams were demonstrated. They also performed a comparison between the Pastor-Zienkiewicz and cap plasticity models through the dynamic analysis of the failure of lower San Fernando dam under the 1971 earthquake and the Mahabad and Doroodzan dams under the 1978 Tabas earthquake [34].

(Adalier, K. and Sharp, M.K., 2004) studied the dynamic behavior and densification remediation of an embankment dam on liquefiable foundation. They studied seismic behavior of a zoned embankment dam with saturated sandy soil foundation through a series of four highly instrumented geotechnical centrifuge model tests under moderate earthquake conditions. They investigated the beneficial effects of foundation densification [35].

(Papalou, A. and Bielak, J, 2004) studied the nonlinear seismic response of earth dams with canyon interaction. Their paper examines the nonlinear earthquake response of earth dams, using a model that considers the deformability of the surrounding medium and effects of spatial variation of the seismic excitation. They developed a finite element based method in which the dam is idealized as a shear beam and the surrounding medium as a halfspace. The nonlinearity of the dam is considered using multiyield surface plasticity theory [36].

4. STRONG GROUND MOTION ESTIMATION

4.1. Introduction

In this section, earthquake hazard in Marmara Region (Turkey) where Alibey Dam is located is outlined. Also, for synthesizing earthquake ground motions Wes Rascal code is summarized and the generated ground motion according to the earthquake hazard in Marmara Region is explained.

4.2. Tectonic Settings of the Marmara Region

The tectonic regime in the Marmara Region is controlled by western portion of the North Anatolian Fault zone (NAFZ). The NAFZ begins to loose its single fault line character and splays into a complex fault system at west of 31.5°E toward the Marmara Sea region (Mudurnu/Akyazi). Several researchers have developed different tectonic models for Marmara Sea based on low-resolution bathymetric data and earthquake occurrences (Figure 4 - 1). In Figure 4 - 2, the active tectonic map of the region prepared by the General Directorate of Mineral Research and Exploration (MTA) Turkey is given. Some researchers developed a fault model based on the data collected in 1997 by the ship "MTA Sismik-1". According to the data obtained during the recent high-resolution bathymetric survey of the Ifremer RV Le Suroit vessel, it is observed that, a single, thoroughgoing strike-slip fault system (Main Marmara Fault) cuts the Marmara Sea from east to west joining the 17.8.1999 Kocaeli earthquake fault with the 9.8.1912 Sarkoy-Murefte earthquake fault (Figure 4 - 3).

From previous researches and the available data, researchers defined the tectonic evolution of the Marmara Sea region as the superposition of two different aged fault systems as illustrated in Figure 4 - 4. They are the early Miocene-early Pliocene Thrace – Eskisehir Fault Zone and its branches and the late Pliocene-recent NAF and its branches. The northwest-southeast trending Thrace-Eskisehir fault is a major dextral strike-slip system, which was active during the early Miocene-early Pliocene.

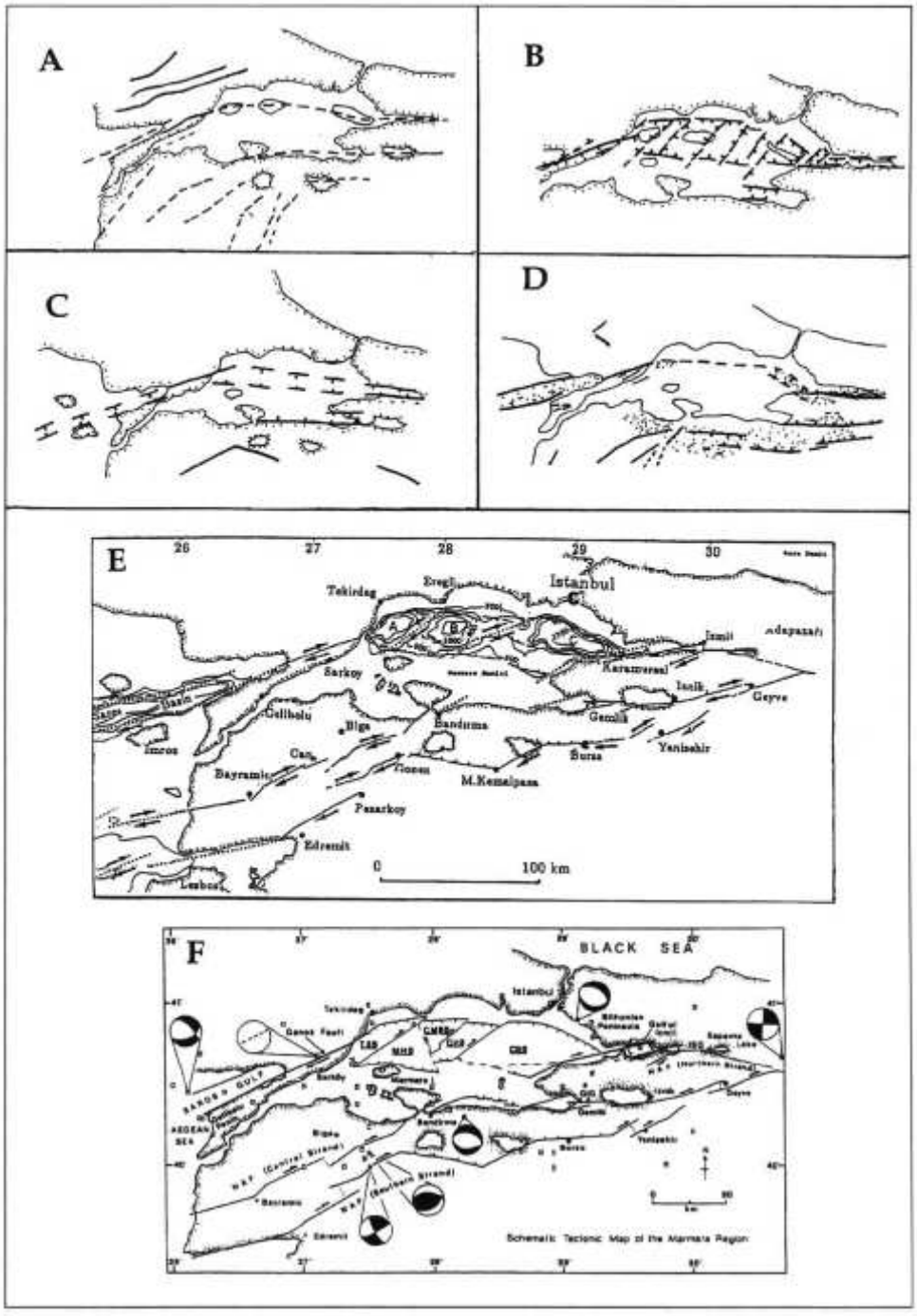

Figure 4 - 1: Comparison of the structural models suggested for the Marmara Region [37].

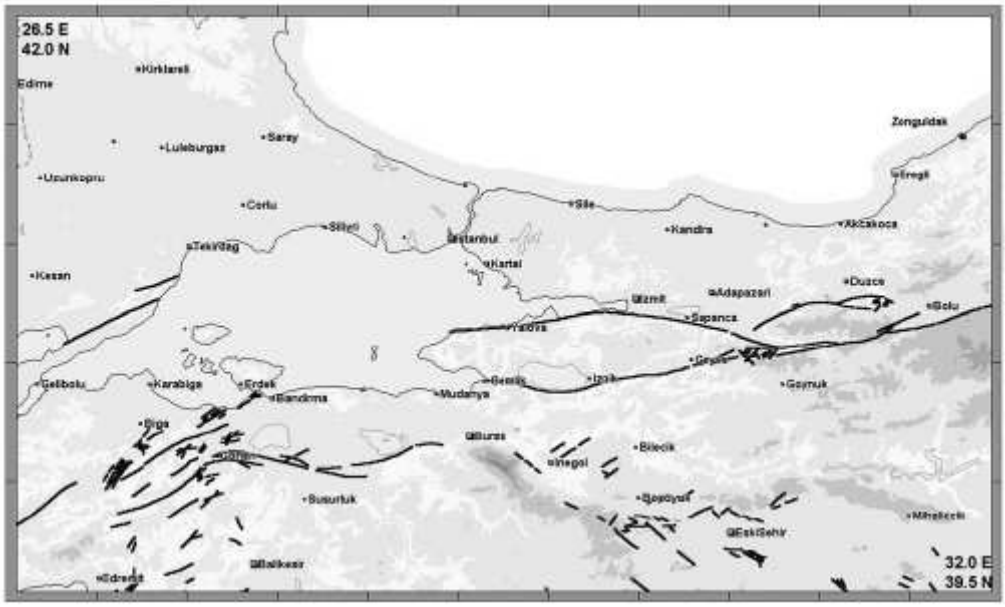

Figure 4 - 2: Active fault map of Marmara Region prepared by General Directorate of Mineral Research and Exploration (MTA) [37].

At the end of the late-Pliocene, it has been divided into four parts by the NAF. The initiation of the late tectonic period is marked by this event. The NAF extended westward as a number of splays by joining the Ganos, Bandirma-Behramkale and Manyas-Edremit Fault Zones during that period. The connection of the northern branch of the NAF to the Ganos Fault Zone in the west resulted the development of a single buried fault in the Marmara Sea and the formation of the troughs and ridges, superimposed onto the negative flower structure formed by the Ganos fault in the early neotectonic period.

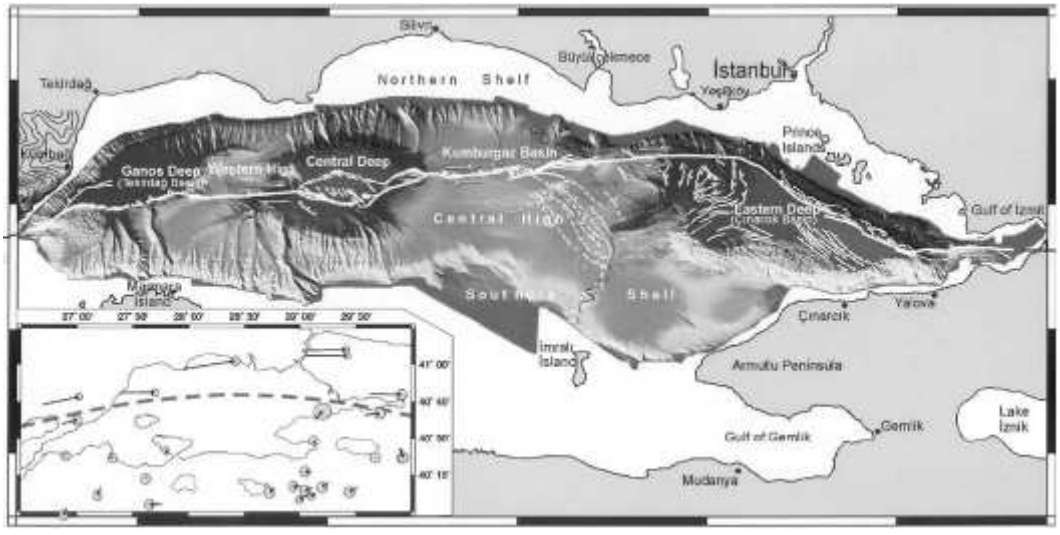

Figure 4 - 3: The recent high-resolution bathymetric map obtained from the survey of the Ifremer RV Le Suroit vessel. A single, thoroughgoing strike-slip fault system can be observed [37].

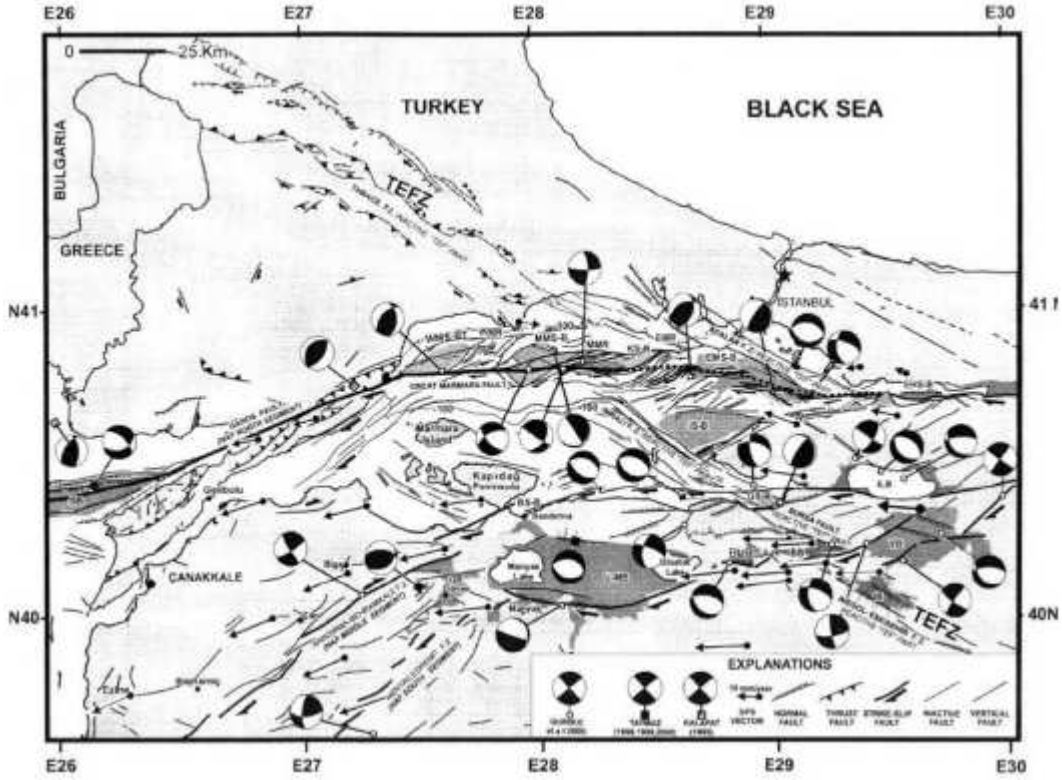

Figure 4 - 4: Tectonic map of Marmara region combined from various studies [37].

The middle strand extends East-West from Iznik Lake to Bandirma and joins to the N60°E-trending Bandirma-Behramkale zone and turns southward near Bandirma. The southern branch of the NAF joins to the Manyas-Edremit Fault zone, forming three pull-apart basins along Yenisehir, Bursa and Manyas segments. The branches of the NAF divide the Thrace-Eskisehir fault at three places: the East Marmara Sea region, in Gemlik Bay and to East of Bursa. The lateral offsets at those locations which amount to 58-59, 7-8 and 10-11 km respectively give an insight about the relative displacements and slip rates along each of the three branches of the NAF in the Marmara Sea region.

Based on latest data, a fault segmentation model for the Marmara Sea region is developed by researchers shown in Figure 4 - 5. The model is based on the tectonic model of the Marmara Sea, defining the Main Marmara fault, a thoroughgoing dextral strike-slip fault system, as the most significant tectonic element in the region. From east to west the Main Marmara fault cuts through Cınarcik, Cental and Tekirdag basins that are connected by higher lying elements. The fault follows the northern margin of the basin when going through the Cınarcik trough in the northwesterly sense, makes a sharp bend towards west to the south of Yesilkoy , entering central highs, cuts through the Central basin and alternates in this manner until it reaches the Murefte-Sarkoy rupture of 1912.

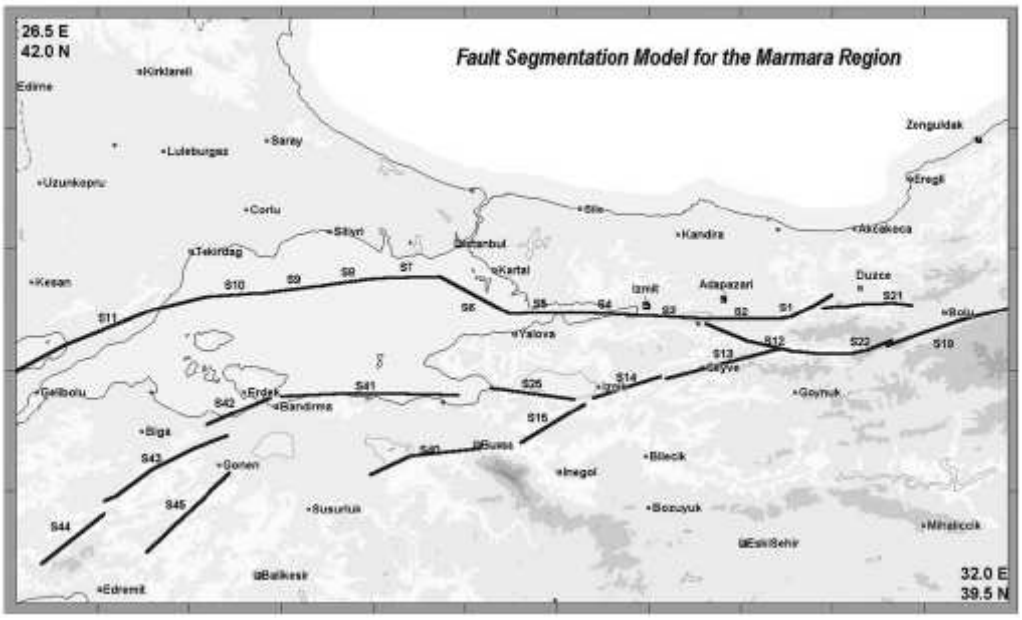

Figure 4 - 5: Fault segmentation model proposed for the Marmara region by [37].

In the model, all these features are interpreted as different fault segments [37].

4.3. Seismicity

Marmara region has been the crossroads between east and west for more than two millennia. As a continuously populated region and having as its center Istanbul, the capital of both Byzantine and Ottoman empires, the historical seismicity record is continuous and relatively complete. The long term seismicity of the Marmara region is illustrated in Figure 4 - 6. Two millennia spanning earthquake records indicate that, on average, at least one medium intensity (I_o = VII – VIII) earthquake has affected Istanbul in every 50 years. For high intensity (I_o = VIII-IX) events the average return period has been 300 years. Also

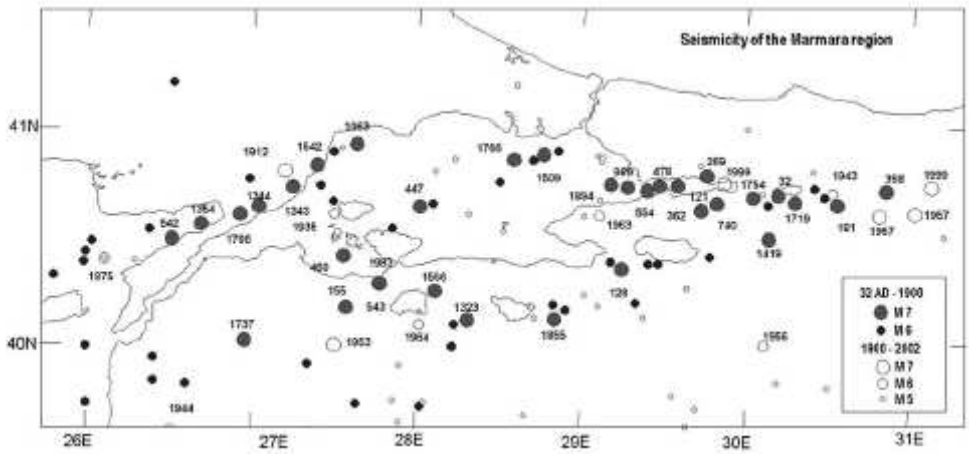

Figure 4 - 6: The long term seismicity of Marmara region (between 32 AD – 1983) [37].

there has not been any earthquake that ruptured the entire length of the Main Marmara Fault from Gulf of Izmit to Gulf of Saros; the seismicity accounts for all of the expected 2.2 cm/year slip and there is a time dependence of seismic activity that should be accounted in earthquake hazard assessments. Figure 4 - 7 illustrates the sequence of occurred earthquakes in the 18th century. It has been claimed that the August 17, 1999 earthquake may be associated with the 1719 earthquake of this sequence. Recent studies conducted after the 1999 Kocaeli (Mw = 7.4) and Duzce (Mw = 7.2) earthquakes indicate (with the assumption that the stress regime in the Marmara Sea remains unchanged) about 65 per cent probability for the occurrence of an Mw ≥ 7.0 magnitude earthquake affecting Istanbul as indicated in Figure 4 - 8. The earthquake damage experienced by regional cities and historical structures in Istanbul has been relatively well documented. It is known that the 1470 years old Hagia Sophia Museum was strongly and repeatedly affected by the

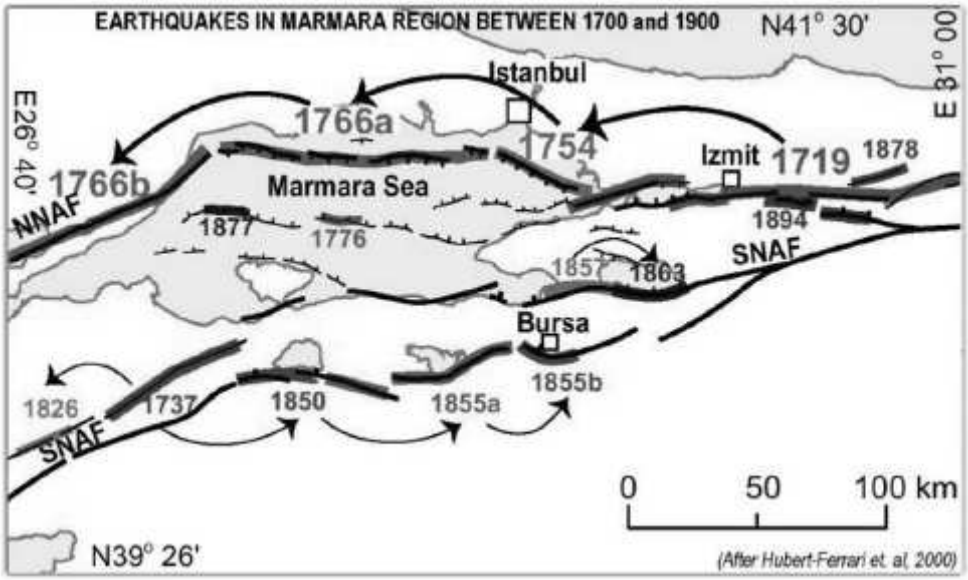

Figure 4 - 7: The sequence of earthquakes in the 18th century [37].

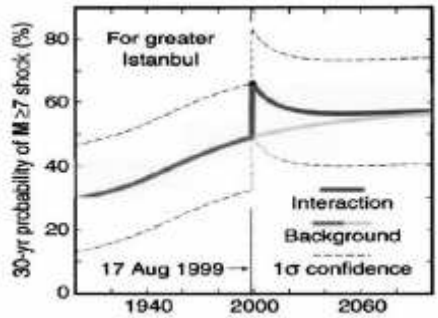

Figure 4 - 8: Probability for the occurrence of a Mw ≥ 7.0 earthquake affecting Istanbul for the next 30 years [37].

earthquakes that took place in the region and was subsequently repaired after every damaging earthquake. Compared to seismic activity in the Marmara region during the past two millennia, th 20^{th} century has been relatively active with five earthquakes of Ms ≥ 7.0 (August 9, 1912 Ms = 7.3; March 18, 1953 Ms = 7.1;May 26, 1957 Ms = 7.2; July 22, 1967 Ms = 7.2 and August 17, 1999 Ms = 7.4). The association of earthquakes between 1950 to present with the segmentation proposed for the North Anatolian Fault in the Marmara Region is given in Table 4 - 1.

Table 4 - 1: Association of earthquakes between 1500 to present with the segmentation proposed for the North Anatolian fault in the Marmara region [37].

Earthquake	Fault segment
9.10.1509 (Ms = 7.2)	7,8
5.10.1556 (Ms = 7.2)	9
5.25.1719 (Ms = 7.4)	2,3,4,5
3.6.1737 (Ms = 7.2)	43
9.2.1754 (Ms = 6.8)	6
5.22.1766 (Ms = 7.1)	7,8
8.5.1766 (Ms = 7.4)	11
2.28.1855 (Ms = 7.1)	40
7.10.1894 (Ms = 7.3)	3,4,5
8.9.1912 (Ms = 7.3)	11
2.1.1944 (Ms = 7.3)	19
3.18.1953 (Ms = 7.2)	45
5.26.1957 (Ms = 7.0)	22
7.22.1967 (Ms = 6.8)	12
8.17.1999 (Mw = 7.4)	1,2,3,4
11.12.1999 (Mw = 7.2)	21

There exist some potential seismic gaps in the Marmara region. As an example, along the middle strand from the Mudurnu Valley region to the Aegean Sea there have not been any significant earthquakes for the last 400 years, except the 1737 earthquake in the Biga peninsula. The most western portion of the southern strand has not ruptured since 1855 to present. Maps of recent seismicity indicate a potential seismic gap in the central part of the

Marmara Sea. The rupture associated with the Kocaeli earthquake is the only remaining gap across the Marmara Sea to the south of Istanbul. This gaps location corresponds to the location of 1766 earthquake and it is well defined. This implies an increased probability for a strong earthquake similar to the 1766 event.

In Table 4 - 1, the May 5, 1719 Ms = 7.4 event has been associated with segments 2-5 of the model. Recent paleoseismological studies show that the surface rupture of this event of this event extended towards Duzce, thus having a similar geometry with the August 17, 1999 event.

A microseismic experiment conducted at 1995 in the Marmara region has revealed a lineament in coincidence with the location of the main Marmara fault. The alignment of the Marmara Fault is also clearly apparent in Figure 4 - 9 and Figure 4 - 10, where respectively the epicentral distribution of earthquakes with M $\geq$ 3 from 1.1.1990 to 8.16.1999 (prior to Kocaeli earthquake) and 8.17.1999 to present are illustrated. There exists a seismic gap associated with segments S6, S7 and S8 that matches up to ruptures associated with 1754 and 1766 earthquakes. The existence of these seismic gaps was also confirmed by the results of a microseismic experiment carried out in the Marmara region. Finally in Figure 4 - 11, epicenters of all events with M $\geq$ 1 are given for the last 10 years. Most of the small events on the Thrace peninsula seen in Figure 4 - 11 to the north of the main Marmara fault are related with rock blasts. Clusters of seismic activity in Yalova and Gulf of Izmir are mostly the aftershocks of 1999 earthquake. The activity in the Marmara

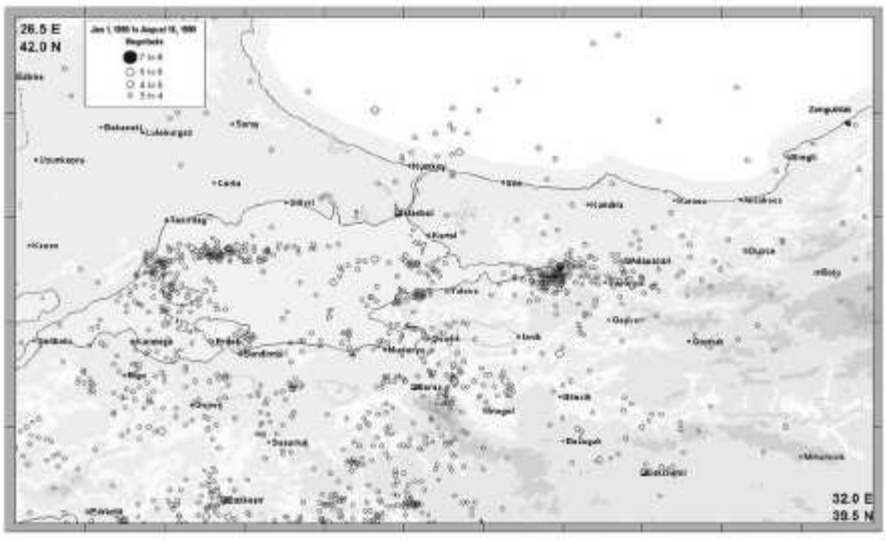

Figure 4 - 9: The seismic activity of the Marmara Sea region with M>3 events from Jan 1, 1990 to August 16, 1999 [37].

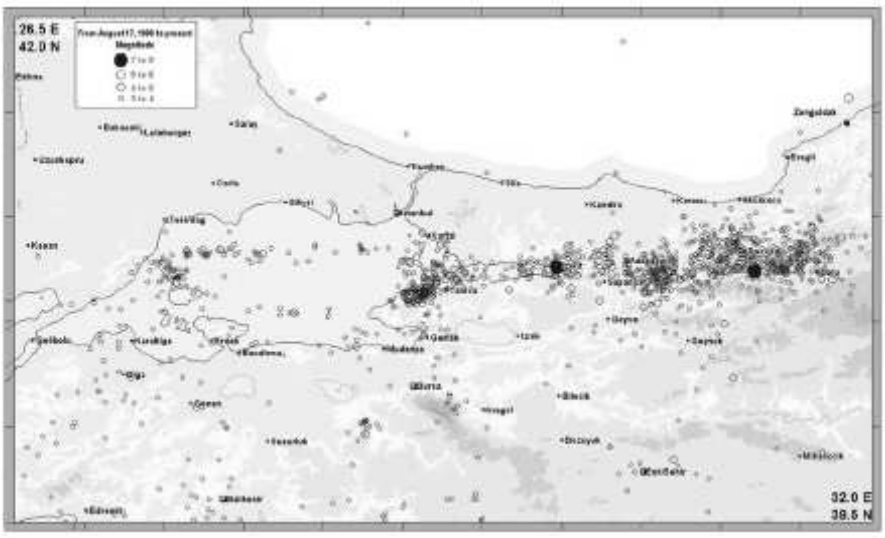

Figure 4 - 10: The seismic activity of the Marmara region with M > 3 events from August 17, 1999 to present [37].

Sea ends to the west of Gazikoy in the Gelibolu Peninsula developing a seismic gap at the location of the 1912 earthquake. Some cluster of seismic activity exists to the south of the Iznik Lake on the mid branch of the North Anatolian Fault. The southern branch of the North Anatolian Fault shows a rather diffuse activity in the region of Bursa.

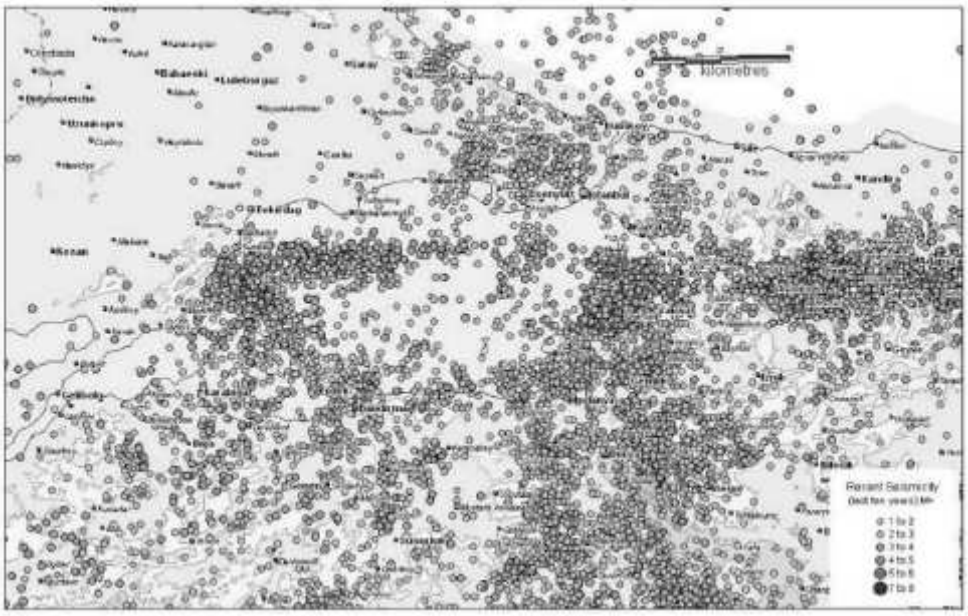

Figure 4 - 11: The seismic activity of the Marmara region with M > 1 events for the last ten years [37].

An earthquake of magnitude Mw 7.4 occurred on the NAFZ with a macroseismic epicenter in the vicinity of the town of Golcuk in the western part of Turkey. Figure 4 - 1 shows the ruptured fault segments and the fault slip distribution model associated with this earthquake. The total observable length of the rupture was about 100 km's. The lateral offset varied between 1.5 and 5 meters at the rupture. Most of the aftershock activity is restrained to the region bounded by 40.5-40.8N and 29.8-30.0E, which covers the area between Izmit and Adapazari to the east of the epicenter.

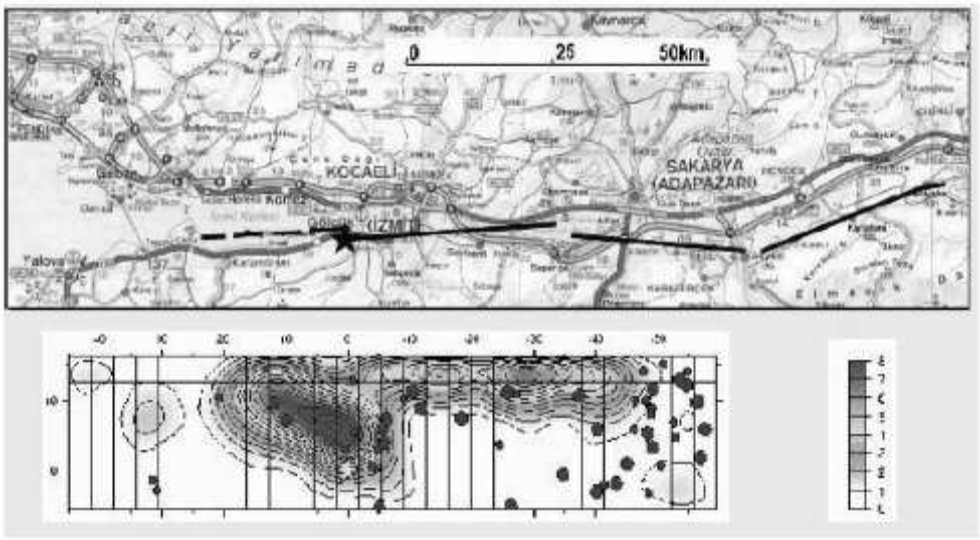

Figure 4 - 12: Surface fault ruptures and slip model of the August 17, 1999 Kocaeli earthquake [37].

Seismic imaging of the Kocaeli earthquake rupture shows almost pure lateral strike-slip rupture that runs west at a velocity of about 3 km/s and towards east at a very high velocity of 4.7 km/s for a distance of about 40 km before dropping to about 3.1 km/s at the easternmost segment. The largest slip (7 m) occurs between 25 to 45 km east of the epicenter. West of the epicenter the slip is large among distances of 10-30 km. The rise time is usually between 2-4 s.

The damage caused by the earthquake covered a very large region ranging from Tekirdag to Eskisehir, cities mostly affected being Sakarya, Yalova, Kocaeli, Bolu and Istanbul. The intensively damaged area tracks a zone of about 20 km in width (10 km to the north and south of the fault) along the fault rupture. The number of condemned buildings after the earthquake totaled 23,400. There were 18,373 reported deaths and 48,901 hospitalized injuries. As much as 120,000 families were left in need of houses after the earthquake. The maximum MSK intensity of the Kocaeli earthquake was X, essentially determined on the basis of fault rupture and excessive ground deformations.

This earthquake is related with fault segments 1, 2, 3 and 4.

4.4. Earthquake Hazard

There are generally two well known methods for the quantification of earthquake hazard. One of them is the probabilistic seismic hazard analysis, which considers all possible earthquake scenarios that could affect the site and results in hazard represented by ground motion parameters at reference ground conditions, such as peak ground acceleration and spectral accelerations. The other is the deterministic earthquake hazard assessment. Probabilistic hazard assessment is usually conducted prior to the deterministic one since, for the deterministic assessment the composite probabilistic hazard is de-aggregated to find the earthquake scenarios (magnitude, distance and the factored standard deviation) at a particular site that would contribute most to the particular hazard. This scenario comprises the basis of the deterministic hazard assessment approach, which also provides the ground motion parameters or simulated strong ground motion time histories.

The deterministic earthquake hazard assessment methodology involves: the determination of the scenario earthquake, identification of appropriate attenuation relationships and proper site response quantification. The deterministic hazard is assessed using both intensity and PGA based attenuation relationships. For both cases median (50 percentile) values obtained from the attenuation relationships were implemented. Based on available geological and seismological information an Mw = 7.5 (similar to 1999 Kocaeli earthquake in magnitude and in total rupture length) related with the unruptured segments of the Main Marmara Fault was preferred as the “Credible Worst Case” scenario event, which is assumed to take place on segments 5, 6, 7 and 8 at Figure 4 - 13. The resulting MSK intensity and PGA distributions are shown in Figure 4 - 14 and Figure 4 - 15. The MSK intensity assessments are actually site-dependent. Nevertheless, they need to be modified for rock and soft soil conditions. The PGA distribution is given for reference ground conditions, specified by NEHRP B/C boundary site-class [37].

4.5. Simulation of Strong Ground Motion

Simulation of strong ground motion is performed with the computer program Wes Rascal. For the simulations, the deterministic PGA values were used. Detailed description about the Wes Rascal code can be found at [38].

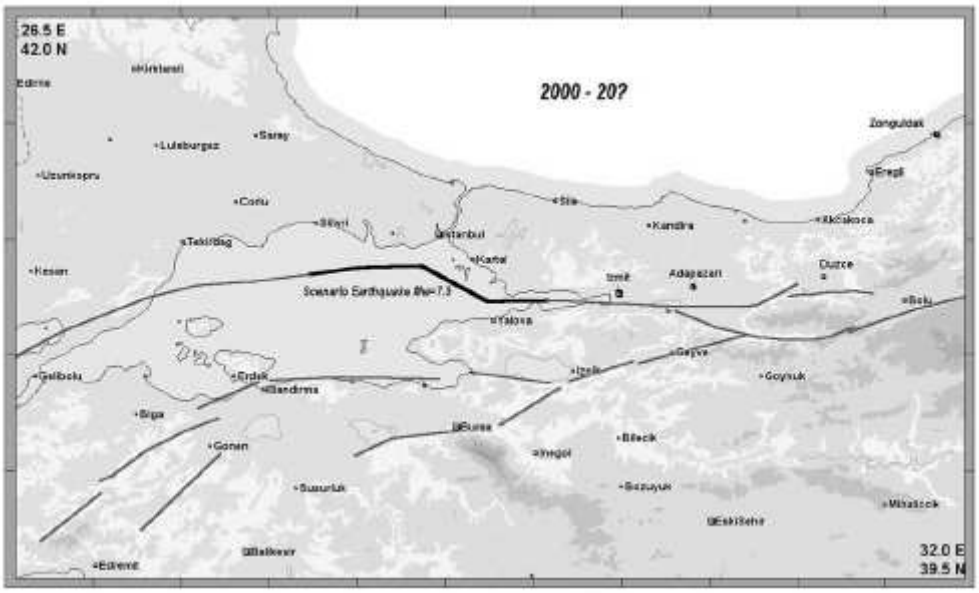

Figure 4 - 13: Mw = 7.5 scenario earthquake for the Marmara Sea region [37].

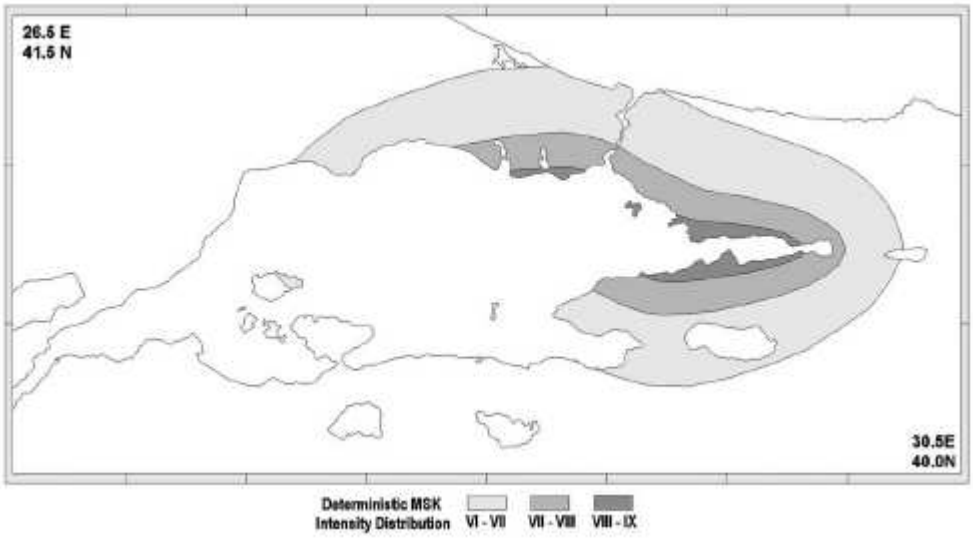

Figure 4 - 14: Intensity distribution plot resulting from the scenario earthquake [37].

The generated strong ground motion is plotted at Figure 4 - 16. The acceleration response spectrum of the motion is plotted at Figure 4 - 17. This is the main input ground motion used in the dynamic time history analyses of the dam.

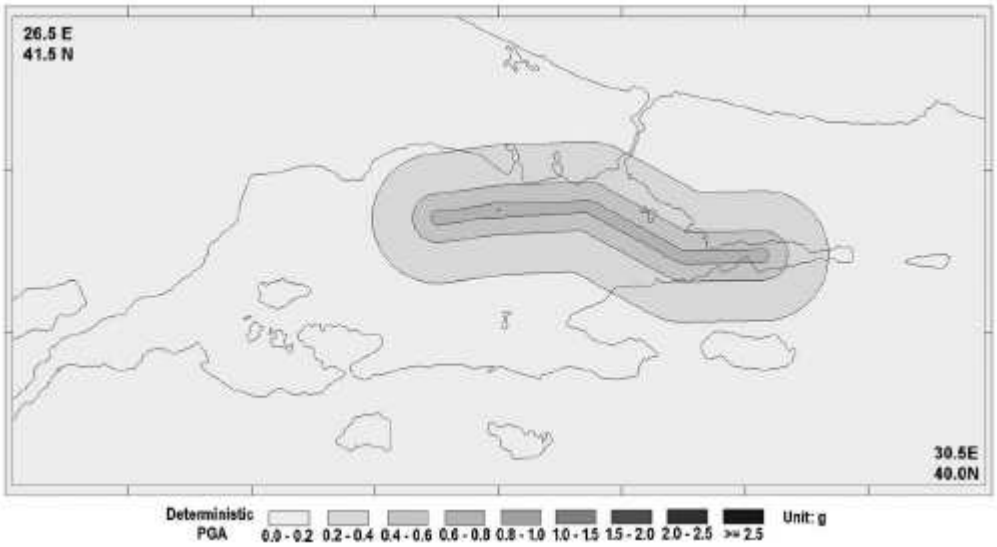

Figure 4 - 15: PGA distribution plot resulting from the scenario earthquake [37].

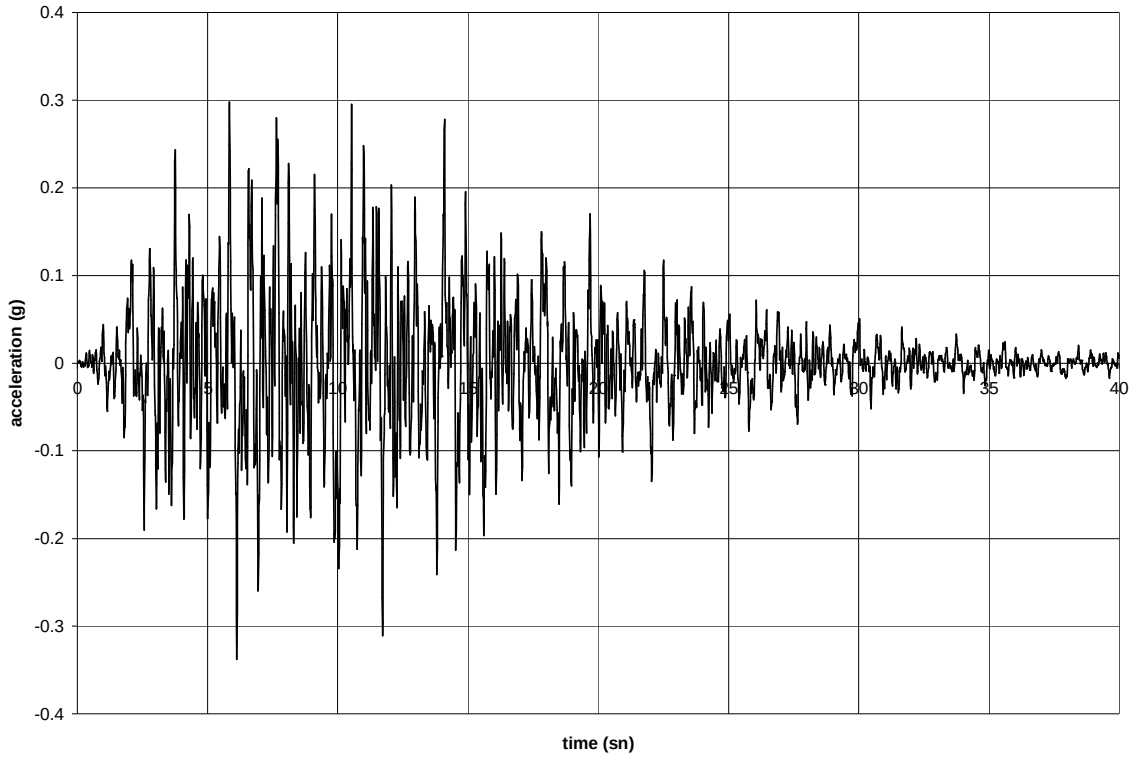

Figure 4 - 16: Acceleration time history plot.

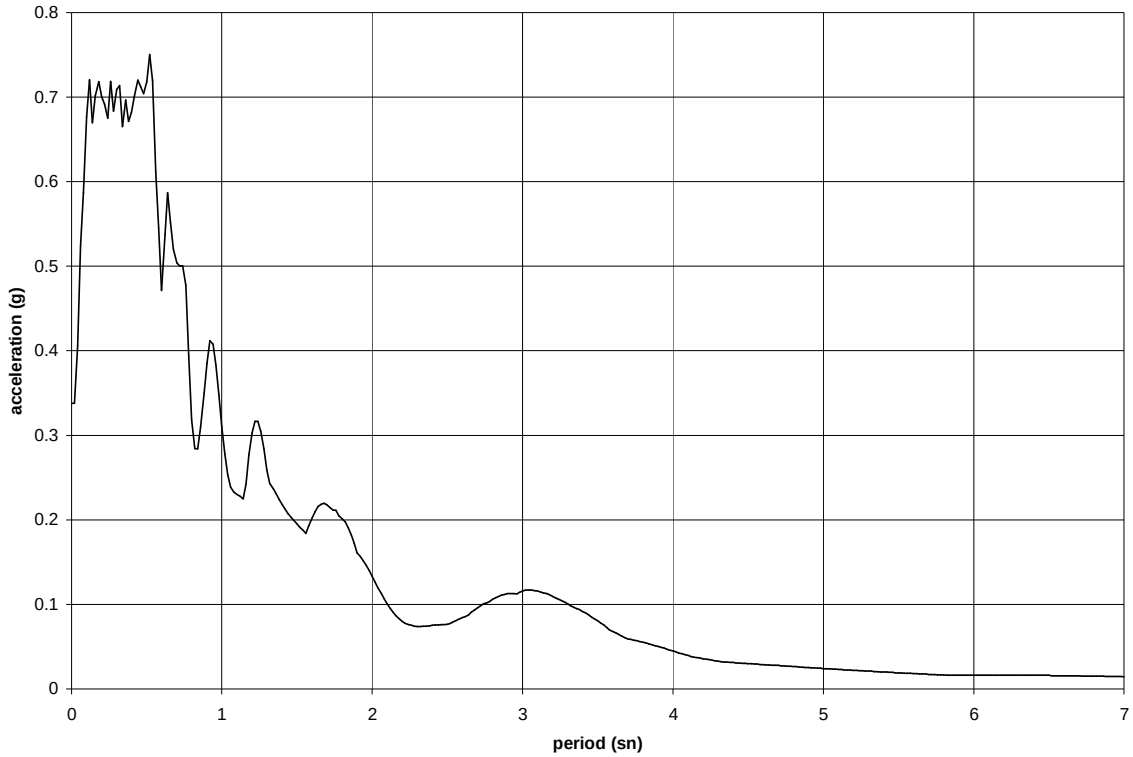

Figure 4 - 17: Acceleration response spectrum.

5. FINITE ELEMENT FORMULATIONS

5.1. Introduction

In this section, governing equations of finite element analyses are summarized.

5.2. Finite Element Formulation

Liquefaction and cyclic mobility are phenomena associated with interaction between the solid and fluid phases. Biot (1957) was the first scientist who developed a general dynamics theory for saturated porous media. Depending on the assumptions, this theory can lead to many different simplified formulations. One versatile and efficient version of them, known as the u-p formulation (in which, the displacements of solid phase, u, and pore fluid pressure, p, are the primary variables), is adopted in the finite element framework OpenSees.

Detailed description of the u-p formulation can be found in (Ragheb, A.M., 1994) [38]. Assumptions made in the u-p formulations are:

- Soil is fully saturated
- Fluid density is constant with respect to space
- Porosity is constant with respect to time
- Solid grains are incompressible
- Fluid is compressible
- Fluid velocity gradient is small and all convective terms are negligible
- Fluid acceleration relative to the solid phase is negligible (excitation at low frequency range, which is sufficient for earthquake engineering applications)
- Soil is considered a continuum (excitation wavelength is large compared to soil pores and grains)
- Small strain and negligible rotation
- Initial strains are not present
- Isothermal process

Following symbols are used in the formulations:

u_i = Displacement of the solid phase

p = Pore fluid pressure

w_i = Displacement of the fluid relative to the solid phase

ρ = Mass Density of the mixture

b_i = Acceleration of body force

Q = Bulk modulus of the (undrained) mixture

R_i = Viscous drag force exerted on the fluid by the solid

k_{ji} = Permeability tensor = $\frac{\tilde{k}_{ji}}{\rho_f g}$ ($\tilde{k}_{ji}$ is D'Arcy's permeability tensor) (Eq. 5.1)

The strain tensor is defined as:

$$d\varepsilon_{ij} = \frac{1}{2}(du_{i,j} + du_{j,i}) \quad \text{(Eq. 5.2)}$$

Effective stress tensor is defined as:

$$\sigma'_{ij} = \sigma_{ij} + \delta_{ij} p \quad \text{(Eq. 5.3)}$$

Equation of motion for the fluid-solid mixture is:

$$\left(\sigma'_{ij} - \delta_{ij} p\right)_j - \rho(\ddot{u}_i - b_i) = 0 \quad \text{(Eq. 5.4)}$$

Equation of motion for the fluid phase is:

$$p_{,i} + R_i + \rho_f (\ddot{u}_i - b_i) = 0 \quad \text{(Eq. 5.5)}$$

Mass conservation of the mixture is:

$$\frac{\dot{p}}{Q} + \dot{\varepsilon}_{ii} + \dot{w}_{i,i} = 0 \quad \text{(Eq. 5.6)}$$

D'Arcy's law is as:

$$k_{ji} R_i = \dot{w}_j \quad \text{(Eq. 5.7)}$$

Combing above equations yields:

$$\frac{\dot{p}}{Q} + \dot{\varepsilon}_{ii} - \left(k_{ji}\left(p_{,i} + \rho_f \ddot{u}_i - \rho_f b_i\right)\right)_{,j} = 0 \quad \text{(Eq. 5.8)}$$

The equations constitute the strong form of the simplified u-p formulation. The associated boundary conditions are as:

- For the solid phase, u, $\dot{u}$ and $\ddot{u}$ can be prescribed on some parts of the boundary and total traction t_i is prescribed on the remainder.
- For the fluid phase, p or $\dot{p}$ is prescribed on some part(s) of the boundary and the rate of inflow (or flux) $\dot{w}$ is prescribed on the remainder.

Boundary traction and boundary flux are natural boundary conditions.

In the context of finite element formulation, the above equations, after spatial discretization and Galerkin approximation, transform into:

$$\mathbf{M}\ddot{\mathbf{u}} + \int_{\Omega} \mathbf{B}^{\mathbf{T}} \boldsymbol{\sigma}' d\Omega - \mathbf{Q}\mathbf{p} - \mathbf{f}^{\mathbf{m}} = 0 \qquad \text{(Eq. 5.9)}$$

$$\mathbf{Q}^{\mathbf{T}}\dot{\mathbf{u}} + \mathbf{H}\mathbf{p} + \mathbf{S}\dot{\mathbf{p}} + \mathbf{G}\ddot{\mathbf{u}} - \mathbf{f}^{\mathbf{p}} = 0 \qquad \text{(Eq. 5.10)}$$

M is the mass matrix, **B** is the strain-displacement matrix, $\boldsymbol{\sigma}'$ is the effective stress vector (defined by the soil constitutive model), $\boldsymbol{\Omega}$ is the entire finite element domain, **Q** is the discrete gradient operator coupling the solid and fluid phases, **u** is the displacement vector, **p** is the pore pressure vector, **G** is the dynamic seepage force matrix, **H** is the permeability matrix, **S** is the compressibility matrix, and $\mathbf{f}^{\mathbf{m}}$ and $\mathbf{f}^{\mathbf{p}}$ are force vectors accounting for prescribed boundary conditions and body force effect for the mixture and the fluid phase respectively in these formulations. Viscous damping is incorporated into the solid phase in the form of Rayleigh damping ($\mathbf{C} = \alpha\mathbf{M} + \beta\mathbf{K}$), where **K** is the initial stiffness matrix. In case of earthquake loading, $\mathbf{G}\ddot{\mathbf{u}}$ can be neglected to attain the symmetry of the global matrix. Also, **M**, **H**, **Q**, **S** and **B** matrices are constant and these matrices are assembled only once at the beginning of a computer run.

The above equations are integrated in time using a single step predictor and multi-corrector Newmark scheme. Newton-Raphson method is used to solve the set of simultaneous equations with the stiffness operator updated to achieve or expedite a convergence [40].

5.3. Constitutive Model Including Cyclic Mobility

During a shear loading process near liquefaction (low confinement levels), a saturated undrained cohesionless soil generally exhibits the following pattern of behavior.

- The soil skeleton experiences a tendency for contraction at low shear strains (phase 0-1 in Figure 5 - 1), leading to development of excess pore-pressure and reduction in effective confinement.
- Significant shear strain may develop without appreciable change in shear stress (essentially, the perfectly plastic phase 1-2 in Figure 5 - 1) as the shear stress approaches the failure envelope (or more precisely the so called Phase Transformation envelope). Numerical versatility is achieved by defining this highly yielded segment of stress-strain response as a distinct phase (γ_y in Figure 5 - 1, where $\gamma = \sqrt{2/3\mathbf{e}:\mathbf{e}}$ refers to octahedral shear

strain, and **e** = deviatoric strain tensor). This feature allows for direct control over the extent of shear strain accumulation in the model.

- Then (above the PT envelope), a dilative tendency (phase 2-3 in Figure 5 - 1) increases effective confinement (and consequently shear stiffness and strength), allowing the soil to resist increased levels of shear stress (by moving along the failure envelope).

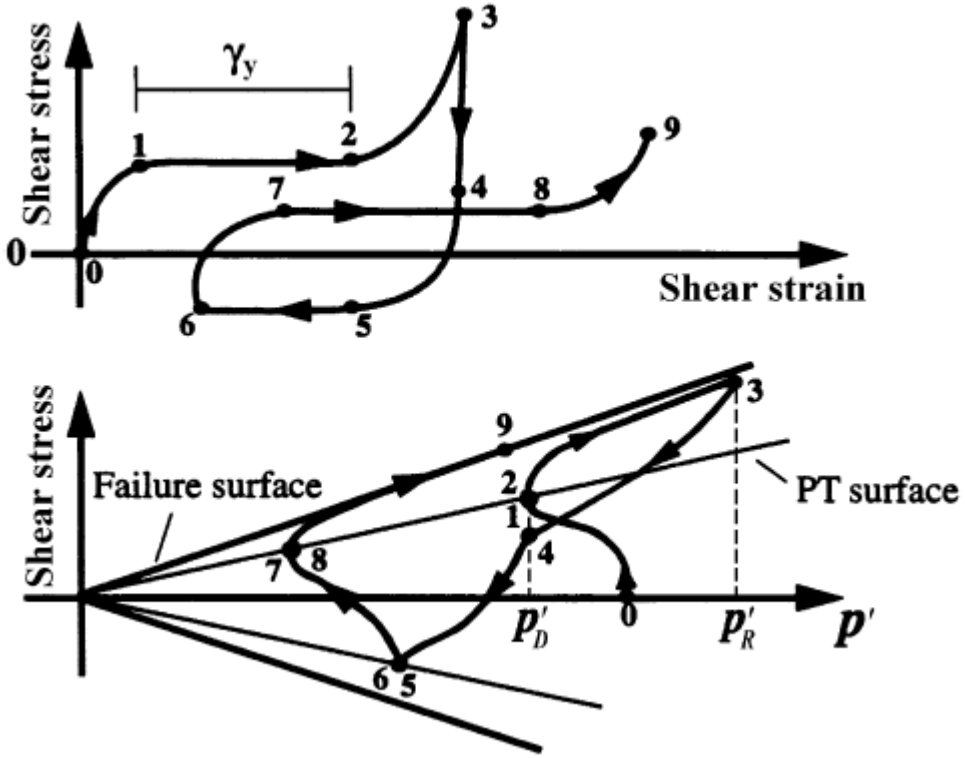

Figure 5 - 1: Constitutive model response showing shear stress, effective confinement, and shear strain [41].

Accurately accounting of the above-mentioned response characteristics in a plasticity model is accomplished by applying a multi-surface approach for cyclic hysteretic response to the original framework of Prevost's plasticity model.

Yield function f is selected of the following form:

$$f = \frac{3}{2}\left(\mathbf{s} - \left(p' + p_0'\right)\boldsymbol{\alpha}\right) : \left(\mathbf{s} - \left(p' + p_0'\right)\boldsymbol{\alpha}\right) - \mathbf{M}^2\left(p' + p_0'\right)^2 = 0 \qquad \text{(Eq. 5.11)}$$

in the domain of $p' \geq 0$, where $\mathbf{s} = \boldsymbol{\sigma}' - p'\boldsymbol{\delta}$ is the deviatoric stress tensor ($\boldsymbol{\sigma}'$ = effective Cauchy stress tensor, $\boldsymbol{\delta}$ = second-order identity tensor), p' is mean effective stress, p_0' is a small positive constant such that the yield surface size remains finite at

$p^{'}=0$, $\boldsymbol{\alpha}$ is second-order kinematic deviatoric tensor defining the yield surface coordinates, **M** dictates the yield surface size, and ":" denotes doubly contracted scalar product of two tensors.

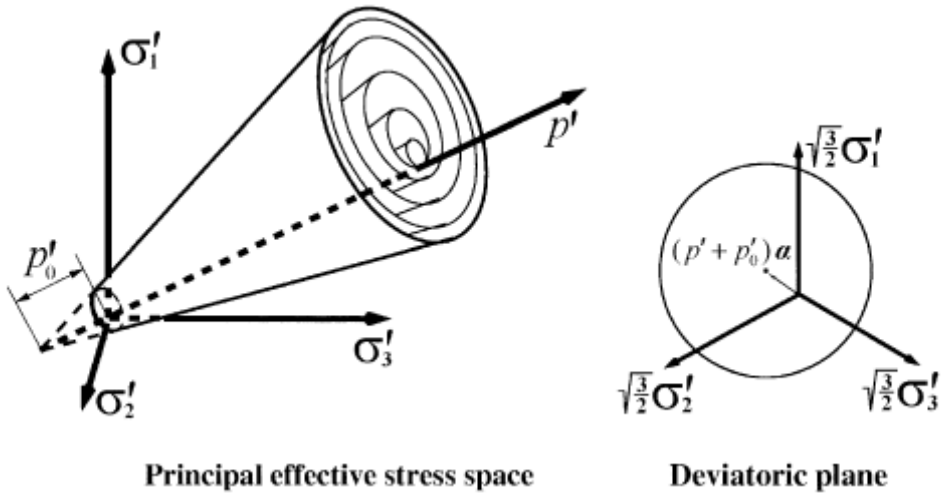

Figure 5 - 2: Conical yield surface in principle stress space and deviatoric plane [41].

Flow rule is given by:

$$3P^{"}=\frac{1-\left(\eta/\bar{\eta}\right)^2}{1+\left(\eta/\bar{\eta}\right)^2}\psi \qquad \text{(Eq. 5.12)}$$

where, P is the direction of plastic flow, and its volumetric component $p^{"}$ defines the desired level of dilation or contraction in accordance with experimental observation, $\eta=\sqrt{(3/2)\mathbf{s}:\mathbf{s}}/\left(p^{'}+p_0^{'}\right)$ is effective stress ratio, $\bar{\eta}$ is a material parameter defining the stress ratio of the PT surface, and ψ is a scalar-valued function for controlling the magnitudes of dilation and contraction.

For the hardening rule,

$$\mu=\frac{M_{m+1}}{M_m}\left[\mathbf{s}-\left(p^{'}+p_0^{'}\right)\boldsymbol{\alpha}_m\right]-\left[\mathbf{s}-\left(p^{'}+p_0^{'}\right)\boldsymbol{\alpha}_{m+1}\right] \qquad \text{(Eq. 5.13)}$$

The translation direction, is defined by **s** as the current (deviatoric) stress state on the active surface f_m and its conjugate point R on the next outer surface f_{m+1}, $\left(p^{'}+p_0^{'}\right)\boldsymbol{\alpha}_m$ and $\left(p^{'}+p_0^{'}\right)\boldsymbol{\alpha}_{m+1}$ are the centers of f_m and f_{m+1} respectively in the deviatoric plane [41].

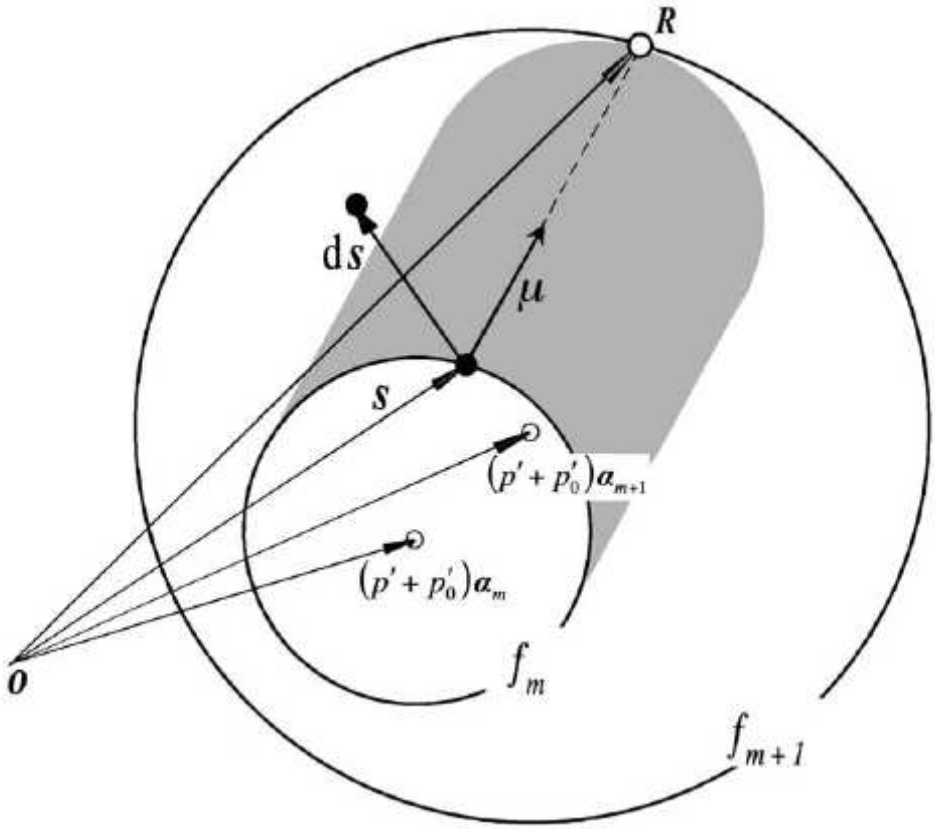

Figure 5 - 3: Deviatoric hardening rule [41].

5.4. Transfer of Seismic Input and Boundary Conditions

The Lysmer-Kuhlemeyer transmitting/absorbing boundary was implemented as described in Zhang, Y. Yang, Z. Bielak, J. Conte, J.P. Elgamal, A. [42] for effective seismic input modeling and for the transmitting boundary conditions. The boundary absorbs the propagating waves in such a way that the incident wave is transmitted entirely into the soil domain of the finite element model without distortion and no waves are transmitted back to the exterior domain.

The one-dimensional vertical shear wave equation can be written in the form as

$$\frac{\partial^2 u(x,t)}{\partial t^2} = v_s \frac{\partial^2 u(x,t)}{\partial x^2} \qquad \text{(Eq. 5.14)}$$

In these equations u denoted the soil particle displacement (perpendicular to the direction of wave propagation) and

$$v_s = \sqrt{G/\rho} \qquad \text{(Eq. 5.15)}$$

denotes the shear wave velocity. The solution of the above wave equation has the form of

$$u(x,t) = u_r\left(t - \frac{x}{v_s}\right) + u_i\left(t + \frac{x}{v_s}\right) \quad \text{(Eq. 5.16)}$$

where $u_r(...)$ and $u_i(...)$ can be any arbitrary functions of $(t - x/v_s)$ and $(t + x/v_s)$, respectively. The term $u_r(t - x/v_s)$ represents the wave traveling at velocity v_s in the positive x-direction, while $u_i(t + x/v_s)$ represents the wave traveling at the same speed in the negative x-direction. Thus, u_i is the incident wave if it points upward into the computational domain and u_r is the reflected wave. Taking the partial derivative with respect to time both sides of the above equation and multiplying by ρv_s gives

$$\rho v_s \frac{\partial u(x,t)}{\partial t} = \rho v_s u_r'(t - x/v_s) + \rho v_s u_i'(t + x/v_s) \quad \text{(Eq. 5.17)}$$

where the prime superscript denotes the derivative of the associated function with respect to its argument. Now, the linear elastic uniaxial shear stress-shear strain relation is given by

$$\tau(x,t) = G\frac{\partial u(x,t)}{\partial x} = -\frac{G}{v_s}u_r'(t - x/v_s) + \frac{G}{v_s}u_i'(t + x/v_s) \quad \text{(Eq. 5.18)}$$

where $\tau(x,t)$ is the shear stress. Combining the above two equations, we get

$$\tau(x,t) = -\rho v_s \frac{\partial u(x,t)}{\partial t} + 2\rho v_s u_i'(t + x/v_s) \quad \text{(Eq. 5.19)}$$

$\partial u(x,t)/\partial t$ represents the velocity of the total soil particle motion, while

$$u_i'(t + x/v_s) = \partial u_i(t + x/v_s)/\partial t \quad \text{(Eq. 5.20)}$$

is the velocity of the incident motion. Therefore, the first term on the right hand side of equation is equivalent to the force (per unit area) generated by a dashpot of coefficient ρv_s, while the second term is equivalent to the force (per unit area), which is proportional to the velocity of the incident wave. As a result, the soil below the soil domain of interest can be replaced with a dashpot and an equivalent force, which defines the seismic input. It is assumed that the response of the soil deposit is predominantly caused by vertically propagating shear waves. The soil below the base of the computational domain is modeled as a linear elastic, undamped and homogeneous semi-infinite half-space. It is expected that any nonlinearities below the base of the computational domain would remain small, since the soil is significantly stiffer than the soil within the computational domain. On each node at the base and on the lateral boundaries of the soil domain, two dashpots are added, normal and tangential to the boundary, respectively. The normal dashpots are set to absorb the reflected compressive waves while the tangential ones are set to absorb the reflected

shear waves. And on each node at the base, an equivalent force, which is proportional to the velocity of the incident wave and the tributary surface area of the node, is applied in the horizontal direction to represent the vertically incident SV-wave.

In the finite element model, horizontal and vertical dashpots are defined at every node along the lateral and base boundaries of the soil domain. The dashpot coefficients (per unit area) were defined as ρv_s and ρv_p (where v_p denotes the compressive or P-wave velocity) for the dashpots tangential and normal to the boundaries, respectively. Since the results derived for one-dimensional wave propagation are applied to a finite size two-dimensional soil domain, the soil domain is made sufficiently long so that the response in the center part of the mesh is close to its counterpart for the one-dimensional case.

It is complicated to implement the transmitting/absorbing boundaries in the nonlinear soil domain of the dam system. In fact, since confining pressure dependent material plasticity models are used to model the behavior of the various soil layers, lateral confinement is needed for these soil layers to develop some strength. However, the dashpots cannot provide any lateral static constraint. Therefore, it is needed to proceed in several steps to apply the transmitting boundaries for a static gravity analysis followed by a dynamic (earthquake response) analysis of the nonlinear dam system. First, the base and lateral boundaries of the soil domain are fixed, various soil constitutive models are set to be linear elastic, and the gravity is applied. In the second step, the soil constitutive models are switched from linear elastic to elasto-plastic accounting for material nonlinearity (and liquefaction if any) effects and the new static equilibrium state under gravity of the soil domain is obtained iteratively. In a third step, all the displacement constraints along the boundaries of the soil domain are removed and replaced with the corresponding support reactions recorded at the end of the second step. After balancing the internal and external forces, dashpots in both the horizontal and vertical directions are added to the base and lateral boundaries of the soil domain to model the transmitting boundaries. Finally in a fourth step, the seismic excitation is applied, in the form of equivalent nodal forces defined earlier, from the static equilibrium configuration under gravity loads [42].

6. NUMERICAL MODEL

6.1. Introduction

In this section, numerical model implemented for simulation of the Alibey Earth Dam is explained.

6.2. Definition of the Finite Element Model

In this study, four node plane-strain finite elements were implemented for the simulation studies. Each degree of freedom of the finite elements has two displacement degrees of freedoms and one degree of freedom for pore fluid pressure. In the study, elastic and pressure dependent/independent multi yield materials were implemented. Cross-section of the dam is outlined in Figure 6 - 1.

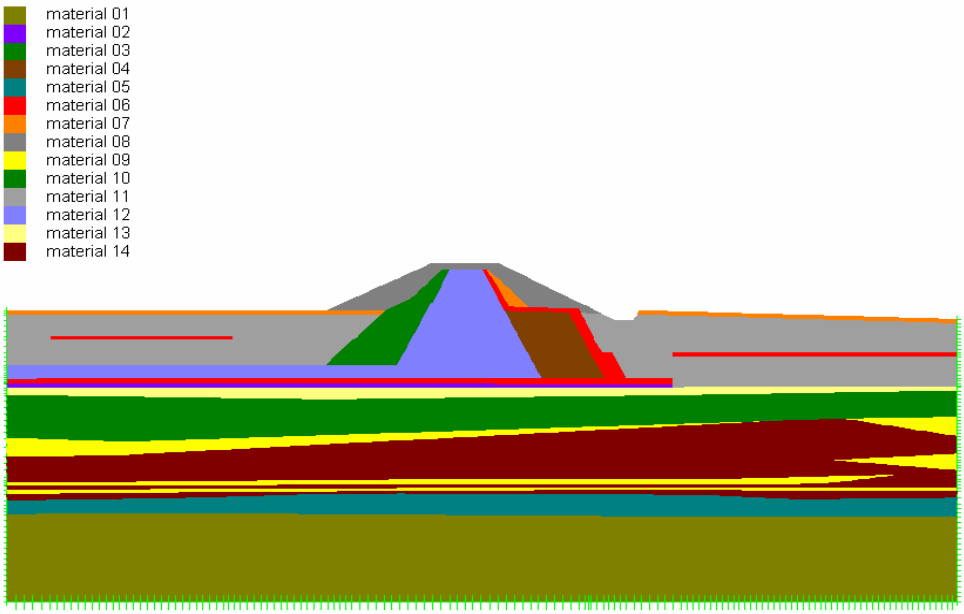

Figure 6 - 1: Cross-section of Alibey Dam according to its material properties.

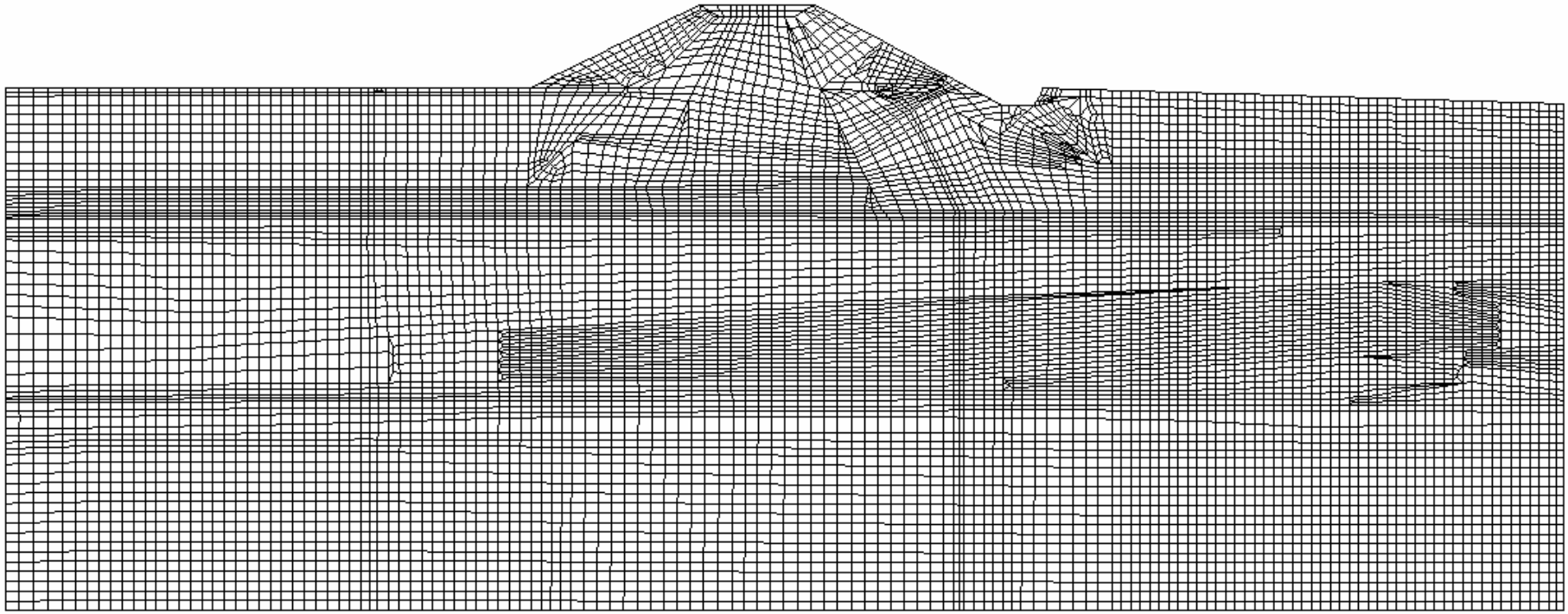

Figure 6 - 2: Finite Element Mesh of Alibey Dam Model.

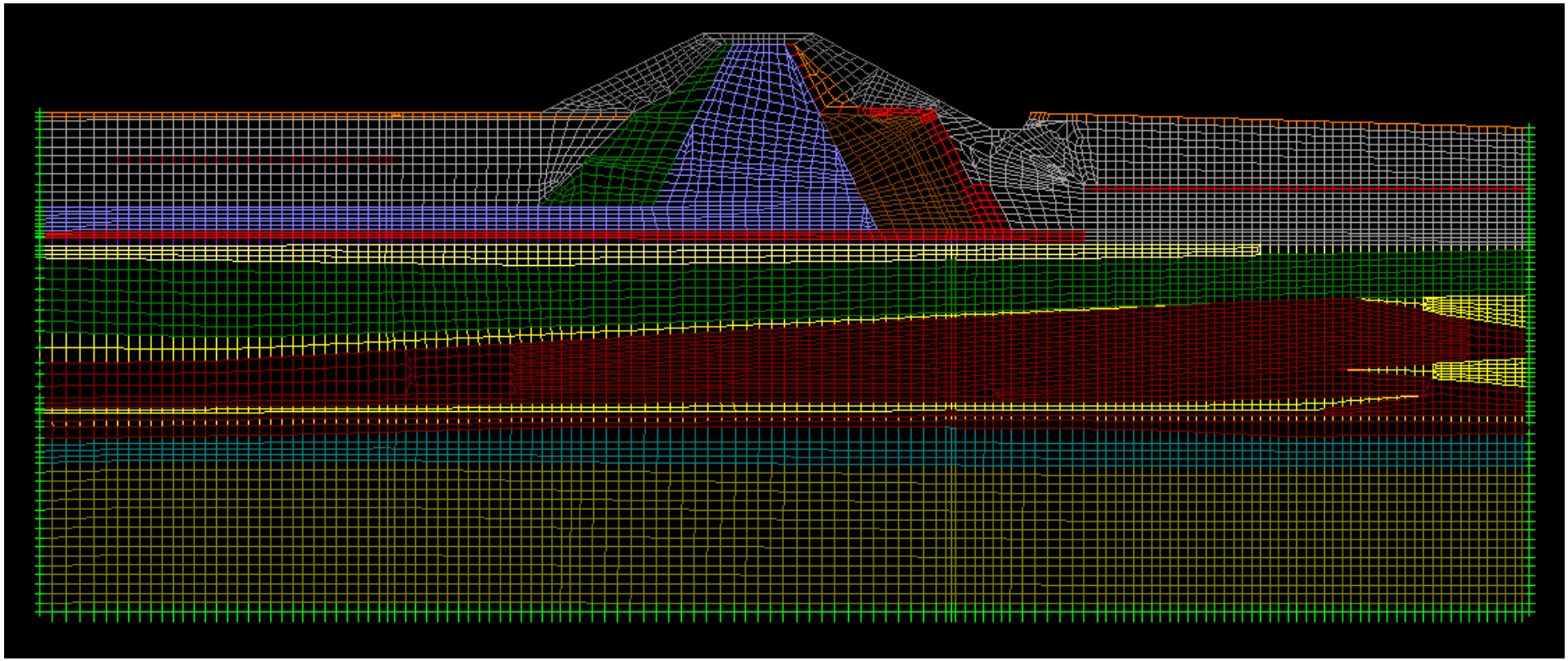

Figure 6 - 3: Finite Element Mesh of Alibey Earth Dam Model

A scaled engineering drawing of the dam was first imported to SAP2000 (a finite element software for structural and earthquake engineering analysis) and the mesh was generated by hand at pre-processor of SAP2000. Database option of the program was used in the generation of the OpenSees model. OpenSees currently involves no pre- and post-processing capabilities and it is only used as a solver. The finite element model prepared at SAP2000 was translated into OpenSees input format with a standard spreadsheet program which can import and export text files.

In the models, zero length elements were also used for modeling transmitting boundaries. Two dimensional dampers were generated by zero length element option of OpenSees and relevant damping coefficients with respect to the soil model were used during the analysis. A model is analyzed in two successive steps. In the first analysis, all the displacement boundary conditions of the dam are taken as fixed and a consolidation analysis is performed and respective joint reactions for the displacement degrees of freedoms are recorded during the analysis. At the second analysis, all the displacement boundary conditions are taken as free and all the boundaries are modeled with zero length elements which can absorb the seismic waves approaching from the domain. These boundaries eliminate the reflection of the seismic waves at the fixed nodes and there exists less transition of waves back into the domain. At the second analysis, the recorded reaction forces for each time interval are applied to the free end of the zero length boundaries and as a result the static equilibrium of the structure under gravity loads is obtained. Also, there exists an alternative formulation of seismic input in the study. In a dynamic time history analysis, the conventional methods used during the analysis are describing prescribed accelerations, velocities or displacements at the fixed nodes. However, at the models generated, it is assumed that the nodes should be free for displacements in order to make the zero length elements work properly. The velocity time history of the model is converted to nodal loads with respect to the method defined at the previous section. These point loads are applied at the bottom free boundaries of the model and the time history analyses were done accordingly. As results, joint displacements at nodes can be extracted. Scientific visualization software called ParaView was used to visualize the displacement contours of the results.

In addition to the time history analyses performed according to the described methods, modal analysis of the model was performed. For modal analysis, uncoupled finite

elements were adopted with plane strain assumption. All the sides of the model are fixed for displacement degrees of freedom during the analysis.

6.3. Material Properties of The Dam

During the analyses, the properties listed at tables below are used.

Table 6 - 1: Material properties 1 [11].

Material Label	Material Name	Material Type	E (kN/m2)	ν
Material 01	Greywacke	Rock	68400000	0.20
Material 02	Fill	Fill	140000	0.30
Material 03	Gravelly-Sand Material	Sand-Gravel	140000	0.30
Material 04	Sands with Gravels	Sand-Gravel	140000	0.30
Material 05	Sand with Gravel	Sand-Gravel	140000	0.30
Material 06	Filter Material	Fill	140000	0.30
Material 07	Light-Weight Rock Material	Fill	140000	0.30
Material 08	Strong Rock Materials	Fill	100000	0.20
Material 09	Sand	Sand Band	140000	0.30
Material 10	Green Clay	Green Clay	140000	0.30
Material 11	Sandy-Clay	Fill	140000	0.30
Material 12	Plastic Clay	Yellow Clay	140000	0.30
Material 13	Yellow Clay	Yellow Clay	140000	0.30
Material 14	Black Clay	Black Clay	140000	0.30

Table 6 - 2: Material properties 2 [11].

Material Label	γ_d (kN/m^3)	γ_s (kN/m^3)
Material 01	25.0155	25.3098
Material 02	19.95	20
Material 03	16	19
Material 04	16	19
Material 05	16	19
Material 06	19.95	20
Material 07	19.95	20
Material 08	19.95	20
Material 09	16	18
Material 10	14	19
Material 11	19.95	20
Material 12	15.4	20
Material 13	15.4	20
Material 14	11.3	17

Table 6 - 3: Material properties 3 [11].

Material Label	H Permeab. (m/sn)	V Permeab. (m/sn)	ϕ' (degree)
Material 01	3.81E-07	3.81E-07	-
Material 02	1.15741E-07	1.15741E-07	-
Material 03	1.27315E-05	1.27315E-05	35
Material 04	1.27315E-05	1.27315E-05	35
Material 05	1.27315E-05	1.27315E-05	35
Material 06	1.15741E-07	1.15741E-07	-
Material 07	1.15741E-07	1.15741E-07	-
Material 08	1.15741E-07	1.15741E-07	-
Material 09	1.27315E-05	1.27315E-05	32
Material 10	2.31481E-08	5.78704E-09	18
Material 11	1.15741E-07	1.15741E-07	-
Material 12	2.31481E-08	5.78704E-09	20
Material 13	2.31481E-08	5.78704E-09	20
Material 14	2.31481E-08	5.78704E-09	17

For nonlinear analysis, pressure dependent multi yield and pressure independent multi yield materials are adopted. Material properties are taken from Table 6 - 4, Table 6 - 5, Table 6 - 6, Table 6 - 7. Rock and fill materials are assumed to behave linear during the analysis. All other materials are assumed to behave nonlinear. All the units are for force kilo-Newton, for length meter, for mass ton and for time second unless otherwise stated.

Table 6 - 4: Material properties 4.

Material Label	mass density	refShearModul	refBulkModul	peakShearStra
Material 01	2.58	28500000.0	38000000.0	-
Material 02	2.04	53846.15	116666.67	-
Material 03	1.94	53846.15	116666.67	0.1
Material 04	1.94	53846.15	116666.67	0.1
Material 05	1.94	53846.15	116666.67	0.1
Material 06	2.04	53846.15	116666.67	-
Material 07	2.04	53846.15	116666.67	-
Material 08	2.04	41666.67	55555.56	-
Material 09	1.83	53846.15	116666.67	0.1
Material 10	1.94	53846.15	116666.67	0.1
Material 11	2.04	53846.15	116666.67	-
Material 12	2.04	53846.15	116666.67	0.1
Material 13	2.04	53846.15	116666.67	0.1
Material 14	1.73	53846.15	116666.67	0.1

Table 6 - 5: Material properties 5.

Material Label	refPress	pressDependCoe	PTAngle	contrac
Material 01	-	-	-	-
Material 02	-	-	-	-
Material 03	80	0.5	27	0.06
Material 04	80	0.5	27	0.06
Material 05	80	0.5	27	0.06
Material 06	-	-	-	-
Material 07	-	-	-	-
Material 08	-	-	-	-
Material 09	80	0.5	28	0.11
Material 10	100	0	-	-
Material 11	-	-	-	-
Material 12	100	0	-	-
Material 13	100	0	-	-
Material 14	100	0	-	-

At these tables, for pressure independent multi yield material, refShearModul represents reference low-strain shear modulus, specified at a reference mean effective confining pressure refPress, refBulkModul represents reference bulk modulus, specified at a reference mean effective confining pressure refPress, cohesi represents apparent cohesion at zero effective confinement, peakShearStra represents an octahedral shear strain at which the maximum shear strength is reached, specified at a reference mean effective confining pressure refPress, frictionAng represents the friction angle at peak shear strength in

Table 6 - 6: Material Properties 6.

Material Label	dilat1	dilat2	liquefac1	liquefac2
Material 01	-	-	-	-
Material 02	-	-	-	-
Material 03	0.5	2.5	7.5	0.0065
Material 04	0.5	2.5	7.5	0.0065
Material 05	0.5	2.5	7.5	0.0065
Material 06	-	-	-	-
Material 07	-	-	-	-
Material 08	-	-	-	-
Material 09	0.2	1.0	10	0.015
Material 10	-	-	-	-
Material 11	-	-	-	-
Material 12	-	-	-	-
Material 13	-	-	-	-
Material 14	-	-	-	-

Table 6 - 7: Material properties 7.

Material Label	liquefac3	e	cs1
Material 01	-	-	-
Material 02	-	-	-
Material 03	1.0	0.63	0.89
Material 04	1.0	0.63	0.89
Material 05	1.0	0.63	0.89
Material 06	-	-	-
Material 07	-	-	-
Material 08	-	-	-
Material 09	1.0	0.78	0.89
Material 10	-	-	-
Material 11	-	-	-
Material 12	-	-	-
Material 13	-	-	-
Material 14	-	-	-

degrees, refPress represents reference mean effective confining pressure, pressDependCoe represents, an optional non-negative constant defining variations in shear and bulk modulus as a function of initial effective confinement.

For the pressure dependent multi yield material, refShearModul represents reference low-strain shear modulus, specified at a reference mean effective confining pressure refPress, refBulkModul represents reference bulk modulus specified at a reference mean effective confining pressure refPress, frictionAng represents friction angle at peak shear strength (in degrees), peakShearStra represents an octahedral shear strain at which the maximum shear strength is reached, specified at a reference mean confining pressure refPress, refPress represents reference mean effective confining pressure at which shear modulus, bulk modulus and γ_{max} are defined. pressDependCoe represents a positive constant defining variations of shear and bulk modulus as a function of instantaneous effective confinement. PTAng represents phase transformation angle (in degrees), contrac represents a non-negative constant defining the rate of shear-induced volume increase (dilation), in which larger values correspond to stronger dilation rates. liquefac1, liquefac2 and liquefac3 represent parameters controlling the mechanism of liquefaction-induced perfectly plastic shear strain accumulation, i.e., cyclic mobility. liquefac1 represents the effective confining pressure below which the mechanism is in effect. liquefac2 represents the maximum amount of perfectly plastic shear strain developed at zero effective

confinement during each loading phase, and liquefac3 represents the maximum amount of biased perfectly plastic shear strain accumulated at each loading phase under biased shear loading conditions. e represents the initial void ratio, cs1, cs2, cs3 and pa represent parameters defining a straight critical-state line.

Four-node plane strain element uses bilinear isoparametric formulation. This element is for simulating dynamic response of solid-fluid fully coupled material, based on Biot's theory of porous medium. Each element has three degrees-of-freedom. DOF one and two are for solid displacements (u) and DOF three is for fluid pressure (p). For this element, combined undrained bulk modulus relating changes in pore pressure and volumetric strain is used which may be approximated by

$$B_c \approx B_f / n \qquad \text{(Eq. 6.1)}$$

where B_f is the bulk modulus of fluid phase (2.2E06 kPa for water), and n is the initial porosity. Also for the formulations of the element, fluid mass density and permeability coefficients are required. Permeability may be given for both horizontal and vertical directions [43].

During the analysis following damping ratios were used for materials. The mass and stiffness proportional damping constants were calculated for damping ratios for periods of 0.1 seconds and 5.5 seconds.

Table 6 - 8: Damping properties of materials.

Material Label	Damping ratio	Mass prop. Damp.	Stiff. Prop. Damp.
Material 01	0.20	0.4488000	0.0062530
Material 02	0.19	0.4264000	0.0059400
Material 03	0.17	0.3815000	0.0053150
Material 04	0.17	0.3815000	0.0053150
Material 05	0.17	0.3815000	0.0053150
Material 06	0.19	0.4264000	0.0059400
Material 07	0.19	0.4264000	0.0059400
Material 08	0.19	0.4264000	0.0059400
Material 09	0.16	0.3590000	0.0050020
Material 10	0.13	0.2917000	0.0040640
Material 11	0.19	0.4264000	0.0059400
Material 12	0.14	0.3142000	0.0043770
Material 13	0.14	0.3142000	0.0043770
Material 14	0.13	0.2917000	0.0040640

6.4. Formation of the Analyses Objects in OpenSees

During the formation of the global stiffness matrix, RCM numberer option of OpenSees was implemented which re-numbers the degree of freedoms to obtain a smaller bandwidth. A plain constraint handler was used since there was no advanced (multiple) constraining of degrees of freedoms. A profile symmetric positive definite linear equation solver was used as the solver. For the solution of the nonlinear equations, Newton-Raphson solution strategy was adopted. During the analyses norm of the displacement increments were tested as a convergence criteria. Newmark transient integrator was constructed for both consolidation and dynamic transient analyses.

6.4. Convergence Criteria

During modal analysis, convergence tolerance for determination of the eigenvalues was 1.0e-7. In the time history analyses, the norms of the displacements were tested with the value of 1.0e-3.

7. VERIFICATION AND VALIDATION

7.1. Introduction

In this section, verification of the modeling assumptions and models were outlined.

7.2. Verification of Transmitting Boundaries and Seismic Input

Dynamic numerical analysis of geotechnical problems requires the decrease of energy as the domain of interest gets larger. This phenomenon is usually referred to as radiation damping or geometric attenuation, and it is distinguished from material damping in which elastic energy is actually dissipated by viscous, hysteretic or other mechanisms. The fact that we must decide the domain of analysis in modeling, however, causes a need for special attention to the boundary.

7.2.1. Transmitting Boundary

To simulate the radiation condition, the “cut off” boundaries must include normal and tangential energy absorption elements. These absorption elements are usually represented by “dashpots”. Using dashpots, the radiation condition can be easily achieved. A schematic of a typical element is shown in Figure 7 - 1. Properly calibrated, these elements absorb the propagating waves in such a way that any incident waves produce zero energy being reflected back into the domain. Even though the energy absorption depends not only on material properties but also on frequency content, the study below shows that this viscous type of infinite element has enough validity to be used in practical applications. The dashpot coefficients are determined in terms of the material properties of the semi-infinite domain.

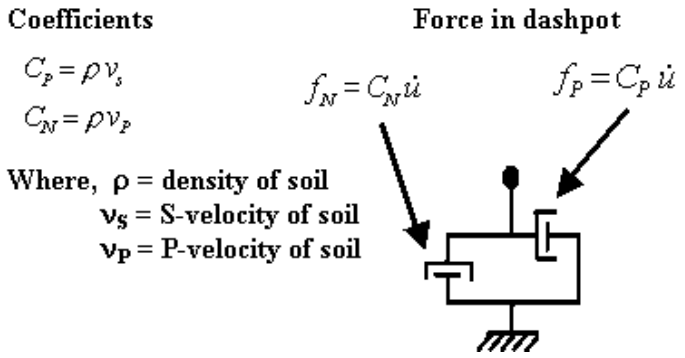

Figure 7 - 1: Energy absorption elements [44].

As a first verification example, a simple 1-Dimensional case has been analyzed by University of Washington researchers using OpenSees. The 1-D condition is enforced constraining both sides of the model to move the same amount. To accomplish this, the OpenSees "equalDOF" command is used. The analysis is performed using two boundary conditions at the bottom; i.e. "fixed" and "transmitted". Model details are shown in Figure 7 - 2. Comparison of recorded displacements at the top and middle nodes show the transmitting boundary absorbs most of the incident energy. The distinct reflections observed in the "fixed" case disappear in the "transmitted" case.

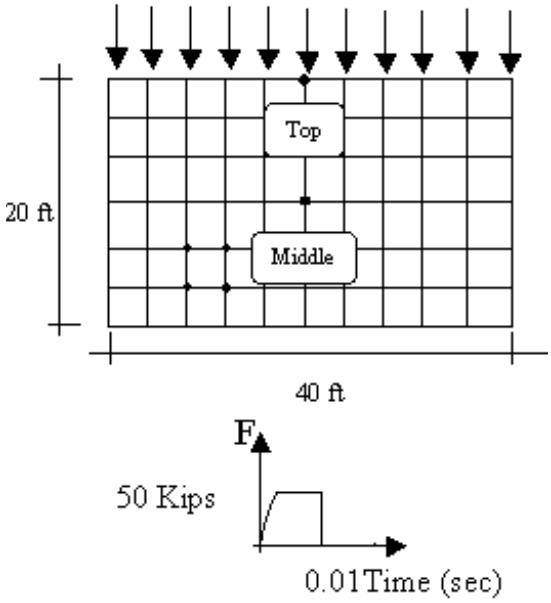

Figure 7 - 2: First verification example [44].

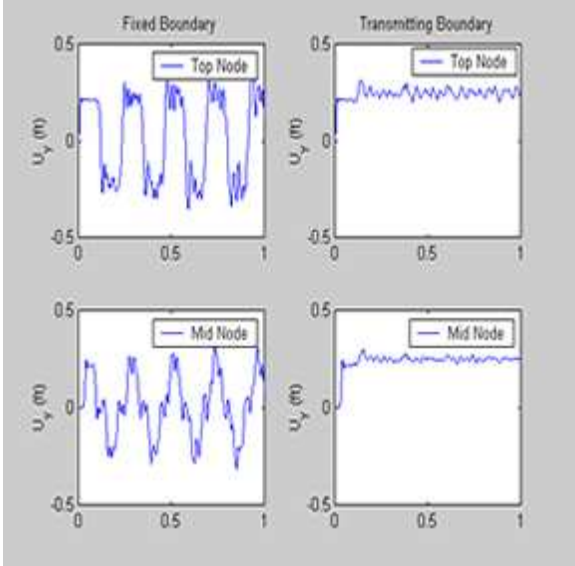

Figure 7 - 3: Results of the 1st verification example [44].

As a second verification example, a half-space model on an irregular domain is analyzed with fixed and transmitting boundaries. In this case the incident wave is no longer normal to the boundary. This geometry allows the use of both dashpots, parallel and normal to the boundary, and verifies the radiation condition in a 2D unbounded domain. The dashpot properties for an inclined side are estimated by considering the slope of the model. The results for "fixed" and "transmitted" cases are compared in Figure 7 - 5. Very small reflections are observed using transmitting elements. Clear reflections are observed in the case of fixed boundaries.

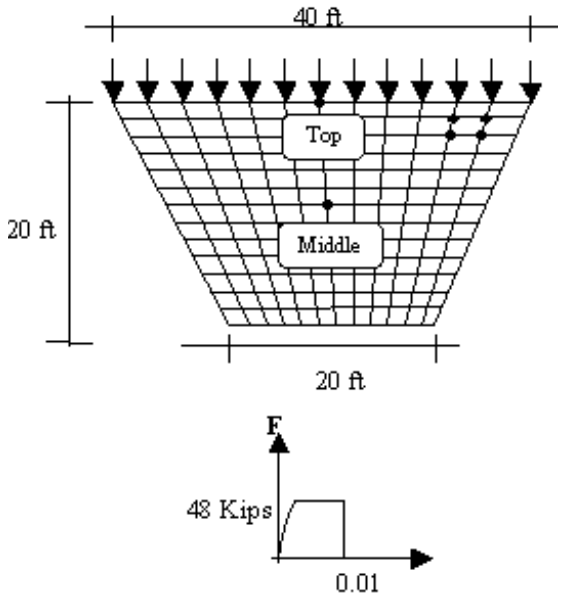

Figure 7 - 4: Second verification example [44].

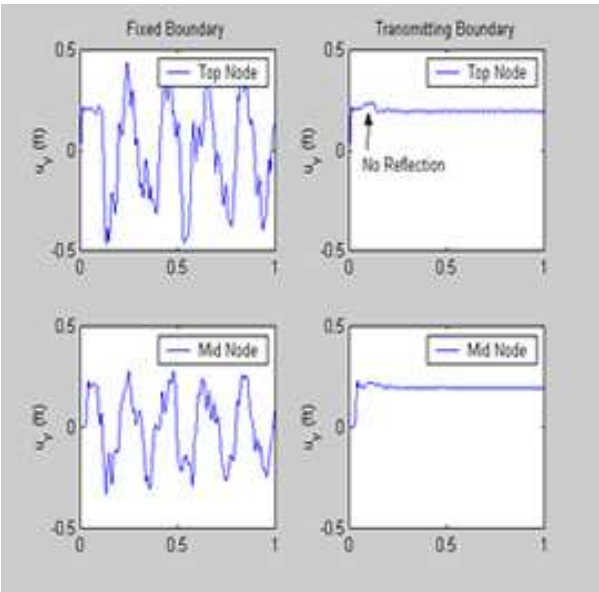

Figure 7 - 5: Results of the second verification example [44].

7.2.2. Effective Seismic Input

Typical finite element dynamic analyses of geotechnical problems apply the excitation to the fixed nodes. Using this method, the nodes which have the excitation are forced to have a specified displacement, velocity, or acceleration. That is, the boundaries are fixed during the analysis. This brings us the questions of how and where to apply the motion. As one possible solution to this problem, the methodology proposed by Joyner (1975) for vertically propagating waves in an underlying elastic medium can be used. The model conditions are represented by a system of horizontal soil layers resting on a semi-infinite elastic medium. The proposed methodology allows obtaining an expression for the shear stresses in the underlying medium at the boundary in terms of the particle velocity of the incident wave and the particle velocity on the boundary.

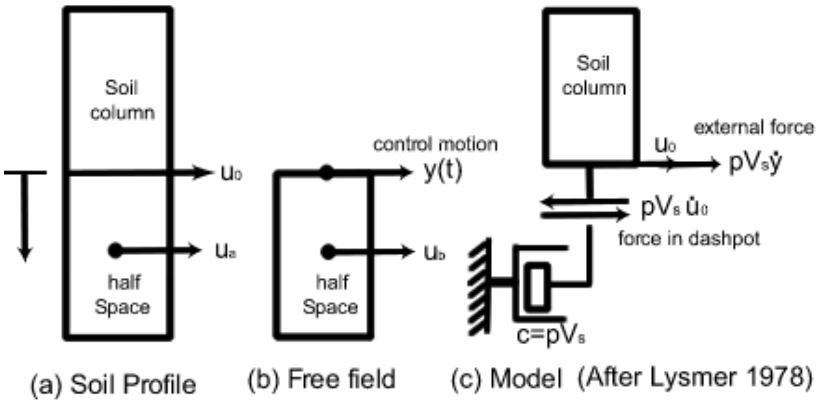

Figure 7 - 6: Effective seismic input model [44].

There are two examples using the effective seismic input loading condition based on an underlying elastic half-space. In the first case, a simple 1-D condition is modeled. Case1 is the target half-space and Case 2 is the reduced model we are trying to use. To find the effective input in terms of velocity, the control velocity ú(t) is obtained (see the middle model). Then, the control motion is applied to Case 2 model in terms of shear force. In this particular case, the loading condition is a uniformly distributed half sine velocity applied along the bottom nodes with duration 0.0002 sec (i.e. a pulse). The comparison between Case 1 and Case 2 indicates the approach is well verified.

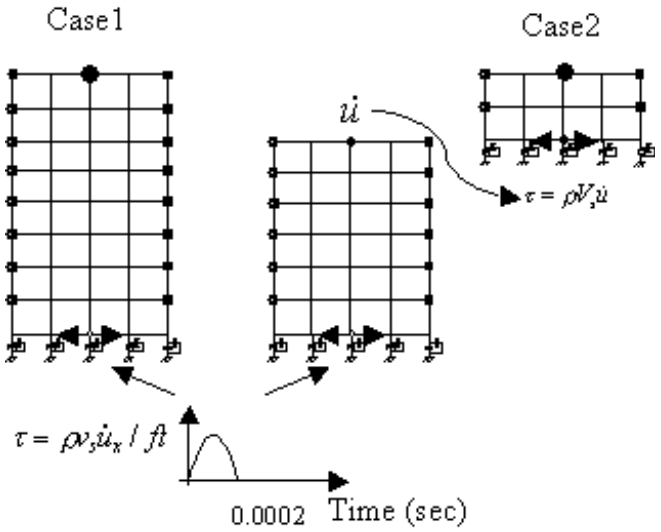

Figure 7 - 7: Effective seismic input verification example 1 [44].

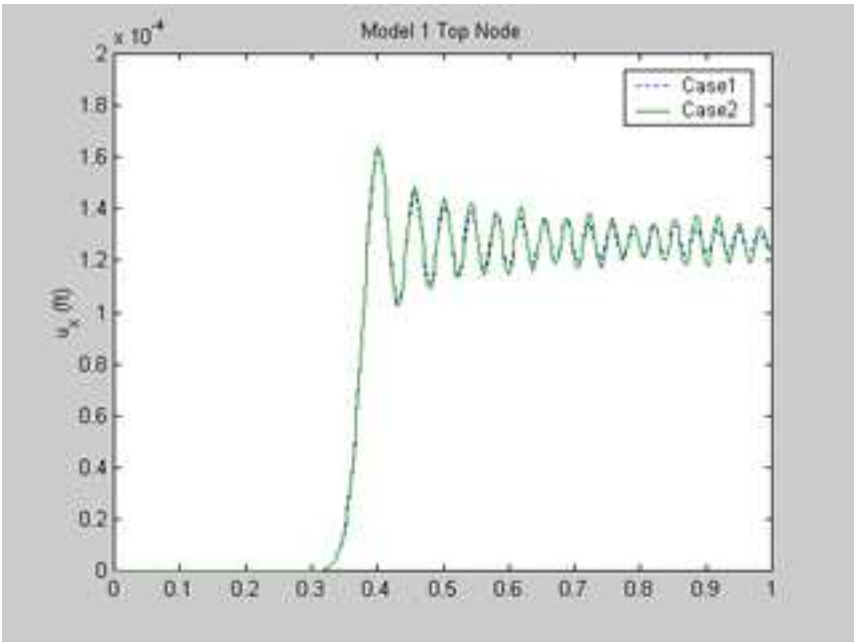

Figure 7 - 8: Results of the first verification example of effective seismic input [44].

The second example represents more realistic loading condition. In this case a 2D model is considered. In this case, the loading is not uniform along the bottom nodes. Its variation in time and space is shown in Figure 7 - 11. As it is shown in Figure 7 - 11, each node experiences a different load. In this case, úx and úy are obtained as control motion and are used to calculate the nodal forces to be applied along the boundaries for Case B. The comparison between Case A and B is not as good as in the first model, but it shows certain level of agreement [44].

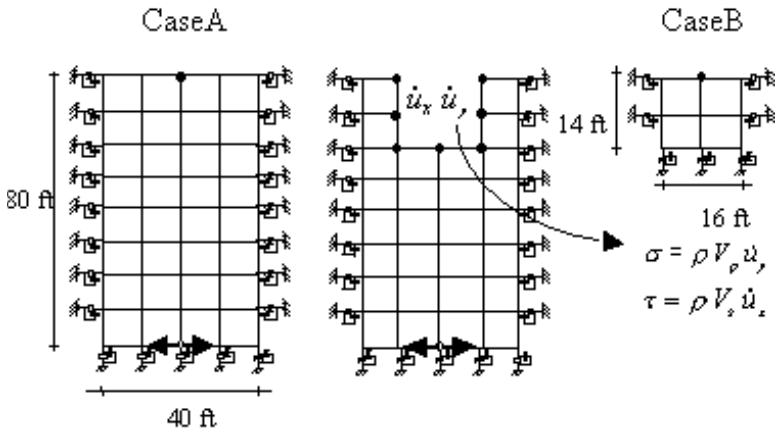

Figure 7 - 9: Second verification example for effective seismic input [44].

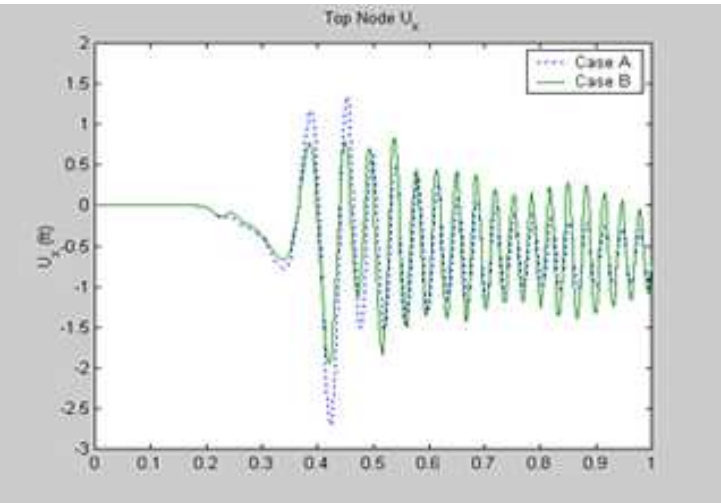

Figure 7 - 10: Results of second verification example for effective seismic input [44].

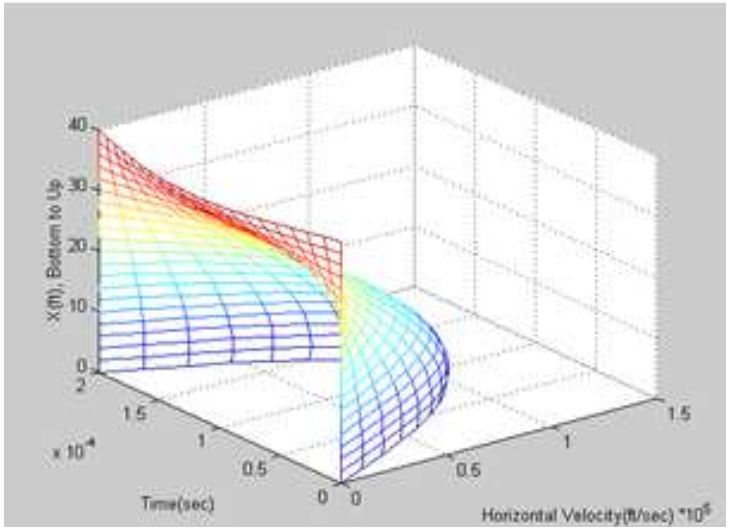

Figure 7 - 11: Results of second verification example for effective seismic input [44].

7.3. Comparison of Results of Plane-Strain Modal Analysis from OpenSees and SAP2000

The fundamental vibration period of the structure analyzed by plane-strain assumptions in OpenSees is found in good agreement with the results obtained from SAP2000.

Period obtained from OpenSees : 0.9256 seconds

Period obtained from SAP2000 : 0.93 seconds.

8. INTERPRATATION OF RESULTS AND COMPARISON WITH PREVIOUS STUDIES

8.1. Introduction

In this section, the results of the numerical models are evaluated and when possible, they were compared with previous studies.

8.2. (Case #1) - Modal Analysis

During the modal analysis, a standard eigenvalue analysis is performed. In the analysis, standard plane strain elements were used instead of coupled elements. All the boundaries of the domain are assumed to be fixed to displacements. According to the results of the modal analysis performed, the 1st fundamental vibration period and frequency of the structure are

1^{st} natural vibration period = 0.93 seconds.
1^{st} natural vibration frequency = 1.075 cycle/seconds.

In a previous study (Cimilli, 1998) [12], modal analysis of the structure and forced vibration tests were performed and it is understood that the first natural vibration frequency of the structure was 1.455 hertz from experimental studies. There is a good agreement between the computed and experimental results.

8.3. (Case #2) - Linear Elastic Material Models - Time History Analysis

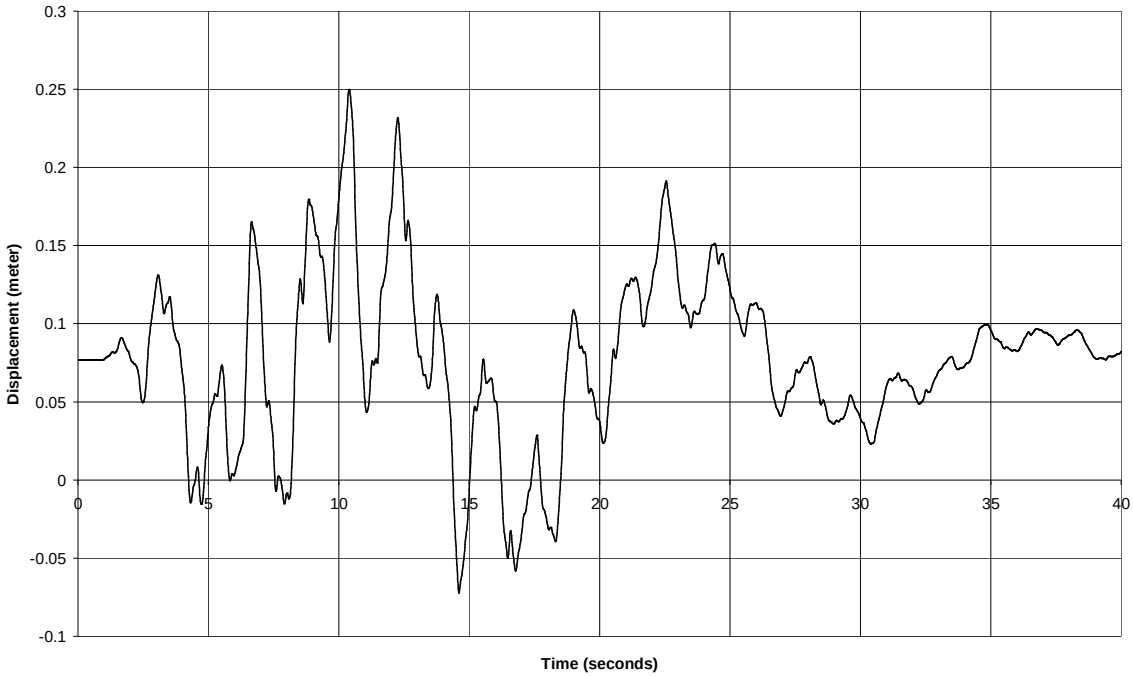

Figure 8 - 1: Dam's crest's horizontal displacements under seismic excitation. Linear elastic case.

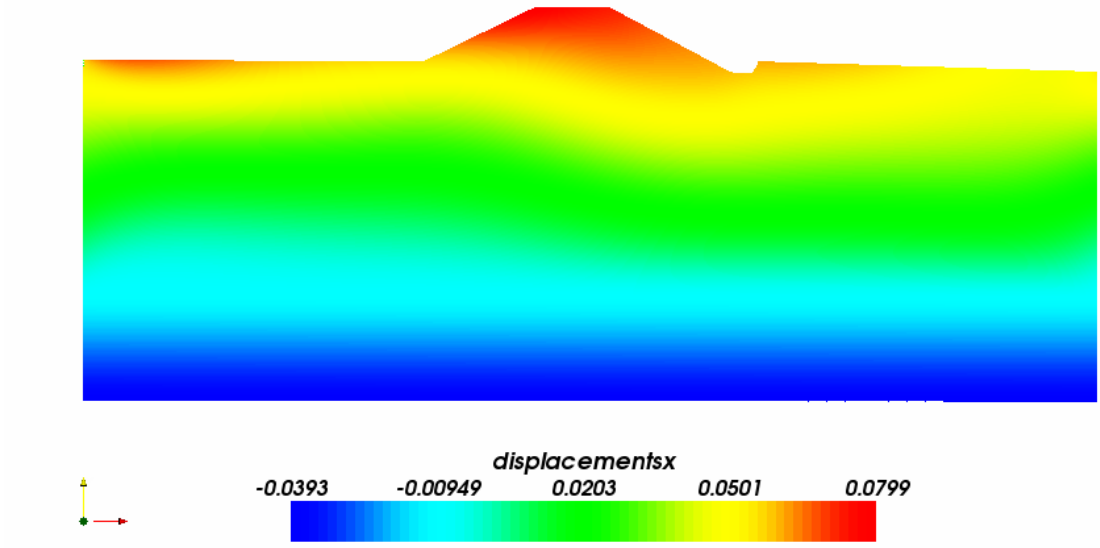

Figure 8 - 2: Horizontal displacements under gravity loads on the deformed shape of the structure. (meter).

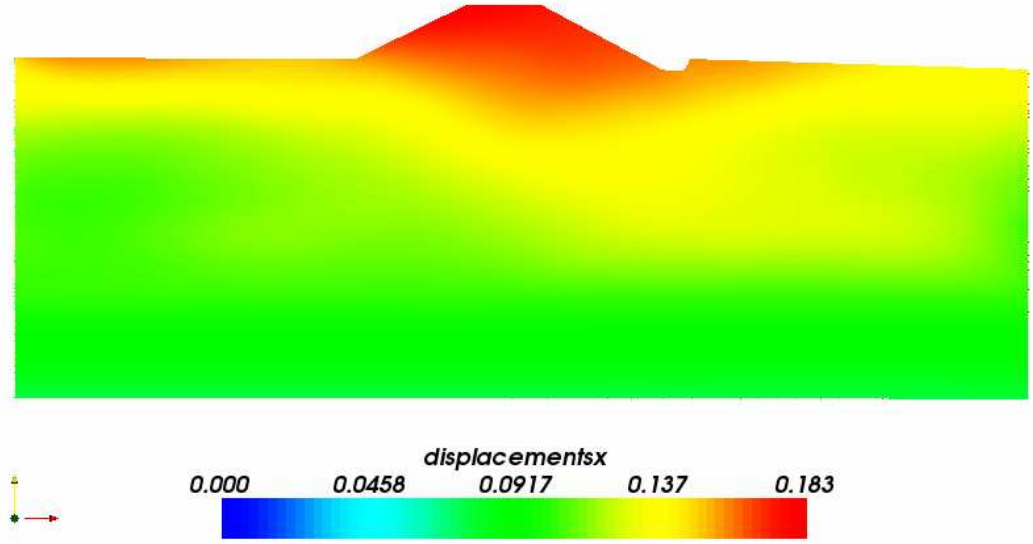

Figure 8 - 3: Horizontal displacements under seismic excitation at t = 10 seconds on the deformed shape of the structure. (meter).

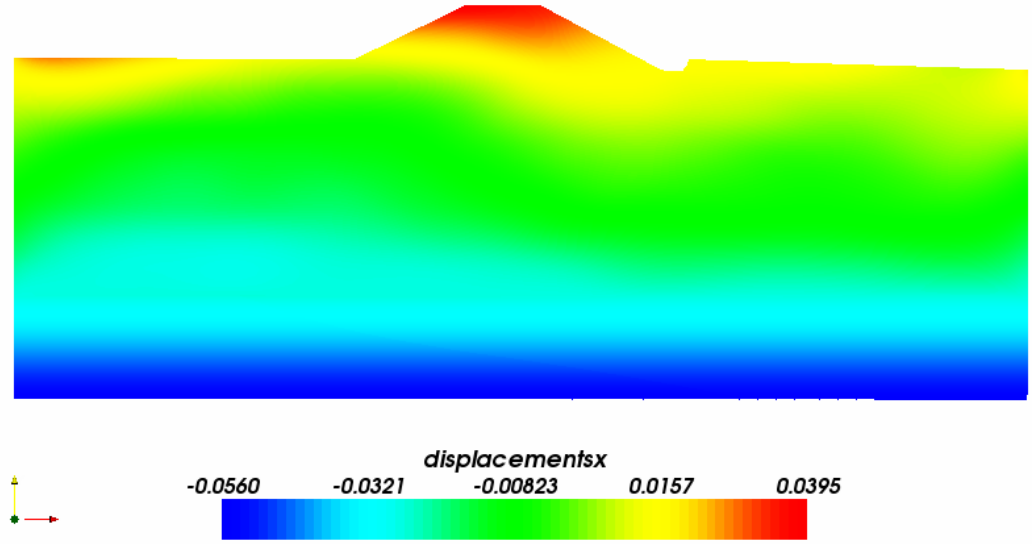

Figure 8 - 4: Horizontal displacements under seismic excitation at t = 20 seconds on the deformed shape of the structure. (meter).

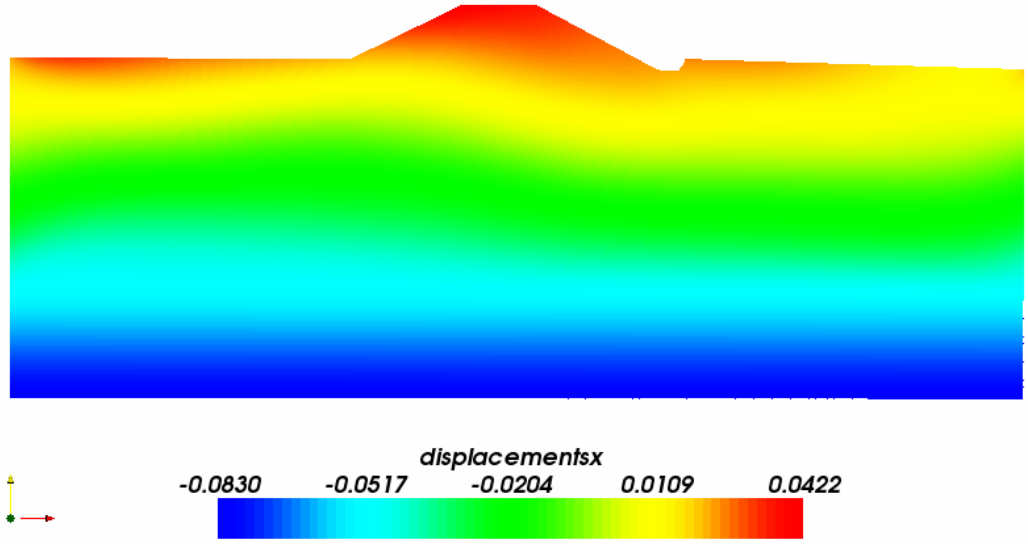

Figure 8 - 5: Horizontal displacements under seismic excitation at t = 30 seconds on the deformed shape of the structure. (meter).

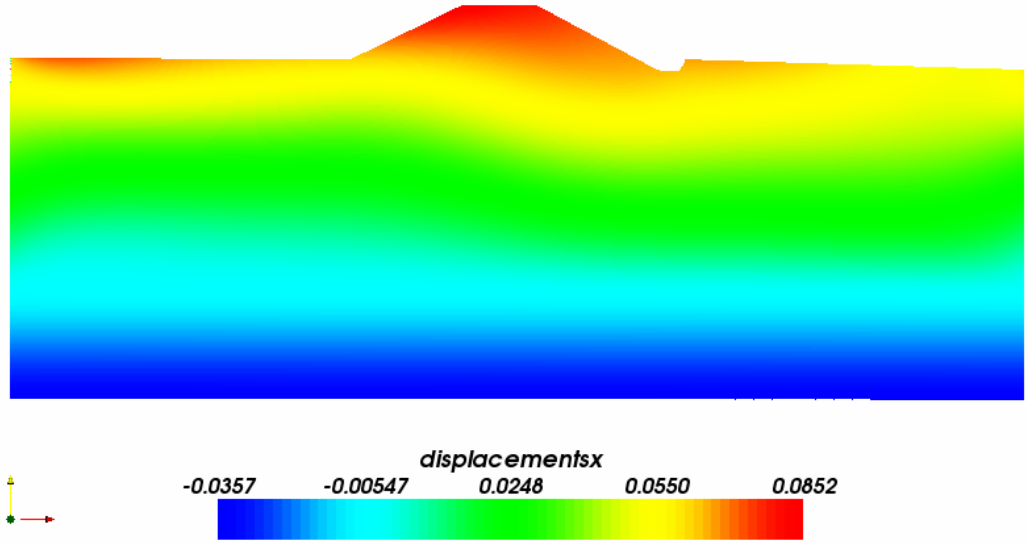

Figure 8 - 6: Horizontal displacements under seismic excitation at t = 40 seconds on the deformed shape of the structure. (meter).

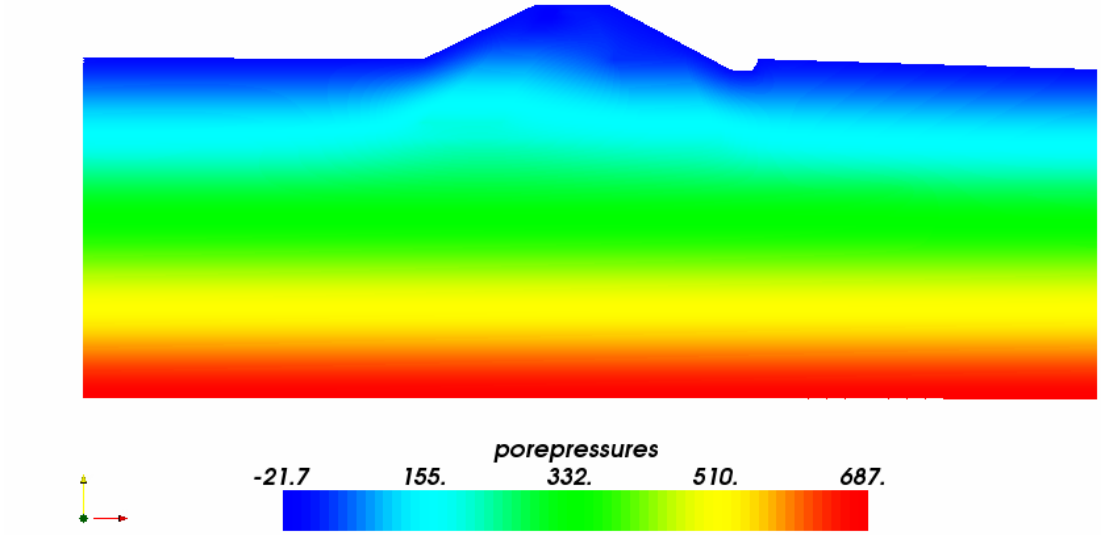

Figure 8 - 7: Pore pressures under gravity loads on the deformed shape of the structure. (kPa).

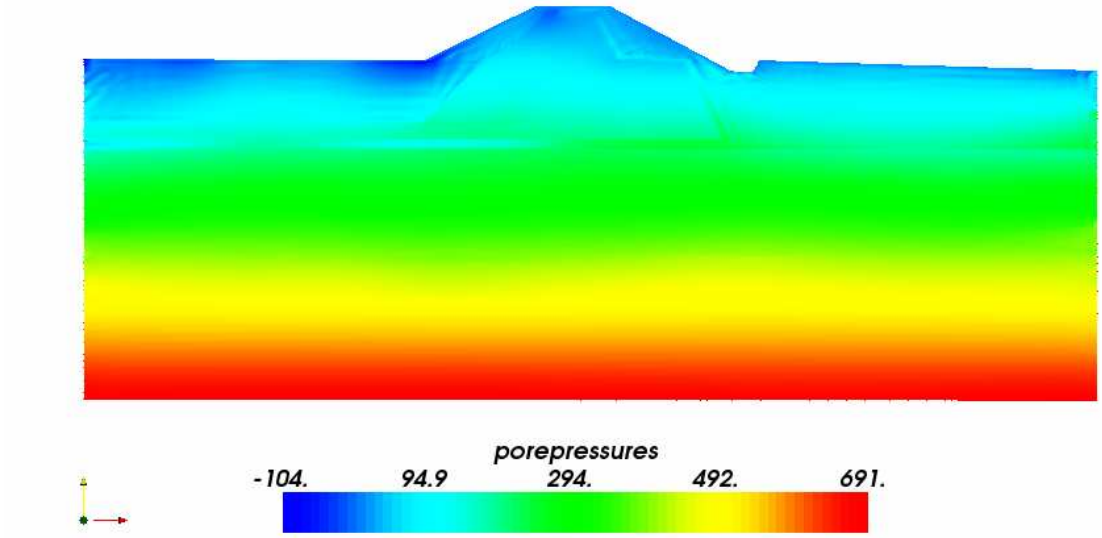

Figure 8 - 8: Pore pressures under seismic excitation at t = 10 seconds on the deformed shape of the structure. (kPa).

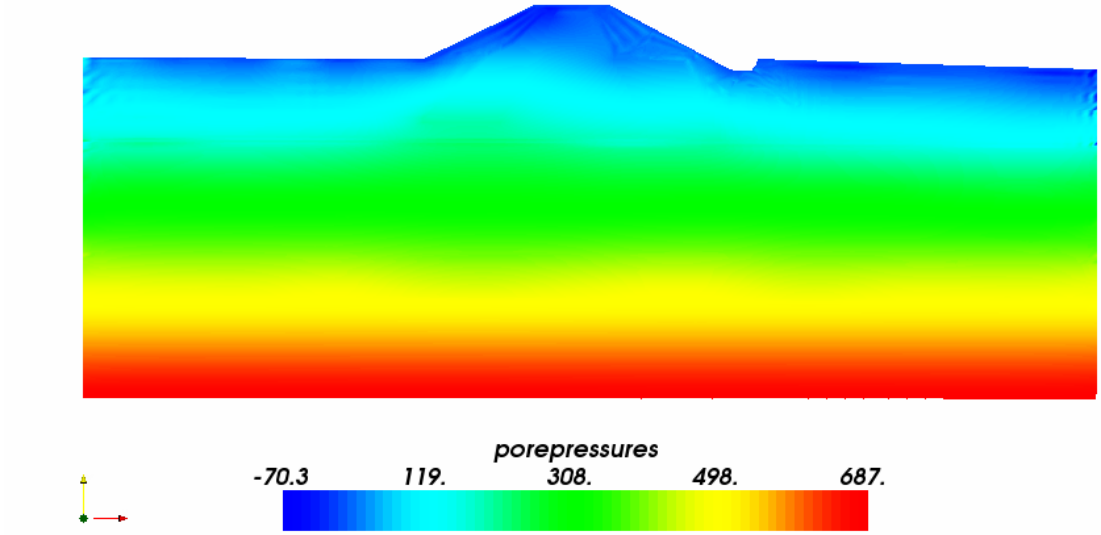

Figure 8 - 9: Pore pressures under seismic excitation at t = 20 seconds on the deformed shape of the structure. (kPa).

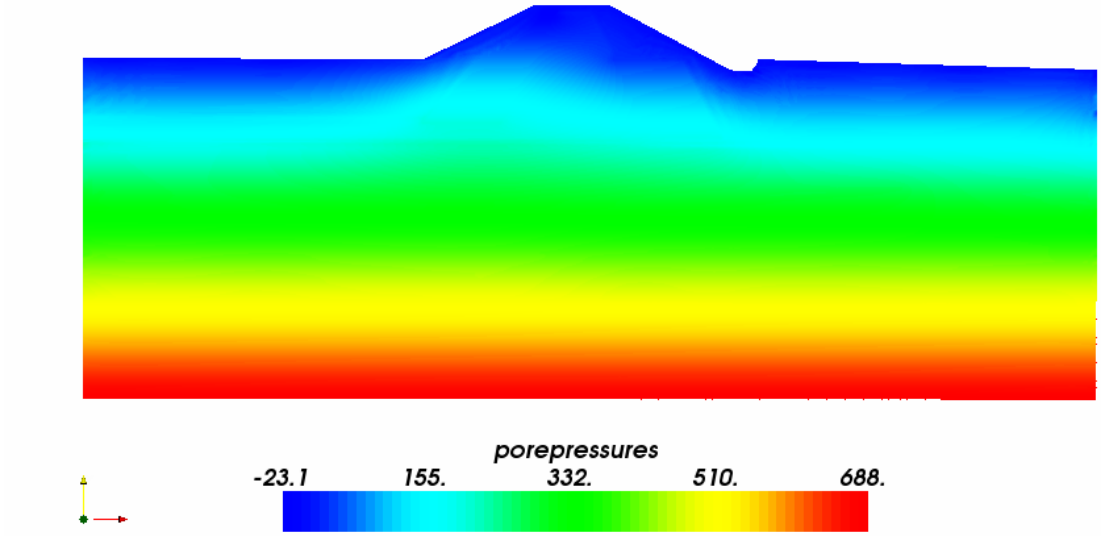

Figure 8 - 10: Pore pressures under seismic excitation at t = 30 seconds on the deformed shape of the structure. (kPa).

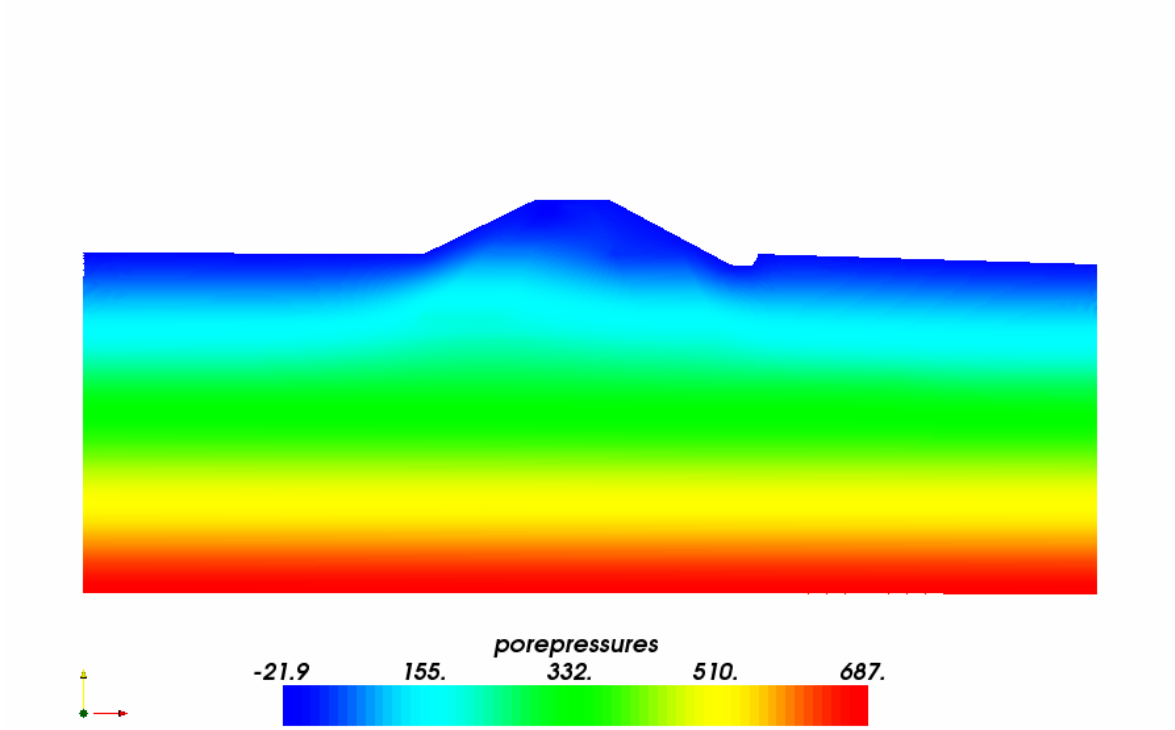

Figure 8 - 11: Pore pressures under seismic excitation at t = 40 seconds on the deformed shape of the structure. (kPa).

8.4. (Case #3) - Pressure Dependent and Independent Multi Yield Material Models - Time History Analysis

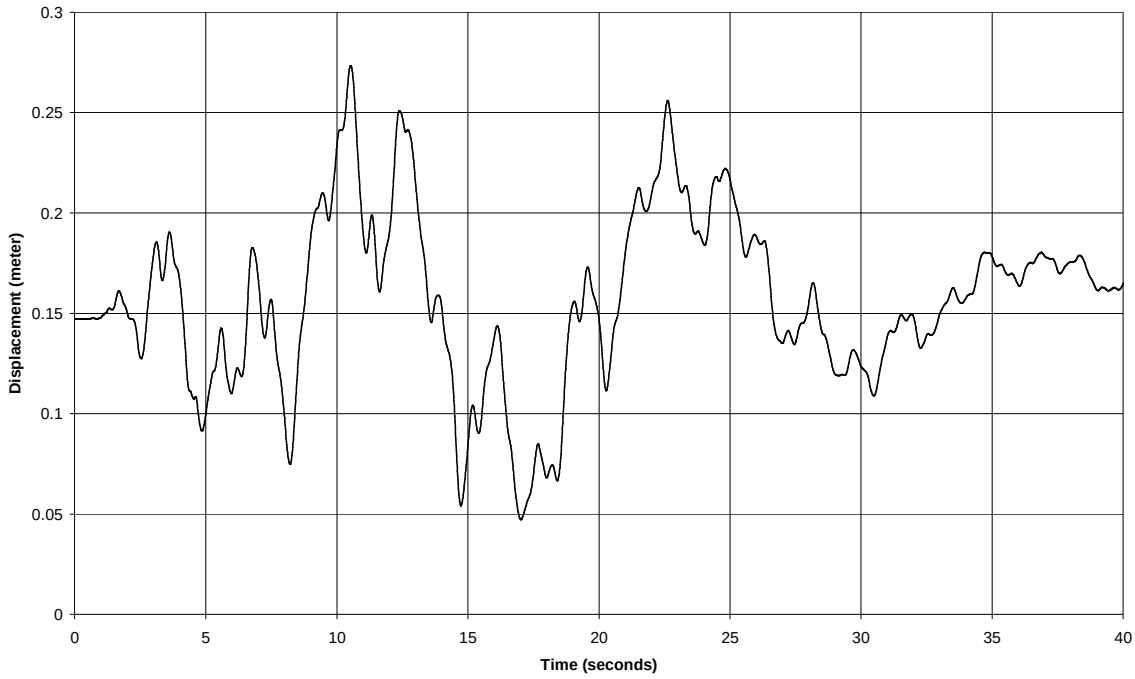

Figure 8 - 12: Dam's crest's horizontal displacements under seismic excitation.

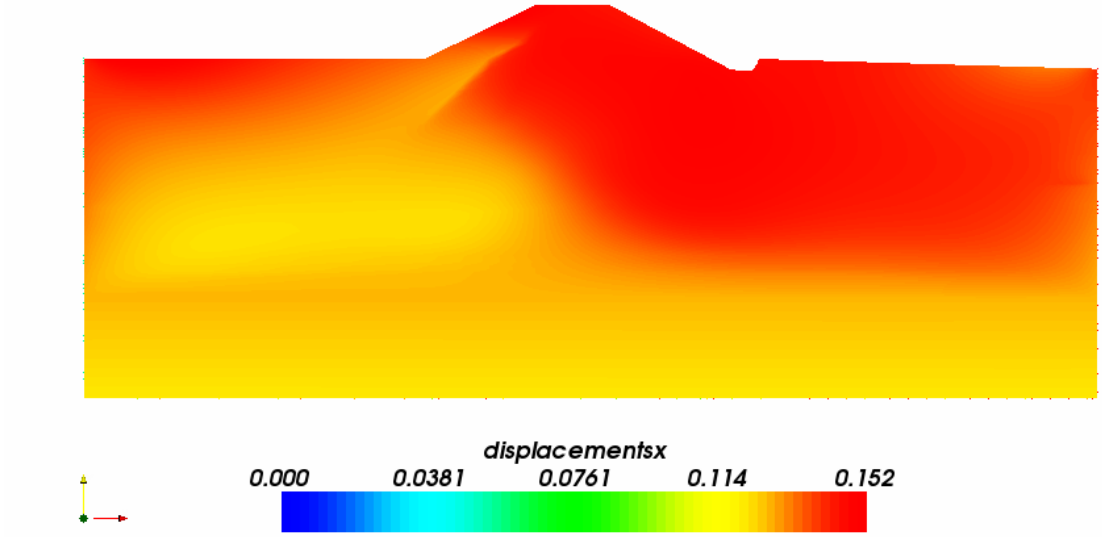

Figure 8 - 13: Horizontal displacements under gravity loads on the deformed shape of the structure. (meter).

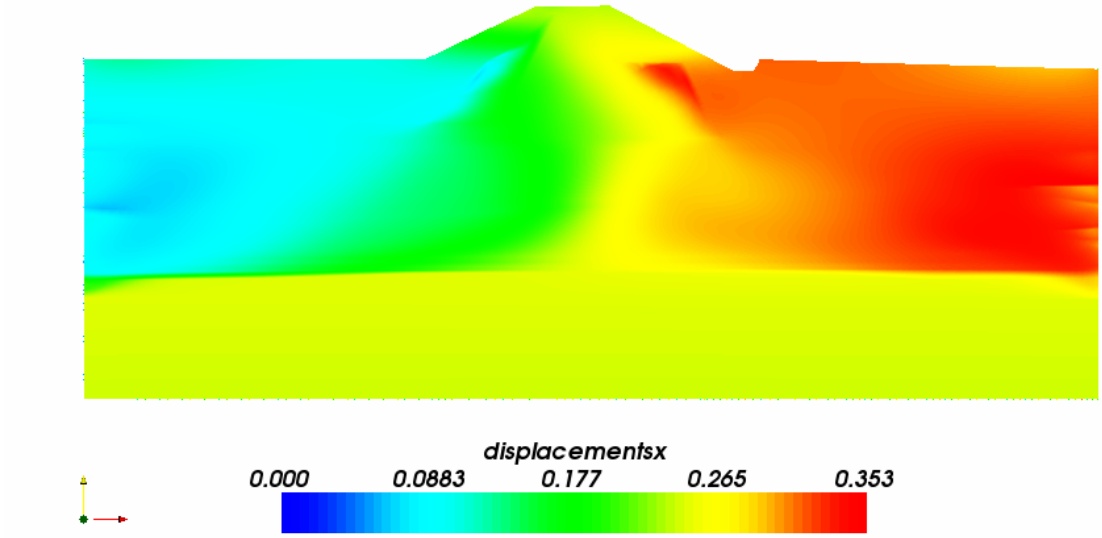

Figure 8 - 14: Horizontal displacements under seismic excitation at t = 10 seconds on the deformed shape of the structure. (meter).

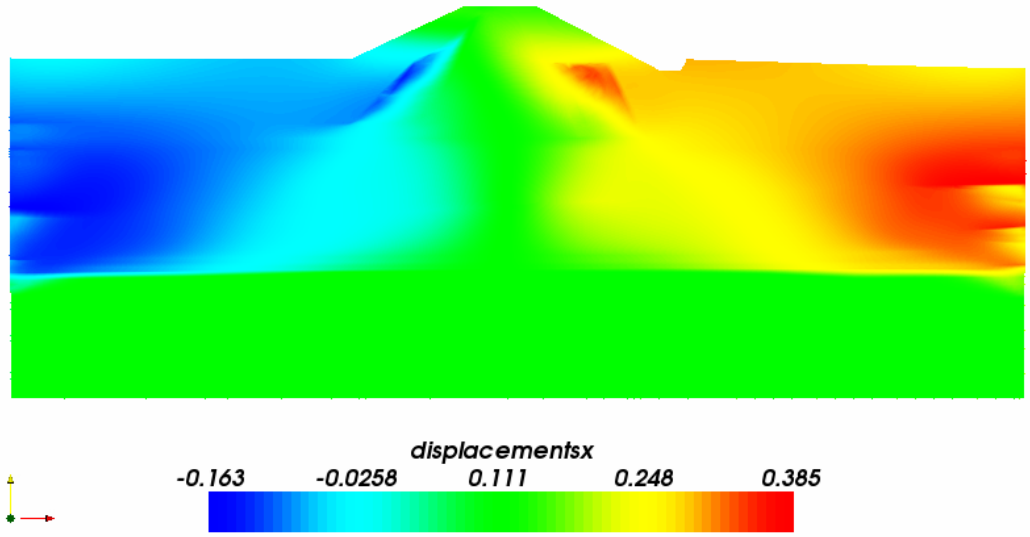

Figure 8 - 15: Horizontal displacements under seismic excitation at t = 20 seconds on the deformed shape of the structure. (meter).

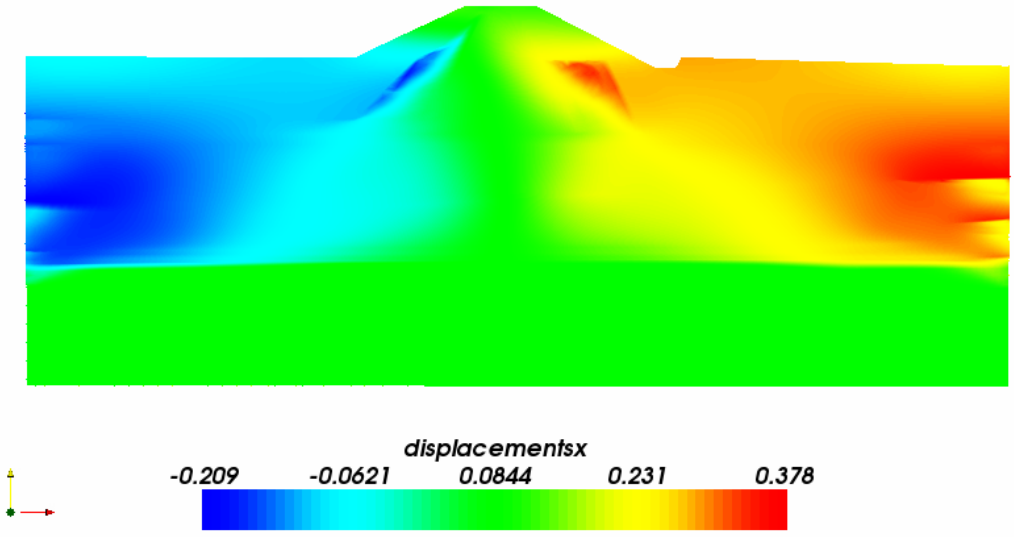

Figure 8 - 16: Horizontal displacements under seismic excitation at t = 30 seconds on the deformed shape of the structure. (meter).

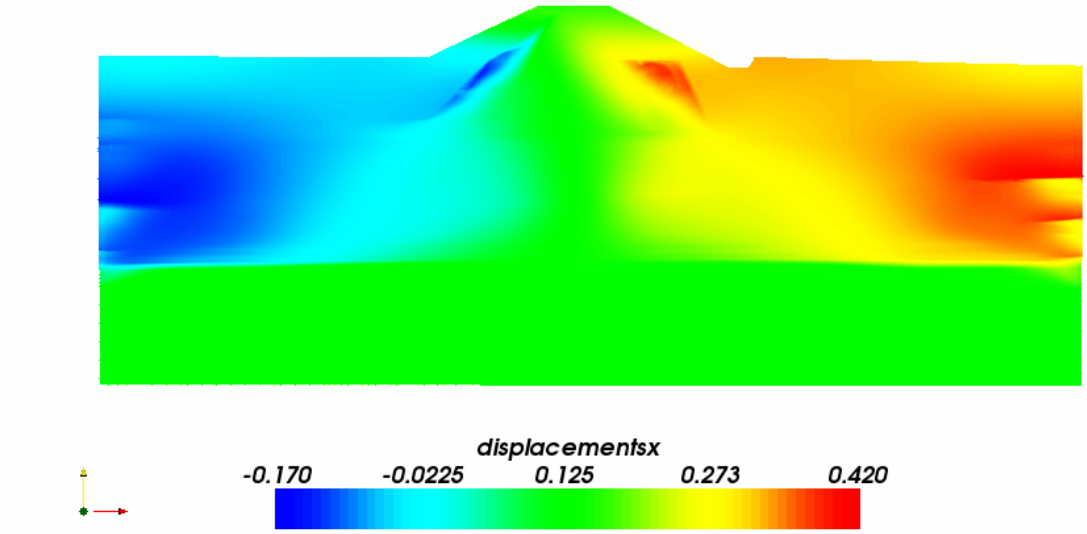

Figure 8 - 17: Horizontal displacements under seismic excitation at t = 40 seconds on the deformed shape of the structure. (meter).

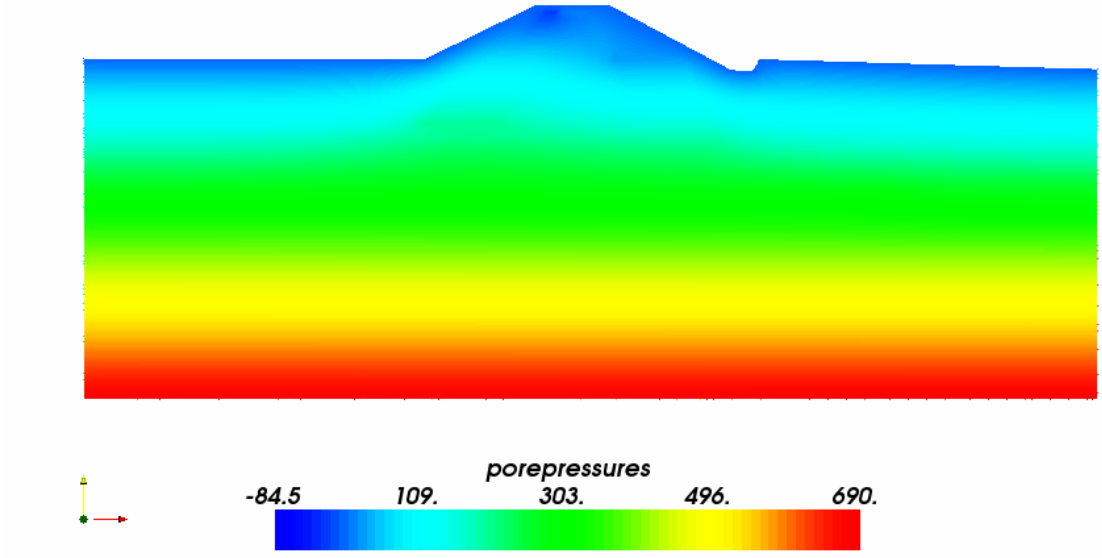

Figure 8 - 18: Pore pressures under gravity loads on the deformed shape of the structure. (kPa).

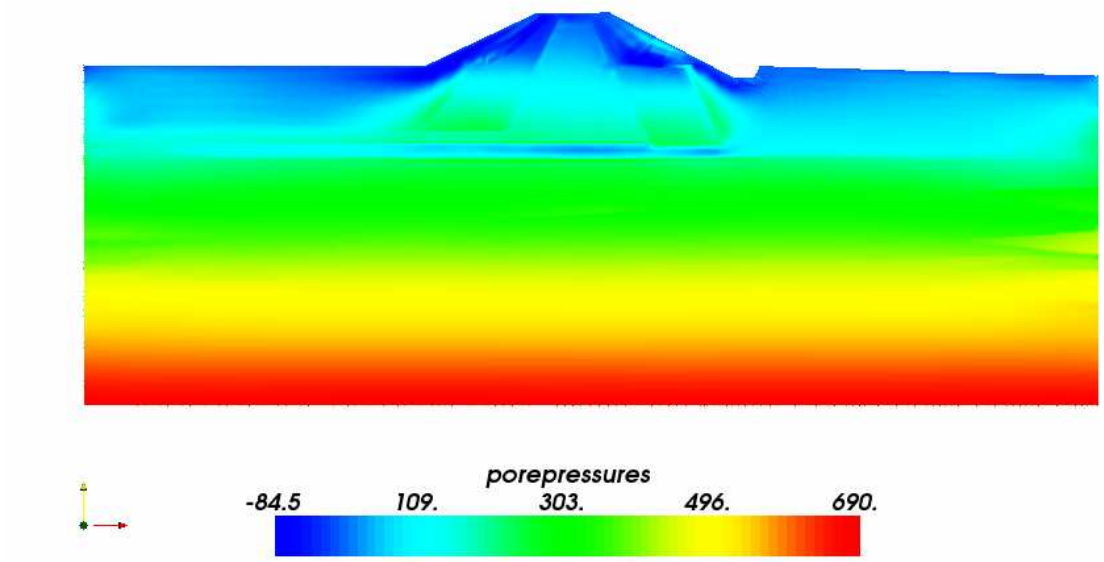

Figure 8 - 19: Pore pressures under seismic excitation at t = 10 seconds on the deformed shape of the structure. (kPa).

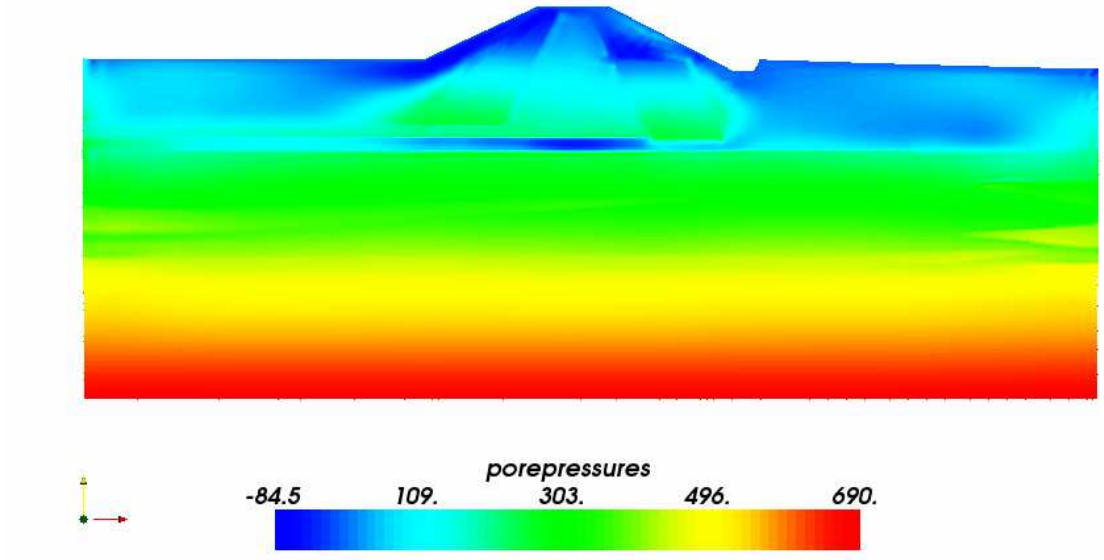

Figure 8 - 20: Pore pressures under seismic excitation at t = 20 seconds on the deformed shape of the structure. (kPa).

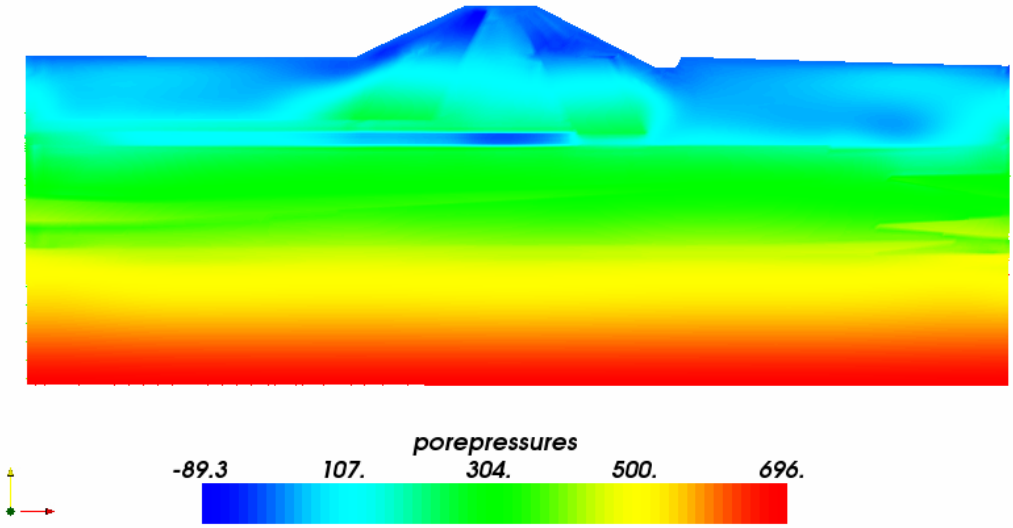

Figure 8 - 21: Pore pressures under seismic excitation at t = 30 seconds on the deformed shape of the structure. (kPa).

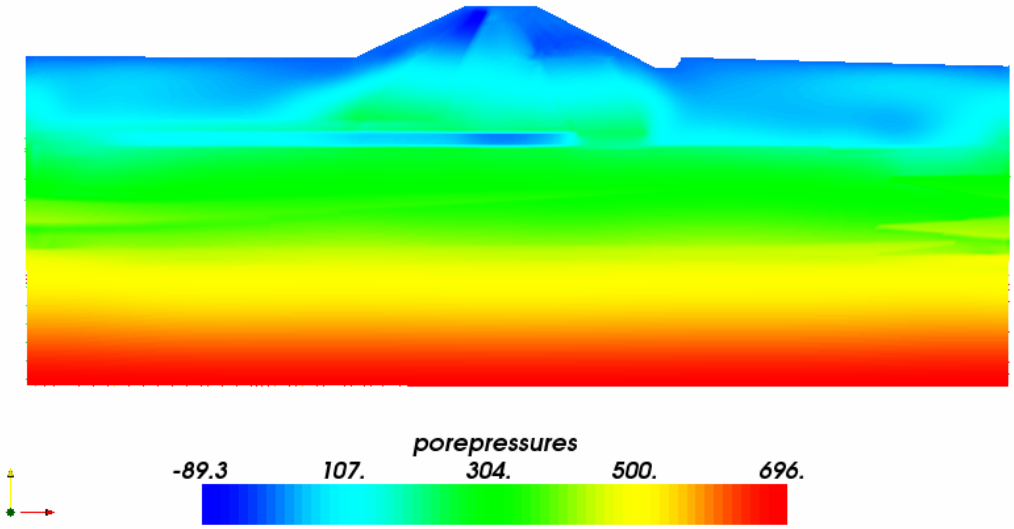

Figure 8 - 22: Pore pressures under seismic excitation at t = 40 seconds on the deformed shape of the structure. (kPa).

9. CONCLUSION

9.1. Introduction

In this section, conclusions drawn from the results of this study are outlined.

9.2. Comparison of Analyses Results

In this study, three different analyses have been performed, one as modal analysis and two as time history (or response history) analysis. There are previous studies that both investigated the modal response and consolidation under gravity loads of the structure. Modal analyses performed by (Cimilli, 1998) [12] states that, most of the research done about Alibey Earth Dam has considered the material properties of the structure more flexible than they were and the real behavior of the structure is more rigid than the proposed material properties. In this study, modal analyses were performed and their results were compared with respect to the study by (Cimilli, 1998) [12] and according to the analyses results, the proposed materials catch the proposed rigidity of the structure.

In the second analysis, linear elastic time history analysis of the dam was performed. In this analysis, displacements up to 0.25 meters are observed at the crest of the dam.

In the third analysis, up to 0.30 meters of displacements are observed at the crest of the structure.

9.3. Conclusion

Alibey Earth Dam is evaluated by nonlinear dynamic time history and modal analysis methods. The dam does not observe excessive displacements under given earthquake excitation. As a result, it is not awaited for the structure to be damaged under the expected Marmara Sea Region earthquake.

REFERENCES

[1] Soralump, S. “Estimating Probability of Earthquake-Induced Failure of Earth Dams”, Ph.D. Dissertation, Civil and Environmental Engineering, Utah State University, UMI No. 3083222, 2002

[2] Mercangoz, B.B. “Yumusak Kohezyonlu Zeminlerin Kademeli Yukleme Altinda Davranisinin Numerik Analizi”, in Turkish, M.Sc. Dissertation, Civil Engineering, Yildiz Technical University, 1996

[3] Kilic, H. Tohumcu, P. Tonaroglu, M. and Ozaydin, K. “Determining the Compressibility and Permeability Characteristics of Foundation Layers of Alibey Dam”, Fifth International Congress on Advances in Civil Engineering, Istanbul Technical University, Vol. 2, pp. 973-982, September 25-27, 2002

[4] Kilic, H. and Yildirim, S. “Prediction of Deformations by Means of Finite Element Computation and Stress Path Testing Technique”, Proceedings of the Fifteenth International Conference on Soil Mechanics and Geotechnical Engineering, Vol. 1, pp. 159-162, Istanbul, 2001

[5] Ozaydin, K. Kilic, H. Berilgen, M.M. Ozcoban, M.S. Yildirim, S. and Erdil, T.B. “Determination of Deformations in Soft Soils with Coupled Analysis-Alibey Dam”, Proceedings of the Fifteenth International Conference on Soil Mechanics and Geotechnical Engineering, Vol. 1, pp. 471-474, Istanbul, 2001

[6] Kilic, H. Berilgen, M. Ozaydin, K. and Erdil, T. “Coupled Analysis of Stress-Strain-Consolidation Behaviour of Alibey Dam Foundation”, “Alibey Baraji Temel Zemininin Kademeli Yukleme Altinda Gerilme-Sekil Degistirme-Konsolidasyon (Coupled) Analizi”, in Turkish, Zemin Mekanigi ve Temel Muhendisligi Yedinci Ulusal Kongresi, Yildiz Teknik Universitesi, Vol. 1, pp. 1-11, 22-23 Ekim, 1998

[7] Kilic, H. and Yildirim, S. “Determination of Soil Deformations Beneath Embankments by Means of Numerical Analyses”, “Dolgu Alti Zeminlerde Deformasyonlarin Numerik Olarak Belirlenmesi”, in Turkish, Zemin Mekanigi ve Temel Muhendisligi Sekizinci Ulusal Kongresi, Istanbul Teknik Universitesi, pp. 121-130, 26-27 Ekim, 2000

[8] Kilic, H. and Yildirim, S. “Soil Parameter Determination of Alibey Dam Foundation”, “Alibey Baraji Temel Zemini Parametrelerinin Belirlenmesi”, in Turkish, Zemin Mekanigi ve Temel Muhendisligi Sekizinci Ulusal Kongresi, Istanbul Teknik Universitesi, pp. 111-120, 26-27 Ekim, 2000

[9] Kilic, H. “The Determination of Deformation Behaviour of Alibey Dam Foundation Soil by Means of Numerical Analyses and Laboratory Testing Techniques”, “Alibey Baraji Temel Zemini Deformasyon Davranisinin Sayisal ve Deneysel Yontemlerle Belirlenmesi”, in Turkish, Yildiz Teknik Universitesi Dergisi, Vol. 1, pp. 31-46, 2003

[10] Ozcoban, M.S. “Yumusak Zeminlere Oturan Dolgu Barajlarin Analizi”, in Turkish, Ph.D. Dissertation, Civil Engineering, Yildiz Technical University, 1997

[11] Kilic, H. “Yumusak Zeminler Uzerine Oturan Dolgu Barajlarda Deformasyonlarin Numerik ve Deneysel Yontemlerle Belirlenmesi”, in Turkish, Ph.D. Dissertation, Civil Engineering, Yildiz Technical University, 2000

[12] Cimilli, I.T. “Seismic Response Analysis of Alibey Earth-Fill Dam”, M.Sc. Dissertation, Earthquake Engineering, Bogazici University, 1998

[13] DSI, Facts and Figures about Alibey Dam, http://www.dsi.gov.tr/?, 2005
[14] Chen, M. “Response of an Earth Dam to Spatially Varying Earthquake Ground Motion”, Ph.D. Dissertation, Civil and Environmental Engineering, Michigan State University, UMI No. 9605849, 1995
[15] Gazetas, G. “Shear Vibration of Vertically Inhomogeneous Earth Dams”, International Journal for Numerical and Analytical Methods in Geomechanics, Vol. 6, pp. 219-241, 1982
[16] Chugh, A.K. “Dynamic Response Analysis of Embankment Dams”, International Journal for Numerical and Analytical Methods in Geomechanics, Vol. 9, pp. 101-124, 1985
[17] Prevost, J. Abdel-Ghaffar, A.M. and Lacy, S. “Nonlinear Dynamic Analyses of an Earth Dam”, Journal of Geotechnical Engineering, Vol. 111, No. 7, pp. 882-897, July, 1985
[18] Elgamal, A.-W. M. Abdel-Ghaffar, A.M. and Prevost, J.H. “Elasto-Plastic Earthquake Shear-Response of One-Dimensional Earth Dam Models”, Earthquake Engineering and Structural Dynamics, Vol. 13, pp. 617-633, 1985
[19] Gazetas, G. “Seismic Response of Earth Dams: Some Recent Developments”, Soil Dynamics and Earthquake Engineering, Vol. 6, No. 1, 1987
[20] Lacy, S.J. and Prevost, J.H. “Nonlinear Seismic Response Analysis of Earth Dams”, Soil Dynamics and Earthquake Engineering, Vol. 6, No. 1, 1987
[21] Lin, J. and Chao, B. “Estimation of Shear Moduli and Damping Factors of Earth Dam Materials”, Earthquake Engineering and Structural Dynamics, Vol. 19, pp. 891-910, 1990
[22] Zeghal, M. and Abdel-Ghaffar, A.M. “Analysis of Behavior of Earth Dam Using Strong-Motion Earthquake Records”, Journal of Geotechnical Engineering, Vol. 118, No. 2, pp. 266-277, February, 1992
[23] Davis, C.A. and Bardet, J.P. “Performance of Two Reservoirs During 1994 Northridge Earthquake”, Journal of Geotechnical Engineering, Vol. 122, No. 8, pp. 613-622, August 1996
[24] Uddin, N. “A Single-Step Procedure for Estimating Seismically-Induced Displacements in Earth Structures”, Computers and Structures, Vol. 64, No. 5/6, pp. 1175-1182, 1997
[25] Dakoulas, P. and Abouseeda, H. “Response of Earth Dams to Rayleigh Waves Using Coupled FE-BE Method”, Journal of Engineering Mechanics, pp. 1311-1320, December 1997
[26] Abouseeda, H. and Dakoulas, P. “Non-Linear Dynamic Earth Dam-Foundation Interaction Using a BE-FE Method”, Earthquake Engineering and Structural Dynamics, Vol. 27, pp. 917-936, 1998
[27] Liang, R.Y. Nusier, O.K. and Malkawi, A.H. “A Reliability Based Approach for Evaluating the Slope Stability of Embankment Dams”, Engineering Geology, Vol. 54, pp. 271-285, 1999
[28] Chen, M. and Harichandran, R.S. “Response of an Earth Dam to Spatially Varying Earthquake Ground Motion”, Journal of Engineering Mechanics, pp. 932-939, September 2001
[29] Wu, G. “Earthquake-Induced Deformation Analyses of the Upper San Fernando Dam under the 1971 San Fernando Earthquake”, Canadian Geotechnical Journal, Vol. 38, pp. 1-15, February 2001
[30] Cascone, E. and Rampello, S. “Decoupled Seismic Analysis of an Earth Dam”, Soil Dynamics and Earthquake Engineering, Vol. 23, pp. 349-365, 2003

[31] Zerfa, F.Z. and Loret, B. “Coupled Dynamic Elastic-Plastic Analysis of Earth Structures”, Soil Dynamics and Earthquake Engineering, Vol. 23, pp. 435-454, 2003

[32] Ming, H.Y. and Li, X.S. “Fully Coupled Analysis of Failure and Remediation of Lower San Fernando Dam”, Journal of Geotechnical and Geoenvironmental Engineering, pp. 336-349, April 2003

[33] Gudehus, G. Cudmani, R.O. Libreros-Bertini, A.B. and Buhler, M.M. “In-Plane and Anti-Plane Strong Shaking of Soil Systems and Structures”, Soil Dynamics and Earthquake Engineering, Vol. 24, pp. 319-342, 2004

[34] Khoei, A.R. Azami, A.R. and Haeri, S.M. “Implementation of Plasticity Based Models in Dynamic Analysis of Earth and Rockfill Dams: A Comparison of Pastor-Zienkiewicz and Cap Models”, Computers and Geotechnics, Vol. 31, pp. 385-410, 2004

[35] Adalier, K. and Sharp, M.K. “Embankment Dam on Liquefiable Foundation-Dynamic Behavior and Densification Remediation”, Journal of Geotechnical and Geoenvironmental Engineering, pp. 1214-1224, November 2004

[36] Papalou, A. and Bielak, J. “Nonlinear Seismic Response o Earth Dams with Canyon Interaction”, Jounal of Geotechnical and Geoenvironmental Engineerin, pp. 103-110, January 2004

[37] Erdik, M. Demircioglu, M. Sesetyan, K. Durukal, E. and Siyahi, B. “Earthquake Hazard in Marmara Region, Turkey”, Soil Dynamics and Earthquake Engineering, Vol. 24, pp. 605-631, 2004

[38] Silva, W.J. and Lee, K. “WES RASCAL Code for Synthesizing Earthquake Ground Motions”, US Army Engineer Waterways Experiment Station, Report 24, Misc. Paper S-73-1, 1987

[39] Ragheb, A.M. “Numerical Analysis of Seismically Induced Deformations in Saturated Granular Soil Strata”, *Ph.D. Thesis*, Rensselaer Polytechnic Institute, September, 1994

[40] Yang, Z. “Numerical Modeling of Earthquake Site Response Including Dilatation and Liquefaction”, *Ph.D. Thesis*, Graduate School of Arts and Science, Columbia University, 2000

[41] Elgamal, A. Yang, Z. Parra, E. and Ragheb, A. “Modeling of Cyclic Mobility in Saturated Cohesionless Soils”, *International Journal of Plasticity*, Vol. 19, pp. 883 - 905, 2003

[42] Zhang, Y. Yang, Z. Bielak, J. Conte, J.P. and Elgamal, A. “Treatment of Seismic Input and Boundary Conditions in Nonlinear Seismic Analysis of a Bridge Ground System”, 16th ASCE Engineering Mechanics Conference, July 16-18, 2003, University of Washington, Seattle, http://www.ce.washington.edu/em03/proceedings/papers/369.pdf, 2003

[43] Mazzoni, S. McKenna, F. and Fenves, G.L. “OpenSees Command Language Manual”, http://opensees.berkeley.edu/OpenSees/manuals/usermanual/OpenSeesManual.pdf, June 14, 2005

[44] Chchoi@u.washington.edu, parduino@u.washington.edu, “Semi-Infinite Domain Characterization Using OpenSees”, Web Page, http://maximus.ce.washington.edu/~geotech/opensees/, April, 2006

REFERENCES NOT CITED

[45] Erdik, M. and Durukal, E. “Simulation Modeling of Strong Ground Motion”, in Chen, W.F. and Scawthorn, C. (eds.), *Earthquake Engineering Handbook*, pp. 6.1-6.67, CRC Press, 2002

[46] Yang, Z. “Development of Geotechnical Capabilities into OpenSees Platform and their Applications in Soil-Foundation-Structure Interaction Analyses”, Ph.D. Dissertation, Civil Engineering, University of California at Davis, UMI No. 3065317, 2002

[47] Sindel, Z. “Tangent Stiffness Approach for the Nonlinear Finite Element Analysis”, Ph.D. Dissertation, Civil Engineering, Bogazici University, 1993

[48] Tezcan, S.S. “CE 601 Finite Elements Lecture Notes”, Lecture Notes, Civil Engineering, Bogazici University, 2005

[49] Jeremic, B. Yang, Z. Cheng, Z, Liu, Q. Preisig, M. and Jie, G. “Lecture Notes on Computational Geomechanics: Inelastic Finite Elements for Pressure Sensitive Materials”, Department of Civil and Environmental Engineering, University of California at Davis, Version: 12, http://sokocalo.engr.ucdavis.edu/~jeremic/CG/CompGeomechanicsLectureNotes.pdf, April, 2005

[50] Algul, E. Arslan, E. Yalin, D. and Alkan, R.M. “The Results of the Deformation Research Project of Alibey Dam between 1987 and 1994”, “Alibey Barajinda Deformasyon Olcmeleri ve 1987-1994 Sonuclari”, in Turkish, Bildiriler Kitabi, Muhendislikte 20.Yil Sempozyumu, Zonguldak Karaelmas Universitesi, Muhendislik Fakultesi, 5-6 Ekim, JDF 07, 1995

[51] Arslan, E. Yalin, D. Algul, E. and Alkan, R. “The Results of the Deformation Research Project of Alibey Dam”, Proceedings of Istanbul-94, 1st Turkish International Symposium on Deformations, September 5-9, pp. 512-523, 1994

[52] Algul, E. Deniz, R. Yalin, D. Arslan, E. and Gurdogan, I.H. “The Research Report of the Deformation Research Project of Alibey Dam for 1987-88 Period”, Geodesy and Photogrammetry Engineering, Istanbul Technical University, 199?

[53] Algul, E. Deniz, R. Yalin, D. Arslan, E. and Ozsamli, C. “Istanbul Alibey Baraji Deformasyon Arastirma Projesi 1991 Yili Arastirma Raporu”, in Turkish, Geodesy and Photogrammetry Engineering, Istanbul Technical University, 1992

[54] Algul, E. Deniz, R. and Yalin, D. “Istanbul Alibey Baraji Deformasyon Arastirma Calismalarinda Bes Yil.”, in Turkish, DSI Teknik Bulteni, Vol. 76, pp. 9-17, 1992

[55] Gulal, V.E. Erkaya, H. Hosbas, R.G. and Ersoy, N. “Deformation Measurements for Earthfill Dams and an Example; Alibey Dam”, “Toprak Dolgu Barajlarda Deformasyon Olcmeleri, Alibey Baraji Ornegi”, in Turkish, I. Ulusal Muhendislik Olcmeleri Sempozyumu, Istanbul, 2003

[56] Samilgil, T. “Istanbul – Icmesuyu Projesi: Alibey Baraji” in Turkish, DSI Bulteni, Vol. 158, pp. 10-23, Nisan, 1972

[57] DSI, “Alibey Dam”, http://www.dsi.gov.tr/tricold/alibey.htm, 2006

[58] Tonaroglu, M. “Sekil Degistirme Hizinin Konsolidasyon Davranisi Uzerindeki Etkisi”, in Turkish, M.Sc. Dissertation, Civil Engineering, Yildiz Technical University, 1998

[59] Chen, W.F. and Mizuno, E. “Nonlinear Analysis in Soil Mechanics Theory and Implementation”, Developments in Geotechnical Engineering, Vol. 53, Elsevier Science Publishers B.V., ISBN 0-444-43043-1, 1990

[60] Tezcan, S.S. “Toprak Barajlarin Deprem Analizi”, Bogazici Universitesi Yayinlari, B.U. -74-33/001, 1974

[61] Potts, D.M. and Zdravkovic, L. “Finite Element Analysis in Geotechnical Engineering Theory”, Thomas Telford Publishing, Thomas Telford Ltd. London, ISBN 0 7277 2753 2, 1999

[62] Crisfield, M.A. “Non-Linear Finite Element Analysis of Solids and Structures”, Vol. 1, John Wiley & Sons Ltd., ISBN 0471 97059 X, 1991

[63] Crisfield, M.A. “Non-Linear Finite Element Analysis of Solids and Structures”, Vol. 2, John Wiley & Sons Ltd., ISBN 0-471-95649-X, 1991

[64] Chopra, A.K. “Dynamics of Structures Theory and Applicatons to Earthquake Engineering”, Prentice-Hall, Inc., ISBN 0-13-086973-2, 2000

[65] Kramer, S.L. “Geotechnical Earthquake Engineering”, “Geoteknik Deprem Muhendisligi”, in Turkish, Gazi Kitabevi, ISBN 975-8640-63-1, Temmuz, 2003

[66] Wieland, M. “Seismic Aspects of Dam Design”, http://www.ewe.ch/linked/en/hydropower/pu_en_seismic_aspects.pdf, ?